The Processes and Factors Controlling Air Filtration by Impregnated Activated Carbon and its Application in Environmental Pollution

C A BARNARDT

Dissertation presented for the Degree of Doctor of Philosophy at the
University of Stellenbosch
Promoter : Prof D K Hallbauer

JANUARY 1998

ii

Declaration

I, the undersigned, hereby declare that the work contained in this dissertation is my own original work and has not previously, in its entirety or in part, been submitted at any university for a degree.

Date: January 1998

OPSOMMING

Die aandag van die plaaslike, nasionale en internasionale gemeenskap word meer en meer gevestig op omgewingsake. Deel van die probleem wat die gemeenskap en die regering in die gesig staar, is die keuse van 'n strategie wat sonder oormatige wetgewing en kostes 'n veilige omgewing handhaaf. Universele persoonlike beskermingstoerusting vir die werker vir beskerming teen enige vorm van kontaminasie is een van die kostebesparings. Hierdie studie is gedoen om die beskermingstyd van 'n geïmpregneerde koolstof filter te bepaal indien dit aan 'n organiese en anorganiese gas onderskeidelik en gelyktydig as 'n mengsel blootgestel word. Daar is gevind dat gelyktydige blootstelling van 'n filter aan twee of meer gasse die filterkapasiteit verlaag.

Die beskerming van 'n gasmaskerfilter teen 'n mengsel van gasse is 'n belangrike aspek aangesien werkers heel waarskynlik in omgewings werk waar meer as een kontaminant teenwoordig is. Twee tipes filtrasiemeganismes is moontlik met geaktiveerde koolstof, naamlik fisiese adsorpsie en chemiese adsorpsie.

Die filtrasie van koolstoftetrachloried (CCl_4) is afhanklik van fisiese adsorpsie terwyl waterstofsianied (HCN) deur middel van chemiese adsorpsie gefiltreer word. Gelyktydige blootstelling aan 'n organiese en anorganiese kontaminant is nog nie in die literatuur gerapporteer nie. Hierdie studie is gedoen om die invloed van gelyktige blootstelling op die kapasiteit en derhalwe die beskermingstyd van geïmpregneerde koolstof vas te stel.

Aangesien die kapasiteit van geïmpregneerde koolstof ook deur ander veranderlikes beïnvloed word, was dit belangrik om die invloed van die verskillende veranderlikes op die kapasiteit van die koolstof te bepaal. Veranderlikes wat by hierdie studie ingesluit is, is die koolstof roumateriaal, die blootstellingskonsentrasie, die relatiewe humiditeit, die koolstofmassa en die gelyktydige blootstelling van die koolstof. Die kapasiteite is eksperimenteel en teoreties met behulp van die Wheeler vergelyking bereken. Die Wheeler vergelyking is ook gebruik om die adsorpsiesnelheidskonstante te bereken. Behalwe vir die beskermingstye en die kapasiteite is die aktiewe oppervlakte en die porievolumeverspreiding ook bereken.

Die invloed van die verskillende veranderlikes op die kapasiteite is vergelyk om die persentasie variasie tussen die resultate te bepaal. Dit is duidelik vanuit die resultate dat die gelyktydige blootstelling van die geïmpregneerde koolstof 'n beduidende impak op die kapasiteit van koolstof vir CCl_4 het. Die beskermingstyd en kapasiteit van HCN is nie beduidend geaffekteer nie.

Die rede vir die groot afname in kapasiteit vir die fisiese adsorpsie-afhanklike kontaminant kan aan gedeeltelike afskerming van die mikroporieë deur die reaksieprodukte van die chemisorpsie proses toegeskryf word. Dit is deur die verandering in die aktiewe oppervlakte, mikroporievolume en kapasiteitsmetings bewys.

Die gevolg van hierdie afname het direk betrekking op die toepassing en gebruik van gasmaskerfilters in die industrie.

SUMMARY

Environmental issues are attracting ever-increasing attention at local, national and international levels. Part of the problem facing society and government alike is the choice of strategies that maintain a safe environment without excessive regulation nd cost. One of the cost-saving exercises is to provide a universal personal protective device that protects the worker against any contamination.   The object of this study was to determine the time for which a worker would be protected by an impregnated activated-carbon filter against an organic gas and an inorganic gas, both simply and as a mixture. It was found that the effectiveness of the filter was reduced when the gas mixture companied two or more gases.

The degree of protection afforded by a gas mask filter against a mixture of gases is an important criterion because workers will most probably work in environments in which more than one contaminant is present. Two types of filtration mechanisms are possible with activated carbon namely, physical adsorption and chemisorption.

The filtration of carbon tetrachloride (CCl_4) depends on physical adsorption whereas filtration of hydrogen cyanide (HCN) depends on chemisorption. Exposure simultaneous to an organic and an inorganic substance has not been reported in the literature to date. In this study the influence was investigated of simultaneous exposure on the capacity and, therefore, on the protection time afforded by the impregnated carbon.

The capacity of impregnated carbon is also affected by other variables, and the influence of a number of different variables on the capacity of the carbon was studied. These variables included the carbon base material, the challenge concentration, the relative humidity, the carbon weight and the exposure of the carbon to mixtures of gases. The capacities were measured experimentally and calculated by means of the Wheeler equation. The Wheeler equation was also used to determine the reaction- rate constant. In addition to the protection times and the capacities, the active surface and pore volume distribution were measured.

The influence of the different variables on the capacities was compared in order to determine the percentage variance between the results obtained. The results have shown that the influence of the simultaneous exposure of the impregnated carbon simultaneous to gas mixture has a significant impact on the capacity of the carbon with respect to the CCl_4. The protection time and therefore the capacity for HCN were not affected significantly.

The reason for the large reduction in the capacity for the physical adsorption dependent vapour was due to the partial masking effect of the micropores by the reaction products of the chemisorption process. This was proved by the change in active surface, micropore volume and capacity. This reduction has direct implications for the application of the gas mask filters and cartridges in industry.

<u>CONTENTS</u>

ACKNOWLEDGEMENTS

I wish to express my sincere thanks and appreciation to Professor DK Hallbauer for his patience, friendliness and support throughout this study.

I am also grateful to Mr A Marquart for his valuable discussion and review of this work.

LIST OF SYMBOLS AND ABBREVIATIONS

ABBREVIATIONS

AR	analytical reagent
ASAP 2010	active surface determination apparatus
AR	analytical reagent
BDDT	Brunauer, Deming, Deming and Teller
BET	Brunauer, Emmet and Teller
CCl_4	carbon tetrachloride
Cl_2	chlorine
CIP	carbon in pulp
CBW	chemical, biological warfare
cm	centimeter
$cm.s^{-1}$	centimeter per second
cm^2	centimeter squared
$cm.g^{-1}$	centimeter per gram
DFT	density functional theory
DR	Dubinin-Radushkevich
EPA	Environmental Pollution Agency
GC	gas chromatograph
GPE	grand potential energy
g	gram
$g.mole^{-1}$	gram per mole
$g.m^{-2}$	gram per meter squared
h	hour
HCN	hydrogen cyanide
HCl	hydrogen chloride
HF	hydrogen floride
$kg.l^{-1}$	kilogram per liter
$l.min^{-1}$	liter per minute
min^{-1}	per minute
$ml.min^{-1}$	milliliter per minute

mm	millimeter
ml	milliliter
min	minute
mg	milligram
mg.m^{-3}	milligram per cubic meter
m^2	meter square
mmHg	millimeter mercury
NATO	North Atlantic Treaty Organisation
nm	nanometer
ppm	parts per million
RH	relative humidity
s^{-1}	per second
SABS	South African Bureau of Standards
SO$_2$	sulphur dioxide
STP	standard temperature and pressure
tpy	tons per year
TVFM	total volume filling of micropores
USA	United States of America
VOC	volatile organic compounds
μl	microliter
μg.cm^{-3}	microgram per cubic centimeter
μg.l^{-1}	microgram per liter
μg	microgram

SYMBOLS

Å	Angstrom
A_{cal}	calibrated integrated counts
A_m	apparent cross-sectional area occupied by a molecule of the adsorbate in the completed monolayer, cm^2
A_s	BET activated surface area, $m^2\ g^{-1}$
a_1	condensation coefficient
b	constant, dependent on temperature but independent of surface coverage, and describing in some way the
B	constant, related to the adsorption potential of the micropores
b_d	bed depth, cm
C_x/C_0	ratio of outlet and inlet concentration, g adsorbate / g carbon
C_0	challenge (inlet) concentration, $g.cm^{-3}$
C_e	gas concentration in equilibrium with the weight pre-adsorbed on the adsorbent, $g.cm^{-3}$
C_x	concentration in the outlet, $g.cm^{-3}$
D_p	diffusivity, $cm.s^{-1}$
D	diffusivity in a straight cylindrical pore, $cm.s^{-1}$
D_m	molecular diffusivity, $cm.s^{-1}$
D_k	Knudsen diffusion, $cm.s^{-1}$
D_s	surface diffusion, $cm.s^{-1}$
D_c	intra-crystalline diffusivity, $cm.s^{-1}$
d_f	film thickness, Å
d_p	sorbent granular size, cm
d_b/V_f	bed depth over superficial velocity for the calculation of τ
E	interaction potential energy, $cal.mol^{-1}$
E_a	energy of adsorption, $cal.mol^{-1}$
F	field strength at the centre of the molecule
f(H)	total area of pores of size H in the sample
h	Planck quantum constant
ΔH_A	heat of adsorption

ΔH_L	heat of liquefaction
H_2	hydrogen
K	Kelvin
K_v	constants for the adsorbed vapour
k_v	pseudo-first-order adsorption rate constant, min^{-1}
k	Boltzman constant
k_a	constant related to the structure of the adsorbent, $(cal.mole^{-1})^{-2}$
k_d	desorption constant
M	molecular weight of the adsorbate
M_1, M_2	molecular weigh
n	quantity of gas adsorbed expressed in moles per gram of solid
N_2	nitrogen
n_m	monolayer capacity
N	Avogadro constant
P	pressure of the vapour, Pa
P^0	saturation pressure, Pa
P_a	ambient pressure, Pa
P/P^0	relative pressure
ρ	density of the adsorbate in liquid form, $g.cm^{-3}$
ρ_β	bulk density of the packed carbon bed, $g.cm^{-3}$
q_L	molar heat of condensation
q_1	isosteric heat of adsorption
Q_a	heat of adsorption (that is the amount of heat liberated when the molecules move from vapour to the adsorbed state)This is also the energy involved in evaporation of the adsorbed molecule from the surface equation
Q	volumetric flow rate of air, $cm^3.min$
r	distance separating two atoms
r_k	kelvin radius,$\mathring{A}$
r_{ij}	distance between the molecule I in the gas phase and the centre of an atom j in the solid
R	molar gas constant, $erg.deg^{-1}.mol^{-1}$

S	surface area ,$m^2.g^{-1}$
t_b	protection time, min
t	thickness of adsorbed layer, Å
t_r	regeneration time, min
T	temperature,°C
T_a	absolute temperature, K
T	residence time, s^{-1}
v°_A, v°_B	characteristic frequencies related to optical dispersion
V	equilibrium amount (m.mol g^{-1}) of gas adsorbed per unit mass of adsorbent at relative pressures P/P^0 equation
V_m	amount of gas required for monolayer coverage of adsorbent (m.mol g^{-1}) equation
V_A	volume of nitrogen adsorbed, cm^3
V_N	micropore volume measured with N_2 ($cm^3 g^{-1}$) at 77K
V_f	superficial velocity, $m.s^{-1}$
V_I	volume of the sorbent, cm^3
V/Q	bed volume over volumetric flow for the calculation of T
W_T	volume of adsorption filling micropore , $cm^3 g^{-1}$
W_e	kinetic adsorption carbon capacity, g/g
W_o	active pore volume of the carbon, $cm^3.g$
W_a	volume of condensed adsorbate per gram of carbon, $cm^3.g$
W	weight of the of carbon, g
W_c	critical mass, g
W_e/C_0Q	gradient in the Wheeler equation used for the calculation of W_e
$-W_e\rho_B ln(C_0/C_x)/C_0 k_v$	y-axis intercept in the Wheeler equation used for the calculation
$W/Q\rho_B$	mass of the carbon bed over the product of volumetric flow times the bed density for the calculation of T
X_A, X_B	magnetic susceptibilities of the atoms A and B
x_m	grams of adsorbate per gram of adsorbent
x_s	saturation uptake
X(P)	experimental quantity adsorbed at pressure P

$x(P,H)$	quantity adsorbed per unit area at the same pressure (P), in a pore of size H
X_m	mass of adsorbate adsorbed on sample, g
z_m	number of sites per unit area (so that $z_m\theta_1$ is the corresponding number of sites adsorbed molecules)
μ	dipole moment of the molecule
θ	angle between the field and the axis of the dipole
Ω	function of ϵ/kT
δ	surface tension of the adsorbate, dynes.cm^{-1}
λ	carbon bed depth, cm
β	adsorbate affinity coefficient
%	percentage
ϵ	adsorption potential of the surface, cal.mol^{-1}
°C	degrees Celsius

1

PREFACE

PROBLEM STATEMENT

The environment is becoming endangered more and more by an ever-increasing number of threats, e.g. extinction of certain fauna and flora, water pollution and air pollution. This thesis concentrates on the environmental geochemistry of air-pollution control.

In recent years legislation has changed drastically to enhance life and living conditions by preventing people from exploiting the environment for personal gain. Drastic measures have become necessary to protect workers against adverse conditions. Threatening environments exist and the challenge is in solving these problems in the most cost-effective manner. A short- term solution is to provide the workers with personal protective equipment, e.g. gas masks, which are freely available and which are currently being sold all over the world. As with all products, the designs and applications are continually updated. However, specifications are often not updated, while inadequate quality- control and quality-assurance measures render many products useless.

The current pollution control requirements specifications for South African manufacturers are SABS Specification number 1455 Part IV (I). This specification has subdivided the application of gas mask filters into the following categories:

Type A	-	Organic Vapours
Type B	-	Inorganic Vapours
Type E	-	Sulphur Dioxide
Type K	-	Ammonia

Filter cartridges are subdivided into the above four categories and sold as Type A, B, E or K filters, which are also colour-coded. With the progress in product development, filters applicable to all four categories at once, namely Type ABEK filters, are now being sold. The SABS specification does not make provision for combination filters and as far as can be ascertained, no institute in the world currently tests against a mixture of gases. Workers therefore use these combination filters in environments contaminated with mixtures of pollutants and

assume that protection times are as specified by the supplier and and according to SABC specifications.

This study was made of the influence of mixtures of gases on the adsorption rate constants and capacities of the impregnated carbon, compared with the results obtained when single gas exposures are used. The implications are significant in environmental geochemistry and the protection of the atmosphere and the workers.

The objectives of this study can be summarized as follows;

a) To investigate the changes in protection when a carbon filter is exposed to a single organic (CCl_4)- and inorganic vapour (HCN) singly and simultaneously to an organic- and inorganic vapour mixture.

b) A semi-empirical equation to be utilized to determine the influence on filtration capacity and the adsorption rate constants theoretically of two types of carbons (coconut shell and coal) for exposure to CCl_4 and HCN singly and simultaneously:

c) To determine the changes in the physical characteristics before and after exposure in order to clarify some of the results.

CHAPTER I

INTRODUCTION

1.1   ACTIVATED CARBON

The adsorption capabilities of activated carbon have been recognized and documented for a long time. The most common adsorptive carbon sources were blood char, coconut char, bone char and lignite char. In 1822, Bussy increased the adsorptive power of blood char by twenty to fifty times by a heating process which ultimately led to the development of activated carbon [1].

In 1865 Hunter investigated coconut shell as a potential precursor for an activated carbon and found surprisingly high capacity of the activated product to adsorb vapours after suitable treatment. Later, Lipsone produced a charcoal for the purification of water, while Stenhouse thought that this material might find use in the purification of sewer and other foul atmospheres as well as in the early forms of mask respirators which he devised.

At the end of the nineteenth century it was discovered that activated carbon could be made from coal. During the twentieth century, many precursors have been used successfully to produce activated charcoal, including lignite and peat, textile waste, newspaper and even recycled polymers. However, coal and nuts have been the favoured sources for charcoal production, mainly because of the denseness nature of these precursors, but there is no scientific reason why any carbonaceous precursor should not give a highly active charcoal product.

The use of chemical warfare in 1915 during World War I should have given a great impetus to the manufacture of porous carbon and charcoal from a wide variety of precursors for the physical adsorption of chemical warfare agents. However, as far as can be ascertained, coconut shell charcoal was the favoured material in the UK, USA and Germany for the whole of the period between the wars. The publicity surrounding the use of activated carbon in air-purifying respirators stimulated much research into new fields of use for activated carbon [1, 2, 3]. The knowledge of activation of carbon accelerated their use as an efficient adsorbent

in many chemical processes. During the process of activation the spaces between the elementary crystallites become cleared of various non-organized carbonaceous compounds, resulting in voids or pores. A suitable activation process causes an enormous number of pores to be formed so that the internal surface of the activated carbon becomes very large, which results in an adsorbent with a large adsorption capacity.   The activation process usually depends upon selective oxidation of carbonaceous material in the presence of impregnations at elevated temperatures, and it is then treated with oxidizing agents such as air, steam, carbon dioxide or chlorine.

During carbonisation all other elements except carbon are first removed in gaseous form by pyrolytic decomposition of the starting material, and these freed atoms of elementary carbon are then grouped into organized crystallographic formations. However, the grouped arrangement becomes filled with tar, and the resulting product has only a very small adsorption capacity [4].   There are many ways to increase the adsorptive capabilities of the carbon; these are grouped into two main categories: chemical and physical activation.

Chemical activation is generally carried out at temperatures between 400 and 1000 degrees Celsius. The most commonly used activation agents are zinc chloride, potassium sulphide, potassium thiocyanate, phosphoric acid and sulphuric acid. The activating agent causes the cellulose to swell and lateral bonds to be broken, which results in an increase in the number of inter-micelle and intra-micelle voids.

Physical activation is a two-step process with the first step being carbonisation which is critical to the activation and quality of the final product. The second step is activation of the carbonised material by treatment, most often by steam, carbon dioxide, or oxygen. This leads to the removal of unorganized carbon, the non-uniform burn-out of elementary crystals, and the formation of new pores. As activation continues, complete burn-out of the walls between adjacent micropores occurs, and this leads to an increase in the number of transitionalpores and macropores.

1.2   CHARACTERISTICS OF ACTIVATED CARBON

In general, the structure of the active carbon is tridisperse, for example, it contains three kinds of pores: micropores, mesopores (transitional pores) and macropores. The micropores are classified according to IUPAC as pores that are smaller than 2 nm. The transitional pores are classified as pores with sizes ranging from 2 nm to 50 nm, and the macropores are greater than 50 nm.

Pores in the particle of the activated carbon are as illustrated in Figure 1.1. The pore structure of activated carbon affects the large surface-to-size ratio. The macropores do not add appreciably to the surface area of the carbon, but provide a passageway to the particle interior and the micropores. The micropores are developed preferentially during carbon activation and result in the large surface areas on which adsorption occurs. Pore structure, like surface area, is a major factor in the adsorption process. Pore-size distribution determines the size distribution of molecules that can enter the carbon particle to be adsorbed. The differential behaviour of the pores is illustrated in Figure 1.2. Large molecules can block micropores and render useless their available surface areas. However, because of irregular shapes of pores and constant molecule movement, the smaller molecules can usually penetrate the smaller capillaries. Since adsorption is possible only in those pores that can be entered by molecules, the carbon adsorption process is dependent on the physical characteristics of the activated carbon and the molecular size of the adsorbate [5].

When a cube, real or imaginary, of 1 m side length is subdivided into smaller cubes each 1 μm (micrometer) (10^{-6} m) in length, 10^{18} particles will be formed, each exposing an area of 6 x 10^{-12} m^2. Thus, the total area of all the particles is 6 x 10^6 m^2. This millionfold increase in exposed area is typical of the large surface areas exhibited by fine powder when compared to undivided material.
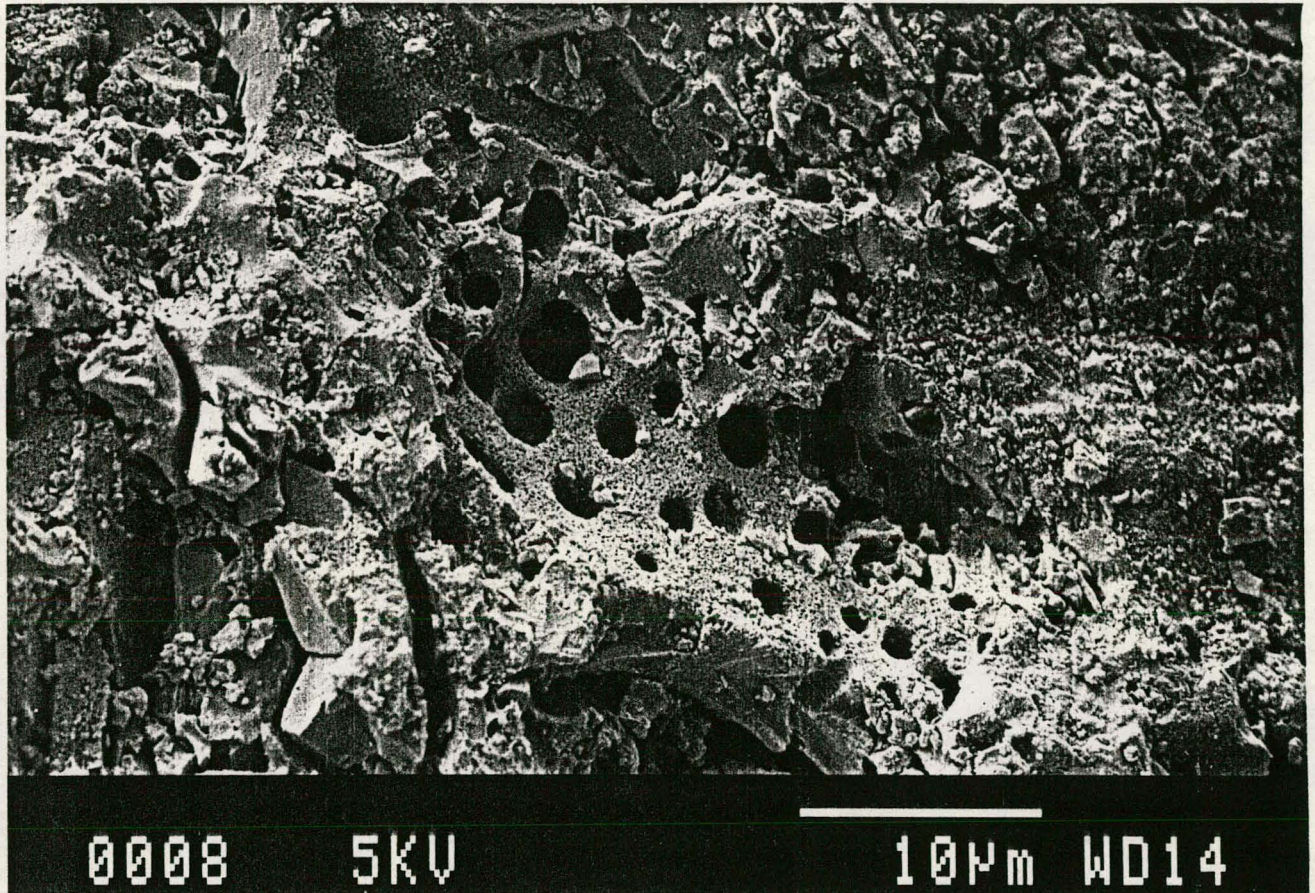
Figure 1.1: The porous structure of activated carbon
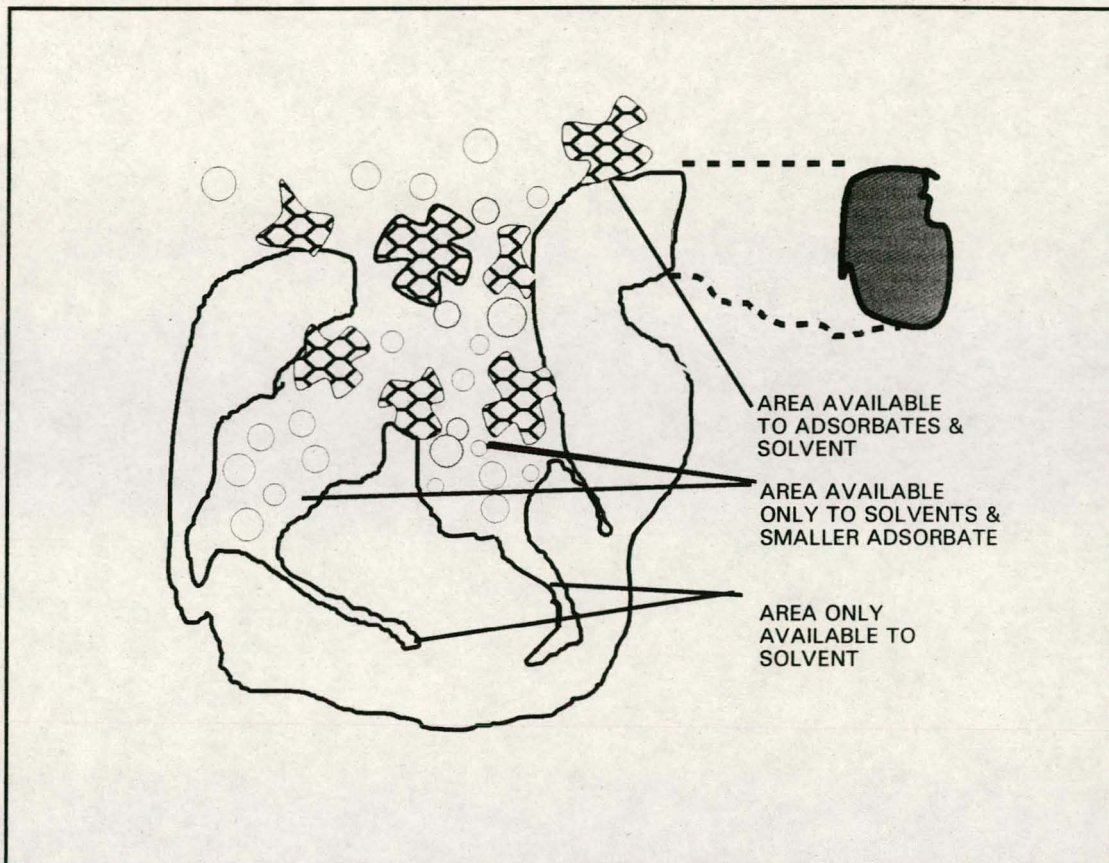
Figure 1.2: An illustration of the differential behaviour of the pores

Examination of powdered materials with an electron microscope can generally disclose the presence of surface imperfections and pores. However, those imperfections or irregularities smaller than the microscope's resolving power will remain hidden. Also hidden is the internal structure of the pores, their inner shape and dimensions, their volume and volume distribution as well as their contribution to the surface area. However, by enveloping each particle of a powder sample in an adsorbed coating, the method of gas adsorption can probe the surface irregularities and pore interiors even at atomic level.

1.3   APPLICATION OF ACTIVATED CARBON IN ENVIRONMENTAL GEOCHEMISTRY

World consumption of activated carbon was estimated at between 400000 tons and 450 000 tons in 1993. Consumption is concentrated in industrialised countries where legislation governing water and air treatment is most stringent. With a consumption of 113 400 tons of activated carbon in 1993, the USA accounts for around one-quarter of total demand. Western Europe and Japan are estimated to account for a further 20% of world consumption.

Following several years of expansion during the late 1980s, overall consumption of activated carbon showed little growth during 1991 to 1993. Although a significant part of the activated carbon market is driven by environmental legislation, many markets were adversely affected by the economic recession in the USA and western Europe. Lower levels of activity in the chemical and petrochemical sectors reduced demand for activated carbon in air and gas purification and in wastewater treatment.

In addition to the economic recession, longer-term trends also depressed demand for activated carbon in the early 1990s. One trend was the increasing substitution of powdered activated carbon by granular material which can be regenerated and re-used several times. The switch towards the use of granular activated carbon has been especially marked in the water-treatment and food-processing sectors. The effect on activated carbon demand is illustrated by American Water Works Service Co. Inc. who estimate that the change to the use of regenerated activated

carbon will reduce the company's consumption of new material from 1,135 tpy to 270 tpy.

In terms of end-use markets, water treatment continued to provide the main area of growth in the early 1990s. US consumption of activated carbon in water purification rose from 40 900t in 1989 (36% of total consumption) to 50 800t in 1993 (45%). In the treatment of industrial wastewater, Du Pont increased throughput capacity using powdered activated carbon treatment (PACT) at the company's Chambers plant by 20% to 60 000t between 1988 to 1993. In the municipal water treatment sector the Cincinnati, Ohio plant alone has an initial fill of 3 270t of granular activated carbon. Similarly, in Europe several large installations of up to 4 000t of granular activated carbon have been undertaken at municipal water treatment plants, with Thames Water of the UK alone purchasing an initial fill of 15 000t for the treatment of London's drinking water. Japanese consumption of granular activated carbon in water treatment, though traditionally low, is estimated to have increased by 25% in 1992.

In 1992 water treatment accounted for 52% of US consumption of activated carbon in liquid-phase uses, while air and gas purification accounted for 45% of consumption in gas-phase end-uses.

Sales by Calgon Carbon to the water treatment sector rose from US$79.6M in 1988 (35% of total sales) to US$116.3M in 1990 (41%). During 1993 water treatment accounted for 45% of total sales; sales to this sector are estimated at around US$120M , based on nine-month figures. Sales of this level would represent an increase of nearly 9% per year since 1988.

1.3.1   FUTURE CONSUMPTION OF ACTIVATED CARBON

Although European demand for activated carbon remains low in early 1994, demand is beginning to pick up in the USA and Japanese consumption, led by demand from the water industry, remains strong. Industry sources forecast that US consumption will increase by 4% per year through the 1990s, driven by stricter environmental legislation. Such a rate of growth gives an estimate of US consumption of around

130 000 to 135 000 tpy in 1997.

Growth in the activated carbon industry in the 1990s will continue to be led by the introduction of more stringent environmental legislation requiring the use of activated carbon to control water and air pollution. In the USA the main area of growth lies in the treatment of chemical process water and municipal water. Stricter limits on pollutants in industrial wastewater have been established under the National Pollutant Discharge Elimination System (NPDES). Most of the newly regulated contaminants are organic compounds in a category for which activated carbon is the best available technology for removal. In the potable-water treatment market, the reauthorisation of the Safe Drinking water Act in 1994 tightened the rules on the levels of trihalomethanes in drinking water. This stimulated growth in the activated carbon market as municipalities moved away from the use of chlorine disinfectants to the use of advanced ozone-granular activated carbon systems.

1.3.2   GAS-PHASE END-USES FOR ACTIVATED CARBON

In gas-phase applications, activated carbon is used to purify gas or air streams by the adsorption of contaminants. Activated carbon is the most effective means for removing contaminants present at parts-per-million levels. As grades of activated carbon consumed in gas-phase uses are generally higher in quality than those used in liquid-phase applications, gas-phase uses are estimated to account for less than 15% of activated carbon sales in terms of volume. Gas-phase uses comprise the purification of process gases, industrial gas separation, air purification, solvent recovery and catalysis.

Activated carbon is widely used to remove contaminants from industrial process gas streams and air streams, to protect catalysts and downstream equipment or to yield a pure intermediate or final gas. Activated carbon is especially effective in applications where impurity levels range up to a few hundred parts per million (ppm). At these low levels activated carbon is nearly always more efficient or more cost-

effective than alternative technologies such as scrubbing, thermal or catalyst incineration or other adsorption technologies.   Impregnated activated carbons are used to remove more volatile compounds, especially those of inorganic origin.

The main applications for activated carbon in gas adsorption are the removal of volatile organic compounds and acidic contaminants, such as sulphur dioxide, nitrous oxides and hydrochloric acid at   low concentrations; the removal of sulphurous contaminants such as hydrogen sulphide, COS and mercaptans; the separation of air streams in the non-cryogenic production of nitrogen and oxygen; the removal of gaseous emissions such as mercury vapour and dioxins and the removal of hydrocarbon fractions from automobile emissions.

The main application for activated carbon in hydrogen sulphide removal lies in sewage plants, where hydrogen sulphide and organic compounds are formed from the anaerobic decomposition of materials containing nitrogen and sulphur. In the Greater Pittsburgh area of Pennsylvania, USA, the Allegheny County Sanitary Authority serves over 1M people, who suffered odour problems from the daily processing of 200M gallons of raw sewage. To solve the odour problem, Calgon Carbon installed a two-stage system comprising of wet scrubbing and adsorption by activated carbon impregnated with sodium hydroxide.   The system removed the offensive odour by reducing hydrogen sulphide levels by over 90% to 0.1 ppm.

Other applications for the removal of hydrogen sulphide using activated carbon are in petroleum refineries, chemical plants and geothermal generating plants.   In control rooms such as computer rooms and telephone exchanges, activated carbon adsorbers continuously remove hydrogen sulphide contaminants to levels below 1 ppm, and protect sensitive instruments and electronic components.

Impregnated granular activated carbons are often used for the removal

of hydrogen sulphide.

1.3.3 ORGANIC COMPOUND REMOVAL

Activated carbon beds provide the final clean-up phase of most vapour streams containing volatile organic compounds, before they are vented to air.   As state environmental and regulatory agencies are imposing tighter volatile organic compound emission levels in air and vapour streams, activated carbon units are required to operate on stream 100% of the time and to maintain optimum efficiency.

Activated carbon beds used for volatile organic compound removal are dual-bed systems; one bed adsorbs while the other regenerates or desorbs. During the adsorption cycle, vapour containing volatile organic compounds enters the top of the bed and leaves from the bottom. The regeneration process generally uses steam.   At the end of the regeneration cycle the bed is dried and remains on standby. Adsorption and desorption cycles depend on the amount and type of activated carbon used, the incoming vapour volume and the concentration of volatile organic compound in the inlet stream.

Activated carbon beds remove a wide range of volatile organic compounds including aliphatics, aromatics, ketones, aldehydes and chlorinated solvents. They are unsuitable for high-boiling compounds and reactive compounds, such as polymers, plasticisers, phenols and some organic compounds, which can foul the carbon and render it ineffective.

1.3.4 MERCURY VAPOUR REMOVAL

Granular activated carbon impregnated with elemental sulphur is used to adsorb mercury vapour from air, hydrogen, liquefied natural gas and certain gas streams. The sulphur, distributed in a thin layer over the large internal surface area of highly porous activated carbon granules, reacts with the mercury vapour to form mercuric sulphide which is

adsorbed onto the activated carbon. In some of the world's largest natural gas plants activated carbon is used to remove mercury vapour to almost undetectable levels.

1.3.5 VINYL CHLORIDE MONOMER

US regulations limit the level of vinyl chloride monomer vapour in effluent gas streams to under 5 ppm. Activated carbon is one of the most effective materials for removing this vapour from plants that manufacture or process vinyl choride monomer gas.

1.3.6 AIR PURIFICATION

Most manufacturing plants, especially in the chemical, engineering, food-processing and printing industries, are increasingly compelled to limit their airborne emissions of harmful or malodorous compounds. Activated carbon treatment is among the most effective technologies for reducing these emissions. Activated carbon is also used to purify intake air to buildings where use or contents impose special demands on air purity.

1.3.7 DIOXIN REMOVAL

Activated carbon is used to reduce emissions of dioxins from municipal and industrial incineration units. Emission limits for dioxins are becoming more stringent. The EC has adopted the highest emission-control standards of any member country for dioxins and furans with those of Germany and the Netherlands, imposing a limit of 0.1 $mg.m^{-3}$ on all incinerators by the beginning of 1997.

1.3.8 AUTOMOTIVE EVAPORATION CONTROL

During the 1990s environmental legislation has aimed at reducing volatile organic compound (VOC) emissions from all stages of the petrol chain. Shell estimates that petroleum vapours that evaporate during the distribution of petroleum, during refuelling and before the catalytic

converter heats up, together account for 15% of VOC emissions.

In Japan, the USA and, since January 1993, in the EC, activated carbon canisters are installed on all new cars to recover evaporative emissions when the car is idling.

In the USA, the EPA ruled in early 1994 that larger canisters will be installed on automobiles, light trucks, mini-vans and other utility vehicles. When fully phased in, the new controls will capture 95% of refuelling emissions and will cut emissions of VOCs and toxic substances by 300 000 to 400 000 tpy.

1.3.9   AIR CONDITIONING

Activated carbon filters are incorporated in heating and air conditioning systems to remove exhaust gases, corrosive gases, noxious odours such as sulphur compounds, allergens and bacteria from incoming air. Filter packs of activated carbon can be placed in series with normal air-conditioning equipment. Industrial filters containing activated carbon are installed in buildings and places where air is recirculated, such as ships, hospitals, aeroplanes, submarines, airports, laboratories, museums and libraries.

1.3.10 PERSONNEL PROTECTION

By the adsorption of harmful or toxic gases, activated carbon protects personnel in both industrial respirators and military applications.

Industrial respirators used in mines and chemical plant contain filters filled with activated carbon to adsorb organic gases, inorganic gases (Cl_2, H_2S, HCN), acidic vapours (SO_2, HCl, HF), ammonia, amines and radioactive iodides. Typical respirator cartridges contain from 270 ml of activated carbon, following the Class 2 CEN norm.

All the gas masks worn by the US Armed Forces and other Allied troops

in the Gulf War in early 1991 contained activated carbon filters as a protection against emissions in possible chemical and biological warfare. In Finland and Sweden a programme has been proposed which would require every house to be equipped with a room containing an activated carbon system for protection against chemical and biological weapons.

1.3.11 CONSUMPTION OF ACTIVATED CARBON IN GAS PURIFICATION

All gas-phase uses, including gas purification, solvent recovery and catalysis, were estimated to account for 20% of US consumption of activated carbon in 1989. This represented 22 400t. In the early 1990s, high rates of growth were forecast for consumption of activated carbon in gas-phase uses, following the passing of the Clean Air Act Amendments in the USA, which listed 189 toxic air pollutants to be regulated by new emissions standards. For many end-of-process streams, activated carbon provides the most effective method of removing contaminants in the parts-per-million range.

The world market for air pollution control technology is estimated to increase by around 5% per year during the 1990s.

1.3.12 WATER TREATMENT

Water treatment is the largest market for activated carbon. US consumption in this sector was estimated at 50 800t in 1993, which represented 45% of total demand. Consumption of activated carbon in water treatment by sector in 1992 was as follows:

drinking water	:	46%
industrial and municipal wastewater	:	40%
groundwater	:	8%
household water	:	6%

Water treatment is an important area of growth for activated carbon. US consumption is forecast to increase by 3% to 5% per year in terms of

volume and by 6% per year in terms of value through the 1990's because of a shift towards the use of higher-value granular activated carbon and higher-activity powdered activated carbon.

1.3.13 GROUNDWATER

Groundwater becomes polluted from landfill leachate, underground piping of chemical products and residues, the injection of residues from wells, the infiltration of sewage and the seepage of fertilizers and pesticides.

Granular activated carbon is also widely used in permanent installations to treat groundwater. Granular activated carbon is one of two materials that effectively removes volatile organic compounds, mainly in the form of solvents, which leak into the water supply through leachate from landfills. Granular activated carbon treatment is concentrated where groundwater is an important source of drinking water.

1.3.14 CONSUMPTION OF ACTIVATED CARBON IN WATER TREATMENT

US consumption of activated carbon in water treatment was estimated at 50 800t in 1993, divided between granular (56%) and powdered (44%) grades. This represented around 45% of total US demand. Consumption is divided between drinking water 46%, industrial and municipal wastewater 40%, groundwater 8% and household water 6%.

The late 1980s saw a significant up-turn in the activated carbon industry, as growing public and government concern over environmental pollution and greater enforcement of legislation led to high growth in demand for activated carbon in water treatment.

In the USA, the main areas of growth for activated carbon lie in the treatment of chemical process water and municipal water. Stricter limits on pollutants in industrial wastewater have been established under the National Pollutant Discharge Elimination System (NPDES). Most of the newly regulated contaminants are organic compounds in a category for

which activated carbon is the best available means for removal.   The Clean Water Act reauthorisation in Congress requires industries that discharge highly persistent or bioaccumulative toxic chemicals to water to reduce their emissions by half.

1.3.15 GOLD RECOVERY

The widespread adoption of carbon adsorption processes for gold recovery was one of the most significant technological advances in gold extraction during the 1980s. Carbon adsorption has become the preferred method of gold recovery for free-milling ores over the past five years. Use of activated carbon processes has made the conventional cyanidation method more effective for gold recovery from low-grade ores and has made the treatment of marginal ore deposits more economical. Three processes using granular activated carbon have been adopted to recover gold from low-grade ores containing down to 0.03 oz gold per tonne of ore:carbon-in pulp (CIP), carbon-in-leach (CIL) and carbon-in-column (CIC). Increasing concern over the environment has also led to the use of activated carbon to reclaim gold from leach-pad rinse solutions.

1.3.16 GOLD RECOVERY FROM ACTIVATED CARBON

Gold is recovered from activated carbon by elution followed by electrowinning. Activated carbon consumption in gold recovery is estimated at 1 kg per ton of ore treated. No data are available for total consumption in the gold industry. Gold recovery is estimated to account for 5% of US consumption in liquid-phase end-uses, but is the largest market for activated carbon in Australia and South Africa.

1.3.17 MINERAL PROCESSING APPLICATIONS

Activated carbon is used to adsorb excess flotation process reagents, such as collectors, which can degrade process-circuit control.

During the processing of uranium, activated carbon removes low

concentrations of natural organic contaminants, ranging from hydrocarbons to humic acids. It also removes trace quantities of molybdenum and vanadium that interfere with processing.

A commercial metal-removal system consisting of a woven activated carbon cathode can be used for the recovery of lead, copper and silver from photographic processing solutions.

1.4   ADSORPTION THEORY

The discovery of the adsorption process, as now understood, is generally attributed to Scheele, who in 1773 was the first to describe experiments on gases exposed to carbon [1].

Adsorption is a physical or chemical process in which a substance accumulates at an interface of two phases. The phase interface may be either solid-vapour or solid-liquid, and its composition is different from that of either bulk phases. The accumulating substance, termed the adsorbate, has a tendency to collect on the surface of the solid, termed the adsorbent [3, 4, 6]. If adsorption occurs at constant volume, the pressure drops, and at constant pressure the volume decreases [7].

Once a substance collects at the surface of a solid, two things can happen. The substance either remains adsorbed on the surface of the solid (this surface includes the external, geometrical surface, and the internal surface formed by the walls of the pores), or it can penetrate into the structure of the solid. Adsorption can be distinguished from absorption in that adsorption usually occurs without a chemical reaction between the adsorbent and the adsorbate, whereas absorption involves a permanent chemical reaction of phase change. It is often difficult to determine the final resting place of the molecules, and therefore a general term "sorption" has been coined to apply when a gas, vapour or liquid is taken up by a solid [3, 4, 7].

Adsorbed molecules are held at the surface by one of two different forces. There

is either a weak interaction between the adsorbent and adsorbate, similar to condensation, or a strong interaction, similar to chemical reactions. The weak interaction is called physical adsorption and the strong interaction is called chemical adsorption [3, 4, 7].

Physical, or Van der Waals adsorption, is caused by forces similar to those that cause condensation of vapours to a liquid, and is determined by three factors, namely: i) the heat of adsorption, ii) the surface of the adsorbent, and iii) the pore structure of the adsorbent. The chemical nature of the adsorbed molecules remains unchanged and the forces are identical to the intermolecular forces of cohesion which operate in the solid, liquid and gaseous states. These forces are electrostatic, and it is now known that there are three effects that jointly account for the attractive forces: i) the orientation effect of Keesom, ii) the induction effect of Debye and iii) the dispersion effect of London. The orientation effect is based on the fact that many uncharged molecules have dipole moments which, when properly orientated, will lead to the development of attractive forces. It is of significance only in the mutual interaction of highly polar molecules possessing permanent dipoles and is inversely proportional to the temperature. The induction effect is caused by a permanent dipole inducing polarization of molecules situated in its proximity; it is independent of the temperature. These two effects explain how Van der Waals attractive forces are developed in highly polar compounds, but they do not help explain attractive forces in molecules which pose no permanent dipoles. The London dispersion effect explains those attractive forces. Molecules without a permanent dipole have fluctuating dipoles which give rise to a fluctuating electric field. When two molecules with fluctuating dipoles approach one another closely their total energy decreases, which is the reason for their mutual attraction. The attractive force decreases with the seventh power of the distance and is independent of the temperature. In most cases of physical adsorption, the dispersion effect is the governing Van der Waals attractive force [1, 3, 4, 7].

Evaluation of heat during physical adsorption during the adsorbate/adsorbent interaction is much lower than for chemisorption, being generally of the same order of magnitude as for heat of condensation. In addition, it does not proceed

at temperatures much higher than the boiling point of the adsorbate, it does not require any activation energy, it is non-specific, and it is capable of multimolecular adsorption [1, 3, 4, 7]. These characteristics are of great importance since they allow the adsorbate to be desorbed from the adsorbent unaltered.

Chemical adsorption or chemisorption, also termed activated adsorption because it requires an activation energy much the same as that in chemical reactions, results from the exchange or sharing of electrons between the adsorbate and the surface of the adsorbent. The bond formed between the adsorbate and absorbent is essentially a chemical bond and is therefore much stronger than in physical adsorption [4]. The heat of adsorption is several orders of magnitude higher than that in physical adsorption and is comparable with the energies of chemical bonds. Chemical adsorption is generally not instantaneous. Also, it is very specific, depending on the chemical nature of both the adsorbent and adsorbate. It is capable of only monomolecular adsorption, and it tends to be irreversible. Because of these characteristics, this type of adsorption would be of no use in industrial hygiene sampling, as collected contaminants could not be qualitatively or quantitatively analysed.

Any process that tends to decrease the free surface energy (the product of the surface tension and the surface area) occurs spontaneously. A molecule adsorbed by a solid saturates some of the unbalanced forces on the surface and decreases the surface tension. Therefore, all adsorption phenomena (physical or chemical) are spontaneous and result in a decrease of the free energy of the system [7]. Adsorption is an exothermic process and the net decrease in heat content of the system is defined as the heat of adsorption [3].

Numerous experimental observations have been made concerning the phenomenon of adsorption and have been accepted as the norm. In 1814, de Soussure found that for porous adsorbents the most easily condensible gases are adsorbed in the largest quantity.[1] He determined that the volume adsorbed increased as the boiling point of the gas increased. Schmidt found a relationship between the heat of vaporisation of gases and their adsorption,[3] all of which correlate Van der Waals [9] adsorption with the condensation properties of the gases. However,

there are exceptions to this general rule, and the adsorbent may retain a certain affinity for one compound over another. Pearce found a relationship between molecular structure and the amount adsorbed, but this is influenced by the pressure during adsorption. [1] At pressures below 1 mm Hg, adsorption increases with molecular size in a homologous series, while pressures above 1 mm Hg preferentially promote adsorption of the smaller molecules [1]. In accordance with the Le Chatelier's principle, the amount of gas adsorbed at equilibrium must always decrease with increasing temperature since adsorption is an exothermic process. Lastly, adsorption also increases with increasing pressure, again relating to the condensibility factor. The amount of gas adsorbed at equilibrium is therefore a function of the temperature, pressure, physical structure and chemical constitution of the adsorbate and adsorbent [1, 3, 4, 7].

Extensive research has been conducted on determining the volume of gas adsorbed per unit weight of adsorbent under various environmental conditions. These data are presented in the form of adsorption isotherms (amount adsorbed at constant temperature and varying pressure), and isosteres (pressure required to maintain constant adsorption at varying temperatures), with the isotherm being the form used almost exclusively because it relates directly to research data. Therefore, at some equilibrium pressure and temperature the weight of gas adsorbed on a unit weight of the adsorbent is given by

$$W = f(P, T, E) \tag{1.1}$$

where

P = the pressure

T = the temperature

E = the interaction potential energy.

Usually the quantity adsorbed is measured at constant temperature and Eg 1.1 reduces to

$$W = f(P, E) \tag{1.2}$$

A plot of amount adsorbed (W) as a function of pressure (P), at constant

temperature T, is referred to as the adsorption isotherm of a particular vapour - solid interface.

In the literature there are recorded tens of thousand of isotherms on a wide variety of solids. Nevertheless the majority of those isotherms which result from physical and chemical adsorption may be conveniently grouped into six types as shown in Figure 1.3. Types I - V are essentially those of Brunauer, Deming, L. Deming, and Teller [8] (BDDT classification), whereas type VI is of a more recent origin [9].
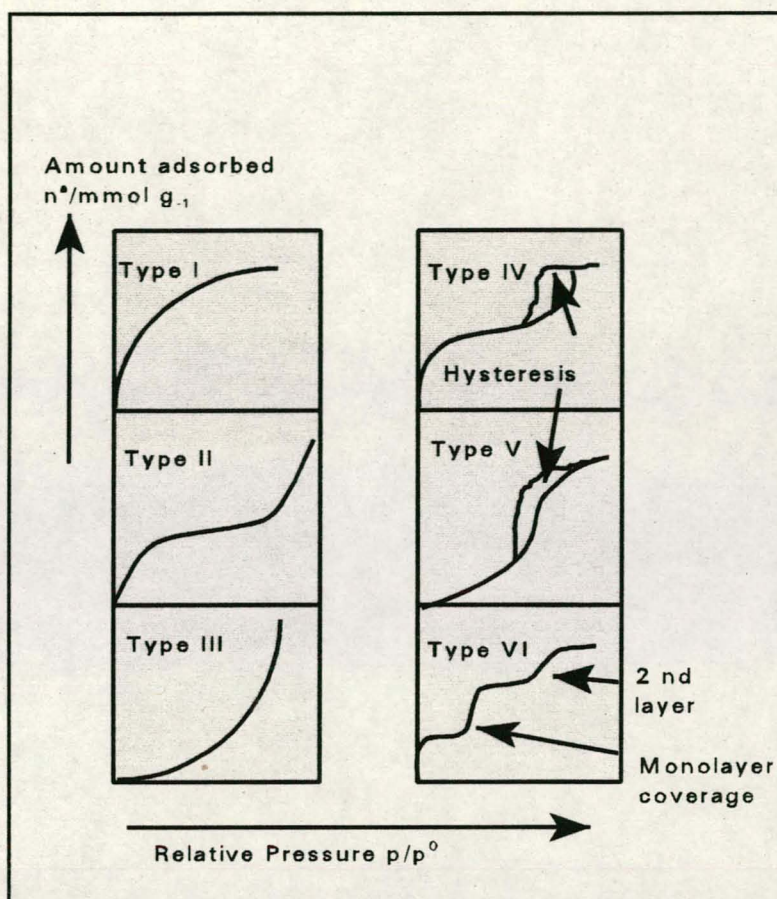
Figure 1.3: Types of adsorption isotherms

TYPE I

These isotherms are found when adsorption is limited to, at most, only a few molecular layers of adsorbate. This condition arises in chemisorption where the asymptotic approach to a limiting quantity indicates that all of the surface sites are occupied. In the case of physical adsorption, Type I isotherms are found with microporous powders whose pore sizes do not exceed a few adsorbate molecular diameters. A gas molecule, when inside pores of these small dimensions, encounters the overlapping interaction potential from the pore walls which

enhances the quantity adsorbed at low relative pressures. At higher pressures the pores are filled by adsorbed or condensed adsorbate leading to the plateau, indicating little or no additional adsorption after the micropores have been filled. Physical adsorption that produces the Type I isotherm indicates that the pores are microporous and that the explored surface resides almost exclusively within the micropores, which once filled with adsorbate, leave little or no external surface for additional adsorption. Furthermore, the primary physisorption process may be regarded as pore filling rather than monolayer coverage [10]. In the extreme cases (e.g. with a molecular size zeolite), the isotherm is nearly horizontal over a wide range of P/P°; this indicates that the external area is very small and that the limiting uptake is controlled by the micropore volume.

Some Type I isotherms going upwards as P/P° approaches 1. The situation is further complicated if this is associated with hysteresis extending to very low P/P°. It is not possible to offer forward a single explanation for these low-pressure hysteresis effects, but irreversible penetration of the adsorbate into the solid structure occurs with some systems [11] (e.g. interrelation of polar molecules into lamellar clay structures [12]). In certain other cases, low-pressure hysteresis is associated with activated entry of adsorbate molecules through fine constrictions [10].

TYPE II

These isotherms are associated with multi-layer adsorption and some reversible capillary condensation phenomena. In the low-pressure region, the amount adsorbed rises less steeply than with Type I. In these types of isotherms, there is an inflection point in the curve that usually occurs near the completion of the first adsorbed monolayer. With increasing relative pressure, second and higher layers are formed until at saturation the number of adsorbed layers becomes infinite. Generally, these types of isotherms are given by non-porous powders or by powders with pore diameters larger than micropores.

TYPE III

The Type III isotherm is convex to the P/P° axis over its entire range and therefore does not exhibit an inflection point. Isotherms of this type are comparatively rare;

the best known examples are for the adsorption of water on carbon surfaces. They are characterized by heats of adsorption that are less than the adsorbate heat of liquefaction. Thus, as adsorption proceeds, additional adsorption is facilitated because the adsorbate interaction with an adsorbed layer is greater than the interaction with the adsorbent surface.

TYPE IV

These isotherms describe mono-layer and multi layer-adsorption plus capillary condensation. These are characterized by the convexity towards the pressure axis at intermediate pressures, giving a point of inflection which shows the completion of a monolayer and the onset of multi-layer adsorption. A characteristic feature of the Type IV isotherm is its hysteresis loop (although this is not indicated in the original BDDT classification). In the simplest case, the initial part of the isotherm follows exactly the same path as the corresponding part of Type II isotherm given by the adsorption on the same area of the adsorbent in a non-porous form. The hysteresis loop is associated with the secondary pore-filling process of capillary condensation; it is this part of the isotherm which is used for the mesopore size distribution calculations. The limiting uptake at high P/P^o, converted to a liquid volume, provides a measure of the total mesopore volume.

TYPE V

These isotherms are associated with pores in the same range as those of the Type IV isotherms. These isotherms result from small adsorbate - adsorbent interaction potential similar to the Type III isotherms. Neither the surface area nor the pore-size distribution can be calculated with any confidence from this type of isotherms.

TYPE VI

The Type VI isotherms, in which the sharpness of the steps depends on the system and the temperature, represent step-wise multi-layer adsorption on a uniform non-porous surface. Each of the first few layers is adsorbed over a restricted range of P/P^o; the step height corresponds to the monolayer capacity and remains nearly constant for two or three layers. Co-operative adsorption contributes to this layer-by-layer process and at very low P/P^o the isotherm is convex to the P/P^o axis. Amongst the best example of Type VI isotherms are those obtained with argon or krypton on graphitised carbon blacks at liquid

nitrogen temperature.

After the development of the isotherms, researchers began to formulate theories to explain the observed results. Highlights of the main theories are presented below.

The Freudlich equation, an empirical equation, is the oldest isotherm equation, but is still widely used in industrial practice, particularly for adsorption from liquids because it fits some data very well, although it has limited application in industrial hygiene sampling. It is also referred to as the exponential equation and it should be realised that it is strictly empirical and not based on theory [3, 4, 7].

In 1915 Langmuir proposed a theory for adsorption based on a belief that it was a chemical process and that the adsorbed layer was unimolecular [3, 7, 13]. No far-reaching forces are envisaged, but when a wandering molecule of vapour collides with a suitable unoccupied surface space, the molecule will adhere [1]. Like the Freudlich equation, it has found wide application in the adsorption from liquids.

It is well known that a liquid that wets the walls of a capillary will rise in it with a concave meniscus and the vapour pressure will be lower than in the bulk liquid. In 1911, Zigsmondy studied the uptake of water vapour on silica gel and attributed it to the numerous small capillaries in the gel. He determined that in small capillaries condensation could occur at pressures below the normal vapour pressure where condensation occurs. The theory of capillary condensation is based on a stepwise filling of the capillaries. The narrowest capillaries fill at the lowest pressure, and as the pressure increases, larger capillaries fill until at the saturation pressure all the pores of the adsorbent are filled with liquid. Capillary condensation is an important factor within the gas- phase pressure where the pressure approaches the saturation pressure for a porous adsorbent [1, 3, 4, 7].

The Brunauer, Emmett and Teller (BET) theory was developed in 1938 by applying Langmuir's ideas to multimolecular adsorption. This theory is based on the assumption that the same forces which produce condensation are also responsible

for the binding energy of multimolecular adsorption. Its general equation can describe the shape of the six isotherm types throughout the entire range of adsorption, which includes unimolecular adsorption (adsorbate formation of a monolayer), multimolecular adsorption (adsorbate formation of multiple layers) and capillary condensation. Furthermore, it represents the first attempt to arrive at a unified theory of physical adsorption and provides an accurate method for adsorbent surface area determinations [1, 4, 7].

The polarisation theory was first developed by De Boer and Zwikker in 1929 and is based on adsorption occurring by the induction of dipoles. It has very narrow applications as it can explain only adsorption of non-polar molecules on ionic adsorbents or polar molecules on non-ionic adsorbent, at conditions not conclusive for capillary condensation [3, 7].

The final theory to be discussed is the potential theory developed by Polanyi in 1914. It assumes that adsorption occurs due to long-range attractive forces from the surface of the adsorbent and that many adsorbed layers can be formed. The layers are under compression, partly from the surface force and partly from the layers adsorbed on top of it. The compression is greatest on the first adsorbed layer where the adsorbate is attributed with liquid-like properties and continually decreases until the last layer, which has properties similar to that of the surrounding gas. It is based on three assumptions: a) the adsorption potential is independent of the temperature, b) the potential is independent of the presence of the adsorbate in the space, and c) under the same conditions, the interaction between adsorbed molecules is the same as that between non-adsorbed molecules. The adsorption potential is a product to which the surface contributes the same share regardless of what the gas is, and the gas contributes the same share regardless of what the surface is [7]. Its significance is that by knowing the affinity coefficient for a given gas on a Type I adsorbent, it is possible from a single isotherm to calculate isotherms for this substance on the same adsorbent. This theory as modified by Dubinin (1975) has been shown to be extremely useful for describing microporous adsorbent [4, 7, 14].

1.4.1 ADSORPTION ON ACTIVATED CARBON

Langmuir's equation holds for non-porous surfaces where the gas molecules have free access and for adsorbents in which the attraction centres are equal in strength and uniformly distributed over the surface. However, neither of these conditions is applicable to activated carbon [3]. The BET theory proves to be very useful for non-porous and macroporous adsorbents, but breaks down and poses serious problems when applied to microporous adsorbents such as activated carbon. Instead, the theory of volume-filling of micropores, which is based on the potential theory (Polanyi), has proved to be best for Type I structure adsorbents such as coconut-based activated charcoal [3, 7, 14].

Adsorption of gases above the critical temperature, 2/3 of its boiling point, is unimolecular and the pore structure of the adsorbent is not particularly important. However, adsorption at below the critical temperature is multimolecular and the pore structure of the adsorbent plays a vital role. Since most filtration applications occur at below the critical temperature, the pore structure of the carbon is important. In addition, it should be recognized that adsorption on activated carbon involves mutual affinities between the surface of the carbon and the substance to be adsorbed [1, 7].

The surface of activated carbon is considered to be heterogeneous, meaning that is consists of randomly distributed sites of various adsorption potentials and is greatly exaggerated by the process of activation. Activated carbon prepared at temperatures below 500°C are more hydrophilic because of the acidic surface oxides that are formed. The surface oxides dramatically increase the adsorption of water vapour and other polar molecules as compared with the basic carbon produced at higher temperatures [1].

As previously stated, the carbon-activation process increases the surface area available for adsorption by creating numerous pores at the external and internal surfaces of the carbon. The pores have been classified by Dubinin into three categories: macropores, mesopores (transitional pores)

Dubinin into three categories: macropores, mesopores (transitional pores) and micropores [3, 14].

A macropore is defined as having an effective radius larger than 500 Angstroms. For typical activated carbons, the effective radius is between 5 000 and 20 000 Angstroms and their specific surface area does not exceed 2% of the total surface area. Adsorption on the surface is negligible and capillary condensation is unlikely. Therefore, macropores function solely as transport passages [3, 14].

A mesopore is defined as having an effective radius of between 20 and 500 Angstroms and its specific surface area does not exceed 5% of the total surface area. The pore is orders of magnitude larger than the molecule being adsorbed and is filled by capillary condensation. Additionally, it provides further access to the micropores [3, 14].

A micropore is defined as having an effective radius of less than 20 Angstroms and its specific surface area is greater than 95 % of the total surface area. The pore is of the same order of magnitude as the molecule being adsorbed and is therefore not filled by capillary condensation but by selective volume filling the adsorption space. The smallest micropores have the greatest adsorption potential and therefore are filled first at the lowest pressure. As indicated, essentially all of the adsorption occurs in the micropores, but very few of the micropores open to the external surface, so that the macropores and mesopores are essential for providing access to the micropores [3, 15].

CHAPTER II

THEORETICAL BACKGROUND
GAS-PHASE ADSORPTION

2.   GAS-PHASE ADSORPTION

In discussing the fundamentals of adsorption it is useful to distinguish between physical adsorption, involving only relatively weak intermolecular forces, and chemisorption, which involves essentially the formation of a chemical bond between the sorbate molecule and the surface of the adsorbent. Although this distinction is conceptually useful, there are many intermediate cases and it is not always possible to categorise a particular process.

In any heterogeneous system consisting of atoms, molecules or ions, the interaction between the phases begins with chemical or physical interaction at the phase interface.   Almost all air pollution problems in which adsorption is considered as a unit operation involve gaseous contaminants.   The number of molecules present at the surface depends on the number that reach the surface and on the residence time of these molecules on the surface. According to *de Boer* [15], if n molecules strike a unit area of a surface per unit time and remain there for an average time t, then σ number of molecules are present per unit area of surface :

$$\sigma = nt \qquad\qquad (2.1)$$

Values of n for H_2, N_2 and O_2 are as follow :

H_2 : $11,0 \times 10^{23}$ molecules.$cm^{-2}s^{-1}$
N_2 : $2,94 \times 10^{23}$ molecules.$cm^{-2}s^{-1}$
O_2 : $2,75 \times 10^{23}$ molecules.$cm^{-2}s^{-1}$

It must be emphasised that there are no special adsorption forces. Forces causing adsorption are the same as those that cause cohesion in solids and liquids, and which are responsible for the deviation of real gases from the laws of ideal gases. Although the theoretical difference between physical and chemical adsorption is clear in practice, the distinction is not as simple as it may seem. Theories are to be viewed, not as blue prints to portray the minor working of a phenomenon, but rather as mental inventions that enable people to make more effective use of the

material world. By simply making a phenomenon more familiar does not enable us to see the inner working mechanisms because we do not know the inner mechanisms.

Early investigators thought that surface tension accounted for the purifying power of activated carbon. It was believed that impurities with low surface tension formed a ready-made film at the surface of a liquid, and that the function of the carbon was to furnish a large surface area on which such a film could gather. Such a mechanism is an important factor but it does not explain all situations, because many substances that do not lower the surface tension of water are removed from an aqueous solution by carbon..

Studies by *Zigsmondy* in 1911 [16] led him to believe that the ability of silica gel to take up water vapour is associated with the presence of small capillaries in the gel. As is well known, a liquid that wets the walls of a capillary will rise in that capillary. *Zigsmondy* deduced that a vapour would condense in small capillaries to a liquid at pressures below those required for normal condensation. The ease of such condensation depends on the diameter of the capillary and as it becomes smaller, condensation occurs at a lower pressure. According to this theory of capillary condensation, then, when capillaries of unequal diameters are present in a solid structure, the narrowest capillaries fill at the lowest pressures; with an increase in vapour pressure there is a stepwise filling of the larger capillaries.

As with surface tension, capillary condensation is associated with forces that bind like molecules - forces commonly known as Van der Waals forces. These attractive forces can cause molecules of different species to unite, for example, chloroform adsorbed on a carbon surface. *Langmuir's* concept [17] has the flexibility to cover homogeneous and heterogeneous surfaces, chemical and physical forces, mono- and multi-molecular layers.

The surface of carbon can be viewed as a patchwork of different kinds of adsorptive spaces, with each kind of space having characteristic affinities. No far-reaching forces are envisaged, but when a wandering molecule of vapour collides with a suitable unoccupied surface space, the molecule will adhere. It does not

adhere indefinitely however, and sooner or later, depending on the thermal energy and the strength of the attractive forces, it evaporates. At first, when the surface is bare, the number of molecules that condense exceeds the number of those that evaporate. As the surface becomes covered, other gas molecules have greater difficulty in finding unoccupied spaces, but there is also an increase in the number of molecules escaping from the surface. When the rate of evaporation equals the rate of condensation, equilibrium is reached. The amount adsorbed at equilibrium is a function of the following factors, some of which are interrelated :

a. The time lag - that is, the average period between the moment the molecules condense and their subsequent evaporation.
b. The total area of the solid surface.
c. The proportion of the total surface which has specific attractive power for the molecules in the gas phase, as well as the accessibility of such surface.
d. The number of adsorbable molecules in the gas state, that is, the pressure.
e. The number of layers of adsorbed molecules.

Considered individually, each factor provides a clear approach to an understanding of adsorption. No single mathematical equation other than a purely thermodynamic one can cover all cases, and much attention has been given to different limiting equations for certain types of adsorption.

2.1 The Langmuir Theory

The *Langmuir* theory regards most of the adsorption as occurring in a layer one molecule deep, although it is recognised that the molecules adsorbed in this layer may have their fields of force altered and thus be able to attract a second layer of molecules, which in turn could attract a third layer. This induced attraction would be weaker and, therefore, molecules in the second layer would have a shorter residence time. Consequently, fewer molecules will be present in the second layer than in the first.

The basic assumptions on which the theory is based are :
a. Molecules are adsorbed at a fixed number of well-defined localized sites.

b. Each site can hold one adsorbate molecule.

c. All sites are energetically equivalent.

d. There is no interaction between molecules adsorbed on neighbouring sites.

The *Langmuir* equation can be written as:

$$\frac{x}{m} = \frac{k_v \, K_v \, P}{(1 + K_v \, P)} \qquad (2.2)$$

where $\quad \dfrac{x}{m} \quad$ = the amount of adsorbed vapour per unit weight of adsorbent

$\quad k_v$ and $K_v \quad$ = constants for the adsorbed vapour

$\quad P \quad$ = partial pressure of the adsorbed substance.

Another form of the *Langmuir* equation is as follow [10];

$$\frac{P}{V} = \frac{1}{(V_m \cdot B)} + \frac{P}{V_m} \qquad (2.3)$$

where $\quad V_m \quad$ = monolayer volume

$\quad B \quad$ = $^{ka}/_{kd}$ = adsorption equilibrium constant

where $\quad k_a \quad$ = adsorption constant

$\quad k_d \quad$ = desorption constant

Commonly suggested procedures for testing the fit of the *Langmuir* model to experimental data involve plotting either $\dfrac{P}{V}$ against P or against $\dfrac{1}{p}$.

B and V_m are then easily obtained from the slopes and intercepts of such plots.

The validity of the *Langmuir* model for physisorption on microporous adsorbent is subject to critical comment [18]. Systems which conform accurately to the *Langmuir* model are exceptional. For most systems the basic assumptions of the *Langmuir* model are not fulfilled, and the

equilibrium isotherms deviate to a greater or lesser extent from the *Langmuir* form.

The *Langmuir* model is of the correct qualitative nature to represent a Type I isotherm. A constant heat of adsorption is one of the requirements of the *Langmuir* model, so that the variation of heat of adsorption with coverage implies that the basic postulates of the *Langmuir* theory are not in fact obeyed. The constancy of the *Langmuir* "constants" evidently results from an almost exact compensation between the variation of the thermal entropy and heat of sorption with loading. The ideal *Langmuir* model gives an appropriate representation of the system behaviour at low concentrations, but breaks down in the saturation region where the effects of molecular interaction become pronounced. However, even at low sorbate concentrations, not all systems conform to the *Langmuir* model. Deviations can occur due to either heterogeneity of sites or interaction between adsorbed molecules.

2.2   The Polanyi Theory

Polanyi [20] quantitatively developed the nature of adsorptive forces further. It is based on a concept that cohesion forces can reach out and attract molecules from distances somewhat greater than molecular diameters. The adsorption affinity, that is, the intensity of the attraction, diminishes rapidly with distance to become zero within small finite spaces. The theory envisions that the captured molecules form a miniature atmosphere in which the outward density diminishes in a fashion analogous to that of the atmosphere on a planet. The theory, originally based on a concept of multi-layers, does not exclude monolayers. When an adsorption isotherm for a system is known at one temperature, the theory provides a means of predicting isotherms for other temperatures. A number of studies have been conducted of various facets of the theory. *Dubinin* [21] has drawn attention to the action of the adsorption potential in pores of molecular diameters. Molecules that enter such pores are held by attractive forces radiating inward from all sides. This reinforced attraction results in volume-

filling. In larger pores, adsorbed molecules lose contact with some sides of the pores and are then held less firmly as adsorbed layers. Because of the limited success which has been achieved with detailed isotherm models, a number of alternative approaches to correlate the adsorption equilibrium data have been followed. The correlation in terms of the *Dubinin-Polanyi* "characteristic curve" is perhaps the most familiar (see example in Figure 2.1). No specific model for the adsorbed phase is required, and data over a wide range of conditions can often be correlated successfully in this way. For adsorption on non-polar adsorbents, such as activated carbon, the basic assumptions of the theory are reasonably well fulfilled since the adsorption
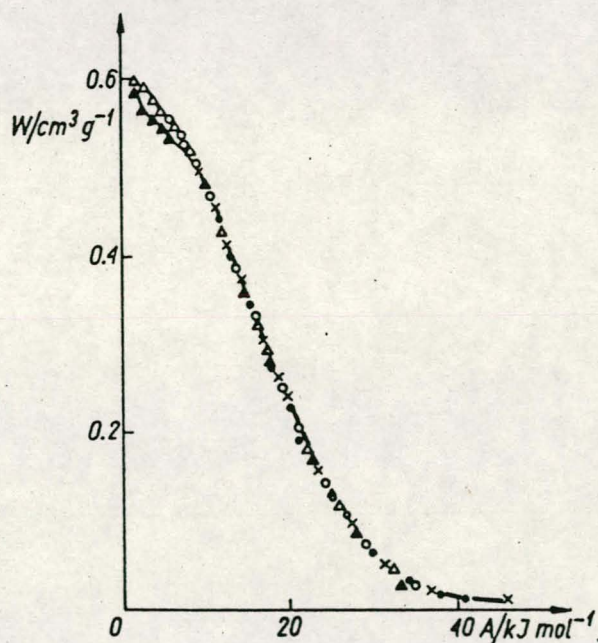
Figure 2.1: The Dubinin-Polanyi "characteristic curve" [10]

potential for carbon is due entirely to Van der Waals forces which are independent of temperature. *Dubinin* [21] and co-workers [22] have shown that the adsorption isotherms of various vapours can be represented by the following *Polanyi-Dubinin* equation :

$$\log W_a = \log W_o - k_a \left(\frac{\varepsilon}{\beta} \right)^2 \qquad (2.4)$$

where

$$\varepsilon = RT \ln \frac{P^o}{P} \qquad (2.5)$$

and

W_a	=	volume of condensed adsorbate per gram of carbon, $cm^3.g^{-1}$.
W_o	=	active pore volume of the carbon, $cm^3.g^{-1}$
β	=	an affinity coefficient that permits the comparison of the adsorption of the test adsorbate to a reference adsorbate.
R	=	gas constant, 1.987 cal/mole, K.
T	=	absolute temperature, K.
P^o	=	saturated vapour pressure of adsorbate at test temperature
P	=	the equilibrium vapour pressure of the adsorbate.
k_a	=	constant related to the structure of the adsorbent, $(cal.mole^{-1})^{-2}$

Equations (2.4) and (2.5) can be used to determine W_o and k from the experimental adsorption isotherm of a reference vapour, for which $\beta_{ref} = 1$. Thus if the affinity coefficient of any given vapour can be theoretically calculated, the equilibrium adsorption isotherm of the given vapour may be predicted. For the non-polar and weak-polar adsorbates, the work of *Dubinin* and co-workers has shown that dispersion forces play a dominant role in determining adsorptive interactions. In these cases the adsorptive interaction is strongly dependent on the polarisability of the molecules. Since the polarisability of a molecule is approximately proportional to the

volume of a molecule or molar volume, V, the affinity coefficient of the given vapour can be expressed as:

$$\beta = \frac{V}{V_{ref}} \qquad (2.6)$$

$$V = \frac{M}{\rho} \qquad (2.7)$$

where $\quad M \quad = \quad$ the molecule weight of the adsorbate

$\quad\quad\quad\ \rho \quad = \quad$ the density of the adsorbate, g.cm^{-3}

More precisely, the affinity coefficient can be calculated from the ratio of the molecular parachors, Ω :

$$\Omega = \frac{M\delta^{1/4}}{P} \qquad (2.8)$$

$$\beta_{vap} = \frac{\Omega_{vap}}{\Omega_{ref}}$$

where $\quad \delta \quad = \quad$ the surface tension of the adsorbate in dynes.cm^{-1}.

For polar adsorbates, *Reucroft et al.*[23] pointed out that the adsorptive interaction may be influenced more by electronic forces than by dispersion forces. They suggested that the ratio of the electronic polarisations, P_e, can be used to calculate the affinity coefficient.

The electronic polarisation is given by :

$$P_e = \frac{(n^2 - 1)m}{(n^2 + 2)p} \qquad (2.9)$$

and

$$\beta_{vap} = \frac{P_e}{(P_e)_{ref}}$$ (2.10)

where   n = refractive index at the sodium D wavelength.

The physical variables in equations (2.7), (2.8) and (2.9) can be obtained from the Handbook of Chemistry and Physics [24]. For optimum prediction of equilibrium values by using the potential theory, the reference vapour should have a similar polarity to the vapour whose adsorption is being predicted.

2.3   Dubinin and Radushkevich theory

Dubinin and *Radushkevich* [25] further developed the micropore-filling theory, based on the *Polanyi* concept of characteristic curves to describe the adsorption on micropores. By combining equations (2.4) and (2.5) the well known *Dubinin - Radushkevich (D-R)* equation can be obtained :

$$\frac{W}{W_o} = \exp\left[-B\,(T/\beta)^2\,\log^2(P^o/P)\right]$$ (2.11)

where   B =   structural constant = kR^2.

Equation (2.11) may be written as :

$$\log W = \log W_o - D\,\log^2\left(\frac{P^o}{P}\right)$$ (2.12)

where   D = $B(T/\beta)^2$

                    β =   affinity coefficient

2.4   Dubinin and Astakhov theory

A more general expression was later developed by *Dubinin* and *Astakhov* (D-A)[26]:

$$W = W_o \exp\left[-(A / \beta E_o)^n\right]$$ (2.13)

where W represents the volume of the adsorbate condensed in the micropores at temperature T and relative pressure P/P^o. This equation is applicable to a wider range of carbons, and a further modification was introduced by *Dubinin* and *Stoeckli* [27] based on the summation of the contributions from individual micropore groups. The so-called affinity coefficient β is a shifting factor that depends only on the adsorbent or of adsorption and, by convention, $\beta(C_6H_6) = 1$. The characteristic energy E_o and exponent n depend only on the micropore system. It has been shown experimentally that in the case of active carbons, n varies in practice from 3 to 1.5, as the micropore system becomes more heterogeneous [27]. The choice of n = 2, corresponding to the original equation of *Dubinin* and *Radushkevich*, is justified when representing the adsorption of vapours by active carbons is represented. From a theoretical point of view, it is shown [27] that exponent n is related to the width of the distribution curve of the adsorption energy, derived from the D-A equation (2.13). The curve becomes sharper as n increases from 1,5 to 3, which implies an increase in the homogeneity of the micropore system, in agreement with simple model calculations based on slit-shaped micropores. The characteristic energy E_o of equation (2.13) is an inverse function of the average pore size, as suggested by the adsorption of molecules of different sizes from the vapour phase. *Dubinin* and *Stoeckli* [27]) suggested the relation:

$$E_o = \frac{k}{x}$$ (2.14)

between the characteristic energy and the average half-width, x, of the slit-

shaped pores, where k = $13,03 - 1,53.10^{-5}.E_o^{3.5}$ (2.15)

Equation (2.15) and the hypothesis according to which the value n = 2 corresponds to a homogeneous system of micropores have been used by various authors to describe heterogeneous micropore systems [28, 29, 30]. Typical D-R plots for benzene (298K) on carbons are illustrated in Figure 2.2.   It is stated that the D-R equation generally underestimates the micropore volume for N_2.
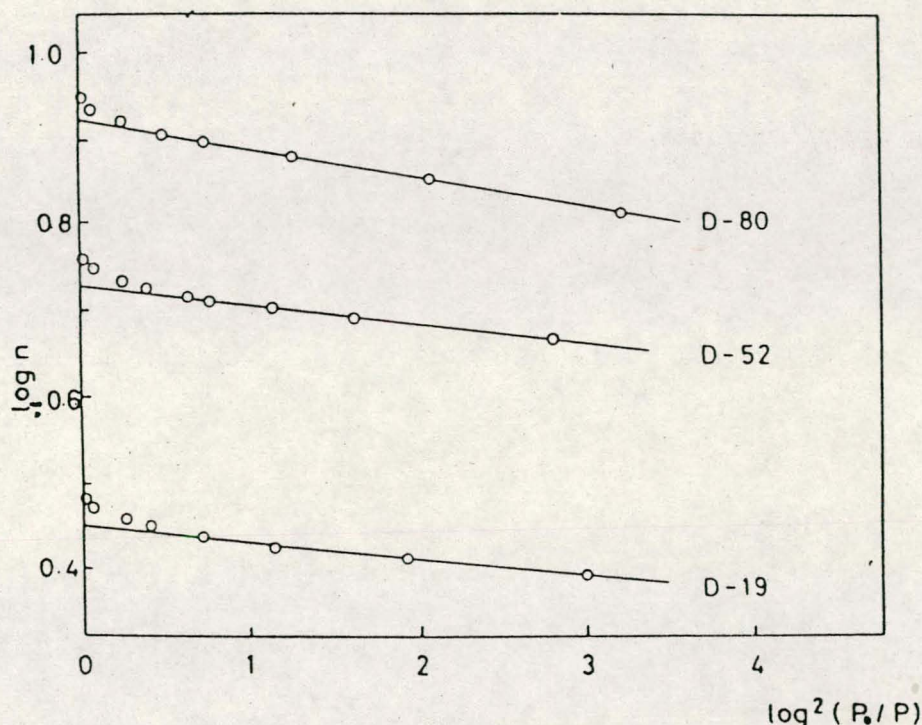

Figure 2.2: D-R plots for benzene (298K) on some carbons of series D

The *mass transfer* of a gas associated with a carrier fluid (i.e. air) to a carbon surface can be effected by a transport phenomenon such as mass flow if a pressure gradient exists, or mass diffusion if a concentration gradient exists in the absence of a pressure gradient. *Fick's* 2nd Law of diffusion [39] shows that the rate of movement of a gas is a function of several variables, especially the concentration gradient.

Diffusion equation:

$$\frac{\partial N\ (x,t)}{\partial t} = D\ \frac{\partial^2 N\ (x,t)}{\partial x^2} \qquad (2.16)$$

For one-dimensional flow in the direction of the x-axis *Fick's Law* can be expressed as :

$$-\frac{dm}{dt} = DA\ \frac{\partial C}{\partial X} \qquad (2.17)$$

where $\quad \dfrac{dm}{dt} \quad =\quad$ rate of decrease in mass (g.sec^{-1}) over A

$\dfrac{\partial C}{\partial X} \quad =\quad$ concentration gradient across the boundary thickness (g.cm-^{4})

$D \quad =\quad$ diffusivity or diffusion coefficient of the gas cm^2.sec^{-1}.

$A \quad =\quad$ boundary area (cm^2)

The limitations of this equation are:

a. no pressure gradient exists;
b. D is a constant independent of the concentration;
c. isothermal conditions exist;
d. the concentration of gas is small compared to that of air; and
e. conservation of mass applies.

Since the true driving force for any transport process is the gradient of chemical potential rather than the gradient of concentration, ideal *Fickian* behaviour in which the diffusivity is independent of sorbate concentration is realised only when the system is thermodynamically ideal.

Diffusion may occur by several different mechanisms depending on the pore size, the concentration of the sorbate, and other conditions. The relationship between the *Fickian* diffusivity, defined by Equation (2.17) and the mobility B, defined by:

$$- \frac{dm}{dt} = B\ A\ \frac{\partial \mu}{\partial x} \qquad (2.18)$$

is easily derived. Considering equilibrium with an ideal vapour phase;

$$\mu = \mu° + RT \ln a = \mu° + RT \ln P \qquad (2.19)$$

$$\frac{\partial u}{\partial x} = RT\ \frac{\partial \ln a}{\partial x} = RT\ \frac{\ln P}{C}\ \frac{\partial C}{\partial X} \qquad (2.20)$$

$$- \frac{dm}{dt} = BRT\ \frac{\ln P}{dc}\ \frac{\partial C}{\partial x} = BRT\ \frac{\ln P}{\ln C}\ \frac{\partial C}{\partial X} \qquad (2.21)$$

therefore the *Fickian* diffusivity is given by :

$$D = BRT\ \frac{\ln a}{\ln C} = Do\ \frac{\ln P}{\ln C} \qquad (2.22)$$

The diffusivity D is normally dependent upon the 3/2 power of T[°K] and can be calculated using the *Gilliland* equation [40],

$$D = 0,0043\ \frac{T^{3/2}}{P\ (V_{m1}^{½} + V_{m2}^{½})}\ \sqrt{\left(\frac{1}{M_1} - \frac{1}{M_2} \right)} \qquad (2.23)$$

where V_{m1} and V_{m2} = molecular volumes of gases 1 and 2 respectively;

M_1 and M_2 = molecular weights of the gases;

P = pressure in atmospheres of the carrier gas;

T = absolute temperature;

D = diffusivity in $cm^2.s^{-1}$

The efficiency of mass transfer plays an important role in adsorption from

moving gas streams.   The basic concepts of mass transfer were investigated by *Grubner and Underhill* [38]. As a general rule, the amount of adsorbate retained by dynamic adsorption from a flowing-gas stream is smaller than the amount corresponding to equilibrium conditions.   The overall adsorption efficiency, calculated from the ratio of the amount of adsorbate actually retained on the bed to the amount of adsorbate required to fully saturate the bed, depends on the distribution of adsorbate across the bed at the time of breakthrough. *Grubner and Underhill* [38] showed that the effects of this distribution can be calculated by the method of statistical moments. Certain basic assumptions have been made however:

a.   the adsorption bed is cylindrical;

b.   the bed is evenly filled with spherical adsorbent particles;
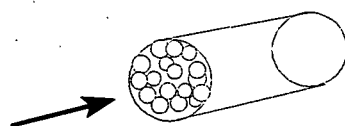
c.   wall effects are negligible; and

d.   the fluid phase streams between the particles in a free volume defined as the interparticle void volume.

INTRA-PARTICLE VOIDS
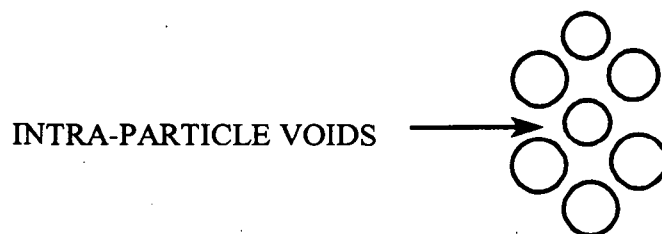
They concluded that *pore diffusion* is the most important mechanism of intra-particle mass transfer and that the nature of *pore diffusion* depends on the diameter of the intra-particle voids. If these pores have a relatively large

diameter (molecular mean free path < pore diameter), intra-particle mass transfer takes place by normal molecular diffusion. As the pores become narrower (molecular mean free path ~ pore diameter) the character of the flow changes to *Knudsen diffusion* and the intra-particle diffusion coefficient must assume a value appropriate to *Knudsen diffusion*. It was also shown that the breakthrough curve is always positively skewed. The breakthrough curve is a plot of concentration, C, measured at the outlet of the filter versus the time when the measurement is taken. The outlet, C, to inlet concentration, C_o, ratio of 0,01 is regarded as the ratio at which the challenge vapour has broken through. This has the important consequence that C/C_o values smaller than ½ are on average nearer the mean than the corresponding C/C_o values higher than ½, which considerably increases the effective adsorption capacity at low values of C/C_o.

The rate of surface migration of gas molecules from their initial contact point on the surface of a sorbent granule to a pore-opening is normally considered to be rapid when compared with the ***intergranular diffusion*** step. Although the mobility of the adsorbed phase will generally be much smaller than that of the gas phase, the concentration is very much higher. Therefore, under conditions such as when the thickness of the adsorbed layer is appreciable, a significant contribution to the flux is possible.
Significant ***physical adsorption*** is thus seen as a prerequisite for the contribution from ***surface diffusion*** to be noticeable, and this requires temperatures not too far above the boiling point of the species considered. Direct measurement of ***surface diffusion*** is not flexible since the flux due to diffusion through the gas phase is always present in parallel. However, if the surface migration step was the slowest step, and therefore rate controlling, the differential rate of gas adsorption would be [41]

$$\frac{\partial W}{\partial t} = 4 \, \pi^2 \, W_e \, \frac{D_s}{d_D^2} \left(1 - \frac{W}{W_e} \right) \qquad\qquad (2.24)$$

where D_s =   surface diffusion coefficient ($cm^2.s^{-1}$)

d_p =   sorbent granular size (cm)

W_e =   the adsorbed weight of gas per unit weight of sorbent in equilibrium with the challenge concentration C_o ($g.g^{-1}$)

W =   weight of gas sorbed per unit weight of sorbent ($g.g^{-1}$)

t =   time in seconds

This equation predicts an adsorption rate independent of linear velocity and nearly independent of inlet gas concentration since W_e is essentially on the plateau of the adsorption isotherm. The rate, however, should vary inversely with the square of the sorbent particle size. The **surface diffusivity** is generally found to be strongly concentration-dependent, except within the Henry's Law region, as illustrated by the data shown in Figure 2.3, taken from the work of *Gilliland et al* [42, 43].
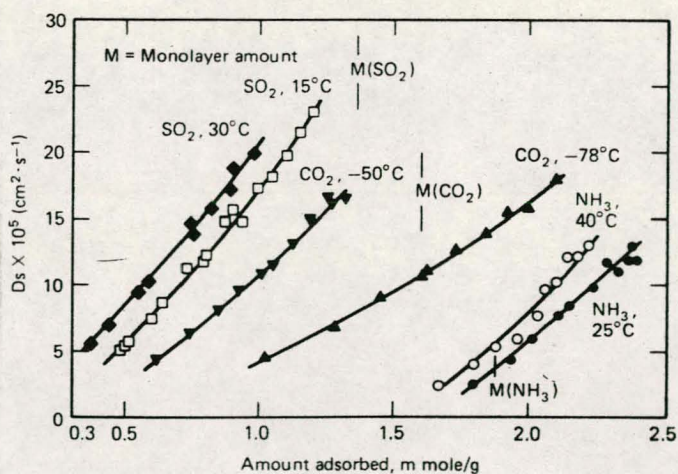
Figure 2.3:   **The variation of surface diffusivity with adsorbed phase concentration**

Intra-granular or *Knudsen diffusion*, also called *pore- or molecular diffusion*, should prevail when the mean free path between intermolecular collisions is large compared with the pore diameter. Macropore diffusion has been widely studied in connection with its influence on the overall kinetics of heterogeneous catalytic reactions [44]. Four distinct mechanisms of transport may be identified: *molecular diffusion, Knudsen diffusion, Poiseuille flow* and *surface diffusion*. Although the individual mechanisms are reasonably well understood, it is not always easy to make an accurate prediction of the effective diffusivity since this is strongly dependent on the shape of the pore structure. In *molecular diffusion* the resistance to flow arises from collisions between diffusing molecules. The effect of the pore is merely to reduce the flux as a result of geometric constraints which are accounted for by the tortuosity factor. *Molecular diffusion* will be the dominant transport mechanism whenever the mean free path of the gas (i.e. the average distance travelled between molecular collisions) is small relative to the pore diameter. However, in small pores and at low pressures the mean free path is greater than the pore diameter and collisions of molecules with the pore walls occur more frequently than collisions between diffusing molecules. Under these conditions the collisions between molecule and pore wall provide the main diffusional resistance, and we have what is known as *Knudsen diffusion*. When a molecule strikes the pore wall it does not bounce back. The molecule is instantaneously adsorbed and re-emitted in a random direction. The direction in which the molecule is emitted bears no relation to its original direction before the collision, and it is this randomness which provides the characteristic feature of a diffusive process. *Knudsen* showed that under these conditions the diffusion constant *(Knudsen diffusion)* per unit cross sectional area of pore is given by:

$$D_K = \frac{2}{3} r \, \bar{v} = 9700 \, r \left(\frac{T}{M} \right)^{\frac{1}{2}} \qquad (2.25)$$

where r =   the mean pore radius (cm)

$\bar{v}$ =   the mean molecular velocity (cm.s^{-1})

$$T \quad = \quad \text{the temperature } (°K)$$

$$M \quad = \quad \text{the molecular weight}$$

$$D_K \quad = \quad \text{diffusion coefficient } (cm^2.s^{-1})$$

The derivation of this equation together with a full discussion of the Knudsen flow regime is given by *Kennard* [45]. **Knudsen diffusion** occurs for gas-phase reactions at one-atmosphere pressure on surfaces whose pores are 20 nm in radius or smaller [46]. Under these conditions the mean free path between gas-phase collisions is about 100 nm. We also note from equation (2.25) that D_K is directly proportional to the pore radius. Molecular flow due to **Knudsen diffusion** is independent of total pressure differences occurring in adsorbent granules. The diffusivity also does not depend on either the composition or total gas concentration. The temperature dependence is slight and there is the usual inverse dependence on the square root of molecular weight. It is therefore evident that there must be a wide range of conditions under which both **Knudsen** and **molecular diffusion** are significant. It is therefore possible in a given adsorbent that **molecular diffusion** is dominant in the larger pores while **Knudsen** flow is dominant in the smaller pores. Because of the dependence of mean free path on pressure, for any given adsorbent and adsorbate there will be a transition for **molecular diffusion** at high pressure to **Knudsen** flow at low pressures. In the intermediate region both wall collisions and intermolecular collisions contribute to the diffusional resistance and the effective diffusivity depends on both the **Knudsen** and **molecular diffusivities**. Both the **Knudsen** and **molecular diffusion** mechanisms involve flow through the gas phase within the pore. If there is a difference in total pressure across a particle, then there will be a direct contribution to the adsorption flux from forced laminar flow through the macropores. This effect is generally negligible in a packed bed since the pressure drop over an individual particle is very small. From Poiseuille's equation it may be shown that the equivalent diffusivity (D_c) is given by:

$$D_c = \frac{P\,r^2}{8\,\mu} \tag{2.26}$$

where P = absolute pressure (dynes.cm^{-2})

μ = viscosity (poise)

r = mean pore radius (cm).

Any flux due to Poiseuille flow simply adds to the diffusional flux through the pore. In order to convert adsorption space W (cm^3.g^{-1}) to an adsorption capacity (g.g^{-1}) one can use the concept of volume pore-filling as expanded by *Bering et al* [31] according to what the adsorbed gas condenses to a liquid and fills the adsorption space of the micropore.

2.5   The Wheeler theory

In a study of heterogeneous gas adsorption by a bed of carbon granules *Wheeler* [32] derived a kinetic adsorption equation from a continuity equation of mass balance between the mass input and the sum of the mass adsorbed, plus that penetrating the bed. The equation was shown as:

$$t_b = \frac{\rho_B \, W_e}{C_o \, V_f} \, [\lambda - \frac{V_I \, \ln \, (C_o/C_x)}{k_v} \,] \qquad (2.27)$$

where C_o = inlet gas concentration in g.cm^{-3}

C_x = exit gas concentration in g.cm^{-3}

λ = carbon bed depth in cm

k_v = the pseudo first order adsorption rate in min^{-1}

ρ_B = bulk density of the carbon bed in g.cm^{-3}

W_e = adsorption capacity in g.g^{-1}

t_b = breakthrough time in min of the gas at the arbitrarily chosen value of C_x.

V_f = velocity in cm.s^{-1}

By definition $Q = V_I A$ and $W = \lambda A \rho_B$

where Q = volumetric flowrate (cm^3.min^{-1})

A   = the cross sectional area of the bed (cm²)

W   = weight of the bed (g).

Equation (2.27) can therefore be converted to (2.28).

$$t_b = \frac{W_e}{C_o Q} [W - \frac{\rho_B \, Q \, \ln \, (C_o / C_x)}{k_v}] \qquad (2.28)$$

In this form of equation, the critical bed mass of the carbon, W_c, or that mass of the bed just sufficient to cause attenuation of the inlet concentration to the chosen exit concentration, can be established as:

$$W_c = \frac{\rho_B Q}{k_v} \ln (\frac{C_o}{C_x}) \qquad (2.29)$$

By maintaining constant values for the conditions of test, namely, C_o, C_x, ρ_B, Q, temperature, carbon type and carbon granule size, but varying W, the plot of experimental values of t_b vs W permits the adsorption capacity W_e to be determined from the slope of the resultant straight line, and the adsorption rate constant, k_v from the X-axis intercept.

The *physical adsorption* process, under heterogeneous adsorption conditions, is characterized by the disappearance of a gas flowing into a packed bed of sorbent granules and can be monitored by the exit stream for appearing concentrations of the gas. The change in exit concentration of the gas with time indicates the progressive rate of passage into, or breakthrough, of the bed. For the study of the adsorption kinetics of a bed of carbon granules exposed to an inlet concentration at a finite volumetric flowrate, and for which the breakthrough time represents the first trace of gas in the bed exit stream, pseudo-first-order kinetics should pertain. Equation (2.25) is the kinetic equation applicable to the study of gas adsorption. The pseudo first order rate constant, k_v, in equations (2.26 - 2.29) is a function of the superficial linear velocity (V_f) of the airflow rate into the carbon bed [34]. The mathematical relationship found, which exhibited a 0,999 correlation coefficient with the experimental data over a

120 -300 cm.min^{-1} velocity range was,

$$k_v = \left[\frac{a + b}{1 + (a/b)\ \exp\ [-(a + b)\ C\ V_l]}\right] \qquad (2.30)$$

where a, b and c were constants of the system. It is expected that one or more of these constants includes the effect of carbon-granule size. Equation (2.30) describes a sigmoidal curve of k_v vs V_l, showing a minimum value b for k_v at a low V_l and a maximum value for k_v of (a + b) at high velocities (V_l).

In a study on heterogeneous catalysis reaction rates *Wheeler* [35] introduced the concept of a maximum or limiting value to the first-order-rate constant governing the adsorption of the gas on the catalyst surface. The maximum value would be mass-transfer limiting and would require, when applied to gas adsorption, an ideal carbon, one for which diffusion and surface adsorption within a single granule would be so rapid that mass transfer of the gas to the external surface would limit the adsorption rate. In addition, *Wheeler* assumed no back-evaporation or desorption of gas after initial adsorption. On the bases of the additional assumptions that all gases have approximately the same viscosity and *Schmidt* number:

$$\left(N_{Sc} = \frac{\mu}{\rho D_G}\right) \qquad (2.30)$$

where μ = viscosity (g.cm^{-1}.sec^{-1}).

     ρ = density (g.cm-^{3})

     D_G = the diffusivity (cm^2.sec^{-1}),

Wheeler showed that the mass-transfer limiting value of the rate constant, k_x, would be approximately

$$k_x \simeq 10 \sqrt{\frac{V_l}{\overline{m} d_p^3 P_T}} \; (sec^{-1}) \tag{2.31}$$

where

V_l = superficial linear velocity $(cm.s^{-1})$

d_p = particle diameter (cm)

P_T = total pressure (atmosphere)

$\overline{m}$ = average molecular weight

By setting P_T equal to one atmosphere and $\overline{m}$ approximately equal to the molecular weight of air, $28.8 \; g.mole^{-1}$, Equation (2.31) can be simplified to:

$$k_x \simeq 1.86 \; V_l^{1/2} \; d_p^3/^2 \; (sec^-1) \tag{2.32}$$

Rehrmann and Jonas [36] showed that the limiting value of the adsorption rate constant, displayed at high linear velocities and / or small carbon granule sizes, is a fundamental property of the activated carbon and probably developed in the carbon as a consequence of its activation. *Jonas et al* [37] reported that the rate controlling step is believed to be internal diffusion rather than mass transfer or external diffusion, and therefore the term $\overline{m}$ representing the average molecular weight of the vapours in equation (2.31) could be replaced by M, the molecular weight of the vapour to be adsorbed, rather than of a mixture of the vapour and air. Thus, in the case where internal diffusion is rate-controlling in heterogeneous adsorption, k_v, the adsorption rate constant, can be expected to be a function of $M^{1/2}$. On the assumption that carbon tetrachloride, or any other chosen vapour, could be regarded as the reference vapour for the adsorption-rate constant of the carbon, as well as for its adsorption space, and considering equation (2.31) in the heterogeneous adsorption case to be equivalent to

$$k_v = k^1 \sqrt{M} \; sec^-1 \tag{2.33}$$

where

$$k^1 = 10 \sqrt{(V_I/d_p^3 \, P_T)} \qquad (2.34)$$

for an activated carbon of a definite mesh size or mean granule diameter and, under fixed conditions of pressure and linear flow velocity, it is possible to calculate the adsorption-rate constant for any vapour knowing that of, for example, carbon tetrachloride.

Thus,

$$k_v M^{-\frac{1}{2}} = k^1 \qquad (2.35)$$

for the system under study.

Wheeler [47] also discussed the aspect of gas desorption. He assumed, as was done for adsorption, that the three differential equations which describe:

a.   desorption at the surface of an individual granule,
b.   diffusion out of the pore structure of the granule, and
c.   desorption from the pore wall at a point in the granule,

may be combined into one differential equation which gives the overall rate of desorption per unit volume as a function of the weight of agent adsorbed, W_t, and of the gas concentration, C, at any time, t. Such an equation, solved simultaneously with the equation of mass balance in the form:

$$- V_I \, \frac{\partial C}{\partial \lambda} = \rho_B \, \frac{\partial W_t}{\partial t} \qquad (2.36)$$

results in the equation,

$$t_R = \frac{W - W_e}{Q\,(C_e - C_o)} \left[W + \frac{\rho_B\, Q\, \ln \frac{1}{1-f}}{k_d} \right] \qquad (2.37)$$

where

t_R	=	regeneration time (min)
ρ_B	=	bulk density (g.cm^{-3})
Q	=	volumetric flowrate (cm^3.min^{-1})
k_d	=	pseudo first order desorption rate constant (min^{-1})
C_o	=	inlet or challenge gas concentration (g.cm^{-3})
W_e	=	mass of adsorbed gas in equilibrium with C_o (g.g)
W_0	=	mass of gas adsorbed per gram of adsorbent (g.g^{-1}) at zero time of regeneration
W	=	carbon mass (g)
C_e	=	gas concentration in equilibrium with the weight, W_o, pre-adsorbed on the adsorbent (g.cm^{-3})
f	=	a rational function defined as :

$$f = \frac{W_o - W}{W_o - W_r} \qquad (2.38)$$

where f is equal to the fractional regeneration of the bed and the terms $W_o - W$ and $W_o - W_r$ represent transformation expressions for the desorption process. In this case f = o represents no regeneration since $W = W_o$ and f = 1 represents complete regeneration since $W = W_r$. In the adsorption case $W_o - W$ would be replaced by W_e and $C_e - C_o$ by C_o as shown in equation (2.28). The time to regenerate a known mass (w) of carbon is the mass before any adsorption took place to the point where arbitrarily chosen regeneration occurred, can be plotted against W. The slope of the resulting straight line will equal:

$$\frac{(W_o - W_r)}{Q(C_e - C_o)} \qquad\qquad (2.39)$$

and the y-axis intercept will:

$$\frac{(W_o - W_r)\rho_B}{(C_e - C_o)k_d} \ln(1/1-f) \qquad\qquad (2.40)$$

The intercept divided by the slope is equal to $(\rho_B/Q\, k_d)$ ln (1/1-f). The difference between the adsorption equation (2.28) and the desorption equation (2.37) is that for adsorption. The term $(\rho_B Q/k_v)$ ln $(C_o - C_x)$ is subtracted from the total carbon mass W, whereas for desorption the $(\rho_B\, Q/k_d)$ ln (1/1- f) is added to the total weight W.

Although physical forces explain many adsorption phenomena, there are adsorptions in which the behaviour indicates that chemical action is involved. Adsorption of this type is designated as *chemical adsorption* or *chemisorption*. Physical adsorption usually involves a smaller energy change than does *chemisorption* [48]. If, between the adsorbate and the adsorbent there is any electron transfer or sharing, or if the adsorbate breaks up into atoms or radicals bound separately, then the adsorption is *chemisorption*. Chemisorption is therefore specific and depends on the chemical nature of both the adsorbent and adsorbate. Physical adsorption decreases at higher temperatures, whereas some elevation of temperature is often necessary to initiate chemisorption. The process of chemisorption is significant in impregnated carbons. The carbons are impregnated in order to remove contaminants that are not removed by physical adsorption. Different impregnants are used, depending on the contaminant to be removed. A summary of chemicals used for impregnation are listed in Table 2.2.

Table 2.2 : Chemicals used for impregnation

CHEMICALS USED FOR IMPREGNATION
1. Cu
2. Cr
3. Ag.
4. Cu, Cr, Ag in NH_4OH and $(NH_4)_2CO_3$
5. Cu, Cr, Ni, Ag in NH_4OH and $(NH_4)_2CO_3$
6. K
7. Na
8. Co
9. S
10. Mn

2.6   SUMMARY OF REACTION STEPS

a.   Mass transfer

b.   Surface diffusion

c.   Intra-granular diffusion - Knudsen diffusion - molecular diffusion

d.   Physical adsorption

e.   Gas desorption

f.   Chemisorption

2.6.1   MASS TRANSFER

External diffusion: - the gas molecules are transported from a variety of neighbouring air molecules to a site on the carbon granule outer surface.

The mass transfer of a contaminant associated with a carrier fluid to a carbon surface can be effected by mass flow, if there is a pressure gradient, or with mass diffusion, if there is a concentration gradient in the absence of a pressure gradient.

The diffusion is expressed by Fick's 2nd Law:

$$\frac{dm}{dt} = DA\ \frac{\partial C}{\partial X} \qquad\qquad (2.41)$$

where   A   =   boundary area (cm^2)

dm/dt   =   rate of decrease in mass ($g.s^{-1}$) over A.

$\partial C/\partial X$ =   the concentration gradient across the boundary thickness ($g.cm^{-4}$).

D   =   diffusion coefficient of the gas ($cm^2.s^{-1}$).

2.6.1.1 LIMITATIONS

a.   There is no pressure gradient.

b.   D is a constant and independent of concentration.

c.   Isothermal conditions obtain.

d.   The contaminant concentration is small compared with that of the carrier gas.

e.   Conservation of mass obtain.

D is dependent upon the $^3/_2$ power of T ($^\circ$K) and can be calculated using Gilliand's equation (1),

$$D = 0,0043 \frac{T^{2/3}}{P (V_{m1}^{1/2} + V_{m2}^{1/2})} \sqrt{\left(\frac{1}{M_1} - \frac{1}{M_2} \right)} \qquad (2.42)$$

where

V_{m1} and V_{m2}	=	molecular volumes of gases 1 and 2.
M_1 and M_2	=	molecular weight of the gases.
p	=	the pressure in atmospheres.
T	=	absolute temperature.
D	=	diffusivity in $cm^2.s^{-1}$.

D can also be calculated by the equation given by Hirschfelder [48].

2.6.2 SURFACE DIFFUSION

This is the transport of gas molecules over a two-dimensional granule surface to the entrance of the adsorbent micropore.

The rate of surface migration of gas molecules from their initial contact point on the carbon surface to a pore opening (inter granular) is normally considered to be rapid when compared with the Intra-granular diffusion step.

If the surface migration step was the slowest step, and therefore

rate-controlling, the differential rate or gas adsorption would be:

$$\frac{\partial W}{\partial t} = 4 \, \bar{\Pi}^2 \, W_e \, \frac{D_s}{d_p^2} \left(1 - \frac{W}{W_e} \right) \qquad (2.43)$$

where D_s = surface diffusion coefficient ($cm^2.s^{-1}$).

d_p = carbon granule size (cm).

W_e = adsorbed weight of gas per unit weight of carbon in equilibrium with the challenge conc. C_o ($g.g^{-1}$).

W = weight of gas sorbed per unit weight of carbon ($g.g^{-1}$).

t = time.

This equation predicts an adsorption rate which is:

a.   independent of linear velocity, and

b.   nearly independent of inlet gas concentration since W_e is essentially on the plateau of the adsorption isotherm.

The rate should vary inversely with the square of the sorbent particle size.

2.6.3 INTRA-GRANULAR DIFFUSION, PORE DIFFUSION OR KNUDSEN DIFFUSION

Transport of gas molecules within the small pores causes the gas to collide, with or come within the force field of, an active site.

This molecular diffusion should prevail when the mean free path between intermolecular collisions is large compared with the pore diameter.

This diffusion occurs for gas-phase reactions at one-atmosphere pressure on surfaces whose pores are 20 nm in radius or less [10]. Under these conditions the mean free path between gas phase collisions is about 100 nm.

The gas molecule is depicted as colliding with a pore wall, then flying to another wall, before colliding with a second molecule.

Knudsen showed that under these conditions the diffusion constant (Knudsen diffusion) per unit cross-sectional area of pore is given by:

$$D_k \ r\overline{V} = 9700 \ r\sqrt{\left(\frac{T}{M}\right)} \qquad\qquad (2.44)$$

$r \quad = \quad$ pore radius (cm).

$V \quad = \quad$ mean molecular velocity (cm.sec^{-1}).

$T \quad = \quad$ temperature (°K).

$M \quad = \quad$ molecular weight.

It is clear that $D_k \sim$ pore radius.

At 300 °K, gas molecules with a molecular weight of 30 will have a Knudsen diffusion constant of 0,005 cm^2.s^{-1} in a 1 nm pore, a constant of 0,05 cm^2.s^{-1} in a 10 nm pore.

Molecular flow is independent of the total pressure differences occurring in a carbon granule as a result of the reaction.

2.6.4 PHYSICAL ADSORPTION

The gas molecule loses translational freedom and is held by, and occupies, the active site. Physical adsorption, under heterogeneous adsorption conditions, is characterized by the disappearance of a gas flowing into a packed bed of carbon and by monitoring the exit stream concentrations of the gas.

The change of exit concentration with time indicates the progressive rate of passage into or breakthrough of the bed.

The kinetic equation, applicable to the study of gas adsorption by a carbon bed, was originally derived by Wheeler [47] from a continuity equation for mass balance between gas entering an adsorbent bed and the sum of the gas adsorbed plus that penetrating the bed.

$$t_b = \frac{W_e}{C_o Q} \left[W - \frac{\rho_\beta Q}{k_v} \ln\left(\frac{C_o}{C_x}\right) \right] \qquad (2.45)$$

where
t_b = gas breakthrough time
C_x = exit concentration at t_b
C_o = inlet concentration $(g.cm^{-3})$
Q = volumetric flow rate $(cm^3.min^{-1})$
ρ_B = bulk density of packed bed $(g.cm^{-3})$
k_v = first order adsorption rate constant (min^{-1})
W = weight of the carbon (g)
W_e = kinetic saturation capacity $(g.g^{-1})$ at the ration C_x/C_o

Values t_b plotted as a function of W yields a straight line from whose shape and x-axis intercept the properties W_e and k_v can be calculated. The x-axis intercept $(\rho_B Q/k_v \ln(c_o/c_x))$ is considered to be

the critical bed weight just sufficient to reduce the inlet concentration to the chosen exit concentration, W_c.

2.6.5 GAS DESORPTION

Gas molecules gain translational freedom and desorb from the active sites in the micropore region, traversing the transition and macropore regions of the carbon on which the chemical impregnants were deposited. The study of gas desorption from a bed of carbon can be approached in terms of regeneration of the bed. The theoretical basis was developed by Wheeler [46].

It was assumed that three differential equations which describe:

a.   desorption at the surface of an individual granule,

b.   diffusion from the pore structure of the granule,

c.   desorption from the pore wall at a point in the granule,

may be combined into one differential equation which gives the overall rate of desorption per unit volume of reactor as a function of the weight of agent adsorbed (W_t) and of the gas concentration C at any time t.

The equation, solved simultaneously with the equation of mass balance in the form of

$$- V_1 \frac{\partial C}{\partial A} = \rho_\beta \frac{\partial W}{\partial t} \qquad (2.46)$$

gives

$$t_R = \frac{W_o - W_r}{Q(C_e - C_o)} \left[W + \frac{\rho_\beta \, Q \ln \frac{1}{1-f}}{k_d} \right] \qquad (2.37)$$

Where

t_R = regeneration time (min)

ρ_β = bulk density (g.cm^{-3})

Q = volumetric flowrate (cm^3.min^{-1})

k_d = pseudo first order desorption rate constant (min^{-1})

C_o = inlet concentration (g.cm^{-3})

W_r = weight of adsorbed gas in equilibrium with Co (g.g^{-1})

W = weight of the carbon (g)

W_o = weight of gas adsorbed per gram adsorbent (g.g^{-1}) at zero time of regeneration

C_e = gas concentration in equilibrium with the weight W_o pre-adsorbed on the adsorbent (g.cm^{-3})

f = rational function; fractional regeneration of the bed

$$= \frac{W_o - W}{W_o - W_r}$$

2.6.6 CHEMICAL REACTION

The desorbing gas molecules react with the chemical impregnants on the surfaces of the larger adsorbent pores.

The chemical compound formed on the carbon after impregnation with chromic oxide, cupric ammonium complex and a ammonium carbonate are the copper tetramine and copper diamine chromates. The slow release of water and the high drying temperature convert the remaining tetramine to the diamine form and then forms a basic cupric ammonium chromate.

A further reaction with water results in an equilibrium mixture of chromate / bronchantite with the basic cupric ammonium chromate:

$$4 \, Cu(OH) \, NH_4CrO_4 + 3 \, HOH \rightleftharpoons Cu_4(OH)_6 \, CrO_4 \cdot NH_3 \cdot H_2O + 3NH_4 \, CrO_4$$

Because of incomplete reactions in the heterogeneous mixture of carbon and solution, it is believed that the final product contains a mixture of cupric diamine chromate, basic cupric A, chromate bronchontite and acid chromate anion.

Reactions with CNCl includes:

(a)   hydrolysis catalysed by the cupric ion to form cyanic acid and hydrochloric acid

$$CNCl + HOH \xrightarrow{Cu^{2+}} HOCN + HCl \qquad\qquad \textbf{(A)}$$

(b)   the cyanic acid is in equilibrium with isocyanic acid

$$HOCN \rightleftharpoons HNCO \qquad\qquad \textbf{(B)}$$

-     Reaction A takes place during the desorption phase, and is several orders of magnitude slower than the adsorption step.

CHAPTER III

EXPERIMENTAL

3.0 EXPERIMENTAL

The characterization of the activated carbon is essential in order to understand the filtration mechanisms. The physical characteristics evaluated before and after impregnation and exposure to HCN were :

a   the specific surface area;

b   the pore volume distribution;

c   the apparent density;

The absorption capacities and adsorption rate constants were determined for :

a $CC\ell_4$ (Type A filters)

b   HCN   (Type B filters)

c $CC\ell_4$/HCN as a dual exposure   (Type AB filters)

3.1 SPECIFIC SURFACE AREA

Since almost all practically important adsorbents are porous solids the key variable which is required to characterize an adsorbent is the specific surface area.   The specific surface areas of activated carbons are very large. Accurate measurement of the surface area presented a significant problem in early studies of adsorption. If the physical adsorption capacity was limited to a close-packed monolayer, then the determination of the saturation limit from an experimental isotherm with a molecule of known size would provide a simple and straightforward method for estimating the specific area. *Langmuir* [49] presented an ideal monolayer adsorption isotherm :

$$V = \frac{V_m \, BP}{1 + BP}$$
(3.1)

where V   =   volume of gas (0°C, 760 mm Hg) adsorbed per unit mass of adsorbent.

V_m =   volume of gas (0°C, 760 mm Hg) adsorbed per unit

mass of adsorbent with a layer one molecule thick.

B   =   empirical constant in reciprocal pressure unit which has limited practical application.

P   =   pressure

The main difficulty is that in chemisorption the sites are usually widely spaced so that the saturation limit bears no obvious relationship to the specific surface area, whereas   physical adsorption generally involves multilayer adsorption.   The formation of the second and subsequent molecular layers commences at pressures well below that required for completion of the monolayer, so that it is not immediately obvious how to extract the monolayer capacity from the experimental isotherm.   This problem was first solved by *Brunauer, Emmett and Teller* (BET) [49] who developed a simple model isotherm to account for multilayer adsorption which they used to extract the monolayer capacity and hence the specific surface area. The resulting equation for the BET equilibrium isotherm is

$$V = \frac{V_m\, Cx}{(1 - x)\,[1 + (C - 1)\,x]} \tag{3.2}$$

where x = P/P^o

C =   constant derived from the heat of adsorption

From equation (3.2) the isotherm equation can be written as

$$\frac{1}{X\,(P^o/P - 1)} = \frac{C - 1}{X_m\, C}\,\frac{P}{P^o} + \frac{1}{X_m\, C} \tag{3.3}$$

where X   =   weight of adsorbate adsorbed at relative pressure P/P^o

P   =   partial pressure of adsorbate

P^o = saturated pressure of adsorbate

X_m = weight of adsorbate adsorbed at a coverage one monolayer

C = a constant which is a function of the adsorbate's heats of condensation and adsorption.

Although the BET equation has its limitations, such as being bound on the assumptions that the heat of adsorption is constant over the entire surface coverage by the monolayer, and that the monolayer is completed before the formation of secondary layers with a heat of adsorption equal to that of the heat of liquefication begins, it is very useful because it enables the numerical surface area to be determined. If the area occupied by a single molecule of the adsorbent and the number of molecules needed to form a monolayer are known, it is possible to express the surface area of the adsorbent in m^2/g. The BET equation (3.3) yields a straight line when $1/X(P^o/P - 1)$ is plotted against P/P^o. The slope, $(C - 1)/X_m C$, and the intercept, $1/X_m C$, are used to determine the weight adsorbed at the monolayer. The value of the weight adsorbed at the monolayer, X_m can be calculated as follows :

$$S = \text{slope} = \frac{C - 1}{X_m C} \tag{3.4}$$

$$I = \text{intercept} = \frac{1}{X_m C} \tag{3.5}$$

Solving equations (3.4) and (3.5) for X_m gives :

$$X_m = \frac{1}{S + I} \tag{3.6}$$

The total surface area, S_t, is determined from :

$$S_t = \frac{X_m N A_{cs}}{M_a} \tag{3.7}$$

where M_a = adsorbate molecular weight

X_m = weight of adsorbate adsorbed at a coverage of one monolayer

N = Avogadro's number = $6,023 \times 10^{23}$

A_{cs} = cross sectional area of adsorbate molecule (See Table 1)

The specific surface area S is given by :

$$S = \frac{S_t}{weight\ of\ sample} \qquad (3.8)$$

Table 3.1: Effective cross sectional areas of various adsorbates

ADSORBATE	AREA (m² x 10⁻²⁰⁾	REFERENCE
Nitrogen	16,2	3
Krypton	20,5	4
Argon	14,2	5
Xenon	25,0	6
Oxygen	14,0	7
Ethane	20,5	8
Butane	46,9	9

Shull [56] suggested that for nitrogen adsorption, the multilayer region may be described by a simple linear function

$$X = \frac{S}{15.47}\ t \qquad (3.9)$$

where t is the average statistical thickness of a layer of nitrogen adsorbed and which can be calculated by the equation

$$t = \frac{13,99}{(0,034 - \log P/P^o)^{\frac{1}{2}}} \qquad (3.10)$$

A simplified alternative to the *multipoint BET* method is the *single-point method* which is based on the fact that the intercept of a BET plot is generally small when compared with the slope and can be ignored. As indicated by equation (3.3), if the intercept is assumed to be zero, the value of X_m tends to be excessively large. However, this error is cancelled out because the measured value of the slope tends to increase if the intercept is taken as zero.

The zero-intercept assumption simplifies the BET equation to

$$\frac{1}{X(P^o/P - 1)} = \frac{1}{X_m} P/P^o \qquad (3.11)$$

or

$$X_m = X(1 - P/P^o) \qquad (3.12)$$

Thus, by measuring the amount of gas adsorbed at one value of P/P^o, the monolayer capacity, X_m, can be calculated by substituting (3.13) into (3.12)

$$X_m = \frac{A}{A_{cal}} V_{cal} \frac{P_a M}{RT} \qquad (3.13)$$

where X_m = mass of adsorbate adsorbed on the sample

V_{cal} = calibrated volume (cm³)

A = sample integrator counts

A_{cal} = calibrated integrator counts

P_a = ambient pressure

M　　=　　adsorbate molecular weight (28 for N_2)

T　　=　　temperature (K)

R　　=　　gas constant (82,1 mℓ atm. deg $^{-1}$ mol^{-1}).

Therefore,

$$X_m = \frac{A}{A_{cal}} \; V_{cal} \; \frac{P_a M_a}{RT} \; (1 - P/P^o) \tag{3.14}$$

Substitution of equation (3.7) into equation (3.14) gives an expression for the **total surface area**.

$$S_t = \frac{A}{A_{cal}} \; V_{cal} \; A_{cs} \; \frac{P_a N}{RT} \; (1 - P/P^o) \tag{3.15}$$

Using R = 82,1 mℓ atm. deg^{-1} mol^{-1}, P_a = 1 atm and T = 298 K equation (3.15) reduces for nitrogen to :

$$S_t = 3,98 \; (1-P/P^o) \; \frac{A}{A_{cal}} \; V_{cal} \tag{3.16}$$

The extent of the error implicit in the single-point method can be calculated as follows:

Solving equation (3.3) for X_m gives

$$X_m = X \, (P^o/P{-}1) \; \frac{1}{C} + \left(\frac{C-1}{C} \right) \; P/P^o \tag{3.17}$$

Similarly, equation (3.11) can be written as

$$X_m^1 = X\,(P^o/P - 1)\; P/P^o \qquad\qquad (3.18)$$

The relative error inherent in the single point method is then:

$$\frac{X_m - X_m^1}{X_m} = \frac{1 - P/P^o}{1 + P/P^o\,(C - 1)} \qquad\qquad (3.19)$$

Equation (3.19) shows that, for a given value of C, the relative error decreases with increasing relative pressure. Therefore, the value of P/P° near 0,3 is recommended since this is generally near the maximum value at which the BET equation remains valid.

3.1.1   INSTRUMENTATION

The ASAP 2010 System (Figure 3.1) consisted of an analyser, a control module, which permits entry of analysis- and report options, and an interface controller, which controlled analyses.
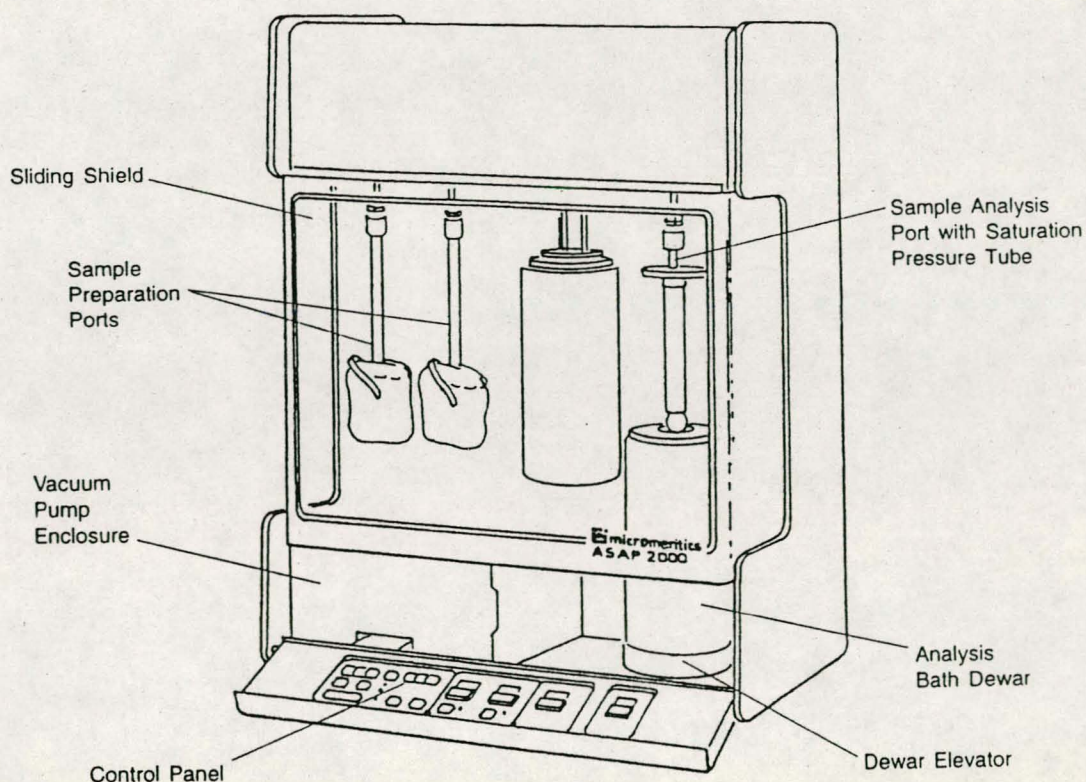
Figure 3.1. The ASAP 2010 porosimeter

The ASAP 2010 analyser contains two sample preparation ports and one analysis port. There were In-line cold traps between the vacuum pump and the manifold in both the analysis and the de-gassing system. The sample saturation pressure (P_{sat}) tube was located next to the sample analysis port.

The analysis bath fluid Dewar rested on an automatically-operated elevator. Controls and indicators on a control panel operated the vacuum systems, de-gas valves, and heating mantles. A sliding shield could be lowered to provide safety or raised to permit access to the sample analysis port and preparation ports.

The ASAP 2010 system was designed and tested to meet the specifications provided in Table 3.2.

Table 3.2: ASAP2010 Specifications

Characteristic	Specification

—— PRESSURE MEASUREMENT ——

Range:	0 to 950 mmHg
Resolution:	
1000 mmHg Range	0.052 mmHg
10 mmHg Range*	0.0005 mmHg
1 mmHg Range*	0.00005 mmHg
Accuracy: (Includes non-linearity hysteresis and non-repeatability. Transducer manufacturer's specifications.)	
1000 mmHg Range	Within 0.1% of full scale
10 mmHg Range	Within 0.15% of reading
1 mmHg Range	Within 0.15% of reading

—— MANIFOLD TEMPERATURE TRANSDUCER ——

Type:	Solid-state absolute temperature device
Accuracy:	$\pm$ 0.02°C (by keyboard entry)
Stability: (Transducer manufacturer's specifications.)	Within $\pm$ 0.1°C per month

—— VACUUM SYSTEM ——

Vacuum Pumps:	Two independent, 2-stage mechanical pumps; one for analysis and one for degas. Ultimate vacuum 5×10^{-3} mmHg.
Molecular Drag Pump:	Ultimate vacuum 1×10^{-5} mmHg.

—— DEGAS SYSTEM ——

Temperature Range:	Ambient to 350°C with glass fibre heating mantles (450°C with optional quartz fibre heating mantles).
Selection:	Digitally set, 1°C increments.
Accuracy:	Deviation less than $\pm$ 10°C of set point at thermocouple.
Backfill Gas:	User-selectable, typically helium or nitrogen.

—— SYSTEM CAPACITY ——

Sample Preparation: 2 degas ports

Analysis: 1 sample port and 1 saturation pressure tube

Total Operating Capacity: 4 complete analysis units can be independently controlled by one control module, effectively doubling the overall capacity.

—— LIQUID NITROGEN SYSTEM ——

Special Features: Patented *Isothermal Jackets* effectively maintain LN_2 level constant on sample tube and Po tube during analysis while evaporation of LN_2 occurs.

Capacity: 1.9 Litre Dewar, which provides up to 60 hours of unattended analysis.

Analysis Time: Unlimited. LN_2 Dewars may be refilled without affecting the accuracy of results.

—— SAMPLE SIZE ——

Sample tubes are available for various size pellets, cores and powders. Sample tube stems are normally ½-inch OD with 9-cc bulbs. Also available are 1/4- or 3/8-inch OD with 9-cc bulbs. Monolithic samples up to 12 mm diameter x 25 mm long fit into a taper-sealed tube. Special tubes can be designed to accommodate unusual samples.

—— ENVIRONMENT ——

Temperature: 10 to 30°C operating; -10 to 55°C storing or shipping

Humidity: 20 to 80% relative, non-condensing

—— GASES ——

Normal: Argon, carbon dioxide, nitrogen, krypton and other suitable gases.

3.2 PORE VOLUME DISTRIBUTION

3.2.1 PORE ANALYSIS BY ADSORPTION

The activated carbon granules contain a complex network of pores of
various shapes and sizes. The shapes include cylindrical, rectangular
cross-sections, as well as many irregular shapes and constrictions.
The size distribution depends on the source materials, formation
procedures and extent of activation.   The method for the
determination of pore structures concern, generally, helium density,
ρ_{He}, mercury density, ρ_{Hg}, nitrogen adsorption and mercury
penetration. The selection of methods depends solely on the range
of pore size.   Helium density is defined as the weight of a solid
sample divided by the volume of helium displaced by that sample.
The molecule of helium has a diameter of approximately 2,3 Å [80].
The mercury density, ρ_{Hg}, is defined as the weight of solid sample
divided by the volume of mercury displaced by that sample. The
volume of mercury displaced at an absolute pressure of 1,6 psia,
which corresponds to a pore radius of about 51μm, is measurable.
Therefore, the total pore value for all pores with a radius less than
51μm is calculated with

$$V_\rho \ (r < 51\mu m) \ = \ \frac{1}{\rho_{Hg}} \quad \frac{1}{\rho_{He}}$$

where V_ρ = total pore volume in cc.g^{-1}

Adsorption at low relative pressures is used to determine the surface
area as described in paragraph 3.1. As the pressure is increased,
capillary condensation takes place in very small pores, and further
increases in pressure cause condensation in large pores. Thus,
adsorption isotherms at high relative pressure will produce cumulative
pore volumes. The lower part of the adsorption isotherm, that is,
0,05 < P/P° < 0,35, is used for measurements of specific surface
area, whereas the entire desorption isotherm is useful for determining

pore size distributions. The desorption isotherm is most frequently used because it represents the branch of lower equilibrium, and is therefore closer to thermodynamic stability. That is, as the adsorbate equilibrium, pressure is decreased, the free energy G_x (G = RT ln P) also decreases.

In some special cases [82], the adsorption isotherm is preferred. Because nitrogen has been used extensively as an adsorbate, it has been well-characterised and, for this reason, serves as the most common adsorbate for pore-size distributions. Assuming that the micropore is cylindrical, the pore radius, r_k, according to the Kelvin equation is

$$r_k = \frac{2X \, V_m \, Cos \, \theta}{ln \, (P/P^o)} RT \qquad\qquad (3.20)$$

where P = saturated vapour pressure in equilibrium with the adsorbate condensed in a capillary or pore

P^o = normal adsorbate saturated vapour pressure

X = surface tension of the adsorbate (8,85 ergs.cm^{-2} at 195,8°C).

V_m = molar volume of the liquid adsorbed = 34,7 cm^3 for N_2

θ = the contact angle, usually taken to be 0°

R = gas constant: 8,134 x 10^7 ergs. deg^{-1}. mol^{-1}

T = 77K

With nitrogen and activated carbon

$$r_k = \frac{4,146}{log \, (P/P_s)} Angstroms \qquad\qquad (3.21)$$

This calculated radius is called the Kelvin radius and must be corrected for the condensed-material effect that has already occurred within the pores at high pressure (t - correction). The actual pore radius is then the sum of r_k and t.

$$r = r_k + t \qquad\qquad (3.22)$$

where r = true pore radius in Angstrom

r_k = Kelvin radius

t = the thickness of the adsorbed layer. The value of t is 3.54 V_a/V_m, where 3.54 is the thickness of one adsorbed nitrogen layer and V_a/V_m is the ratio of the volume adsorbed at relative pressure P/P^o to the volume adsorbed at the completion of one monolayer for nonporous solids.

Several workers [83-85] have attempted to determine values for t and have found reasonable agreement for many different nonporous solids. The average of various experimental values are given in Table 3.3 [83, 84].

Table 3.3: Adsorbed layer thickness at various relative pressures

P/P^o	t (Å)	P/P^o	t (Å)	P/P^o	t (Å)	P/P^o	t (Å)
.3	5.6	.62	7.7	.75	9.1	.87	11.5
.35	5.9	.64	7.8	.76	9.2	.88	11.9
.40	6.2	.66	8.0	.77	9.4	.89	12.2
.425	6.3	.67	8.1	.78	9.5	.90	12.7
.45	6.5	.68	8.2	.79	9.7	.91	13.1
.475	6.6	.69	8.3	.80	9.9	.92	13.7
.50	6.8	.70	8.5	.81	10.1	.93	14.4
.52	6.9	.71	8.6	.82	10.3	.95	16.2
.54	7.0	.72	8.7	.83	10.5	.96	17.3
.56	7.2	.73	8.8	.84	10.7	.97	19.2
.58	7.3	.74	8.9	.85	11.0	.98	22.1
.60	7.5	-	-	.86	11.2	.99	27.8

The Halsey [86] equation (3.23) conveniently fits the data in Table 3 and can be used as an alternative to calculate values of t.

$$t = 3.54 \left(\frac{5}{2,303 \log P^o/P} \right) 1/3$$ (3.23)

3.2.2 PORE-VOLUME DISTRIBUTION BY THE DENSITY FUNCTIONAL THEORY (DFT)

Density functional theory offers a practical alternative to both molecular dynamic- and Monte Carlo simulations. When compared with reference methods based on molecular simulation, this theory provides an accurate method for describing inhomogeneous systems and yet requires fewer calculations. Because the theory provides accuracy and fewer calculations, it is the basis of the technique embodied in the DFT software.

The system modelled consists of a single pore represented by two parallel walls separated by a distance H. The pore is open and immersed in a single component fluid (adsorptive) at a fixed temperature and pressure. Under such conditions, the fluid responds to the walls and reaches equilibrium. In this condition (by the definition of equilibrium), the chemical potential* at every point equals the chemical potential of the bulk fluid. The bulk fluid is a homogenous system of constant density; its chemical potential is determined by the pressure of the system using well-known equations. The fluid near the walls is not of constant density; its chemical potential is made up of several contributions that must at every point add up to the same value as the chemical potential of the bulk fluid.

---

* Chemical potential may be thought of as the energy change felt by a probe particle when it is inserted into the system from a reference point outside the system. It can also be defined as the partial derivative of the grand potential energy with respect to density (or concentration).

As noted previously, at equilibrium the system has a minimum (Helmholtz) free energy (H), known thermodynamically as the *grand potential energy* (GPE). Density functional theory describes the thermodynamic grand potential as a function of the single-particle density distribution. Therefore, calculation of the density profile that minimizes the GPE yields the equilibrium density profile. The calculation method requires the solution of a system of complex integral equations that are implicit functions of the density vector.

Since analytic solutions are not possible, the problem must be solved by using iterative numerical methods. Although calculations with these methods still require supercomputing speed, the calculation of many isotherm pressure points for a wide range of pore sizes is feasible.

The following graphs and accompanying text illustrate the results of using density functional theory to predict the behaviour of a model system.[62]

Figure 3.2 shows the density profile for argon at a carbon surface as calculated by density functional theory for a temperature of 87.3 K and a relative pressure of about 0.5.
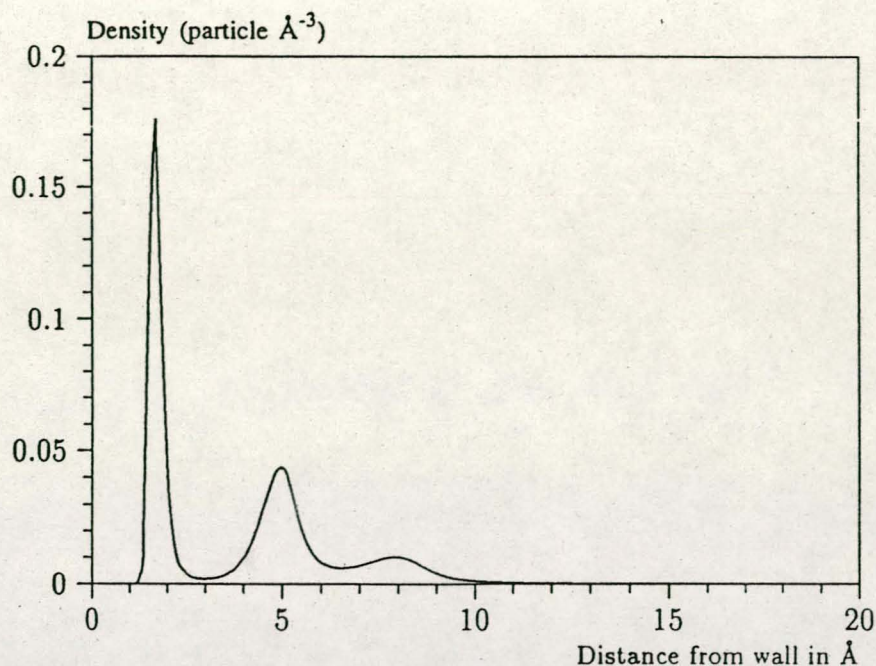
Figure 3.2: **Density profile for argon on carbon at 87.3 K and a relative pressure of 0.5.[62]**

This figure represents a cross-section of the region near the surface. Note the layered distribution of adsorbate; the first monolayer is sharply defined and a third layer can be distinguished. The area under the profile curve represents the amount adsorbed per unit area at this pressure. The positions of the maxima are separated by a distance determined by the size of the adsorptive atom.

Given the density profile, the amount adsorbed at the stated pressure can be easily calculated. Repeating this calculation over a range of pressures yields the adsorption isotherm for the model. If the value of H is very large, the isotherm obtained corresponds to that of an external, or *free*, surface. If H is smaller, a range of pressures will be reached at which two minima exist for the grand potential, showing the presence of two metastable phases having different density distributions but the same chemical potential. The phase with the lower GPE will be the stable one. As the pressure is increased, a point will be reached at which the other phase becomes the stable one. This *phase transition* reflects condensation of adsorbate in the pore; the pressure at which it occurs is called the *critical pore-filling*

pressure. This pressure corresponds to the condensation pressure predicted by the Kelvin equation in the classical model of pore filling.

Figure 3.3 shows how the profiles change with pressure for a model pore with H = 40 Ångstroms. The insets show the density profiles for the corresponding points of the isotherm.
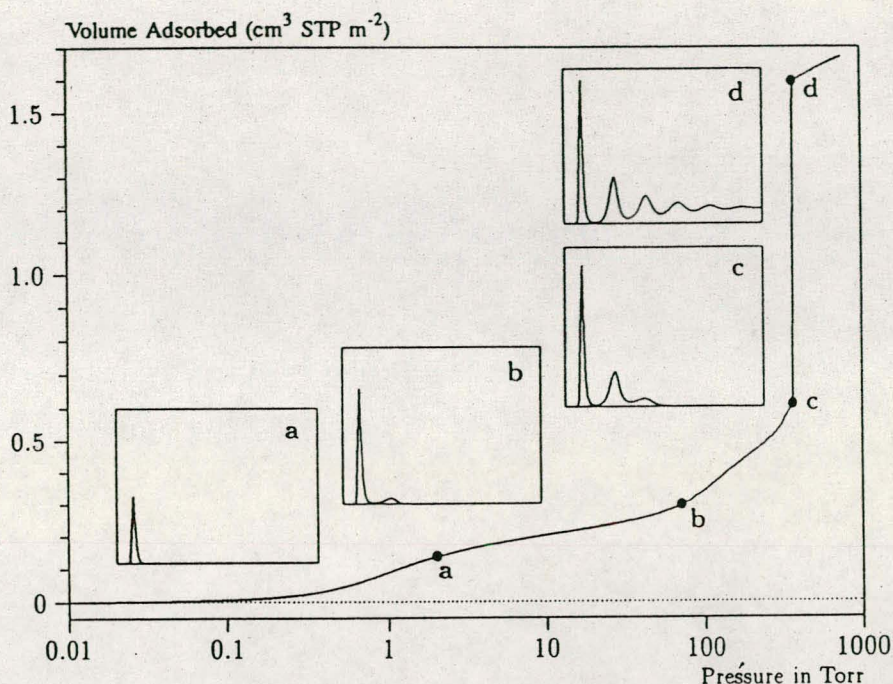
Figure 3.3:   **Model isotherm for argon at 87.3 K in a 40 Å slit in a carbon substrate [62]**

The profiles show the density distribution from one wall to the centre of the slit; the other half of the distribution is a mirror image of the profile.

As the pressure is increased from zero, almost all the adsorbed atoms occupy a position close to the surface. Inset *a* shows the profile corresponding to point *a* on the isotherm where the surface is about half-covered. At point *b*, the first layer contains sufficient atoms that it is more favourable for a new layer of atoms to be started. At point

c, a third layer is forming. Point *c*, for this size of slit, is the critical pore-filling pressure.   In inset *c*, the profile shows the density decreasing to near zero (actually the gas density) at 4 or 5 molecular diameters from the surface. Inset *d* shows the profile converging on a density similar to that of bulk liquid argon in the centre of the pore, indicating a phase transition.

It is worth noting that the adsorption isotherms for pores larger than the one shown in Figure 3.3 will be identical up to point *c*. The lower branch of the isotherm will simply continue to a higher pressure for larger pores. This trend is illustrated in Figure 3.4, where isotherms for some larger size pores are shown. It is clear that pore size is uniquely characterized by a corresponding critical pore-filling pressure. For large pore sizes, density functional theory produces results for the critical filling pressures that are in good agreement with those produced by the Kelvin equation.
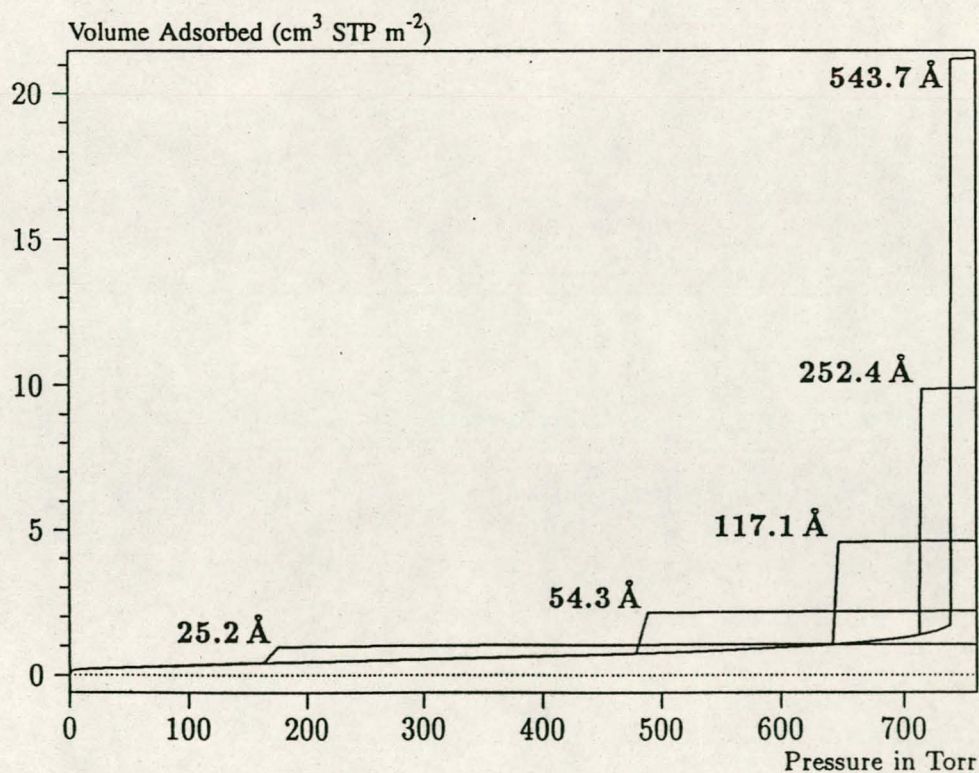
Figure 3.4:   **Model isotherms for some larger pore widths argon on carbon at 87.3 K. [62]**

Figure 3.5 shows model isotherms for pores in the micropore size range. Note the logarithmic scale for pressure.
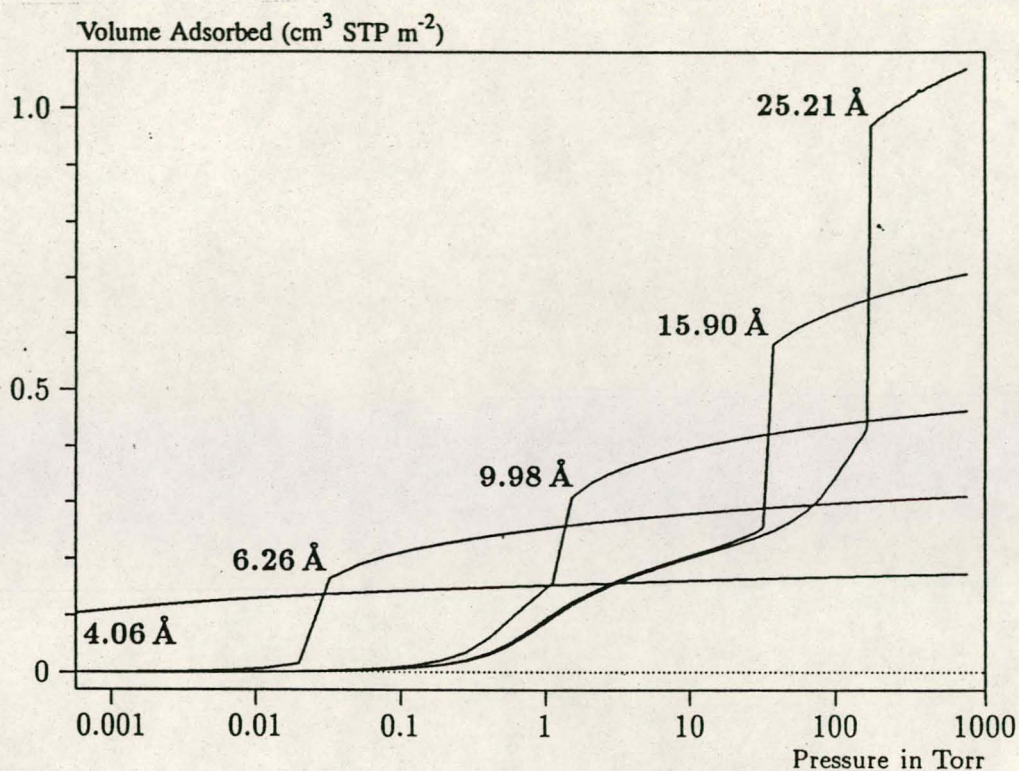
Figure 3.5:   Model isotherms for argon on carbon at 87.3 K in the micro pore size range of pore width.[62]

Pores of 4 Å width, barely larger than the argon atom (3.38 Å), fill at pressures below 1 millitorr. Pores below 15 Å fill before a monolayer is completed on the surface of the larger pores. In the micropore-size range, the pore volume fills more gradually with pressure and the total shape of the isotherm is important in characterizing the pore size.

The following section describes how the model isotherms can be used to obtain a pore size distribution from experimental data.

3.2.2.1   BASIS OF THE DFT METHOD

A sample of porous material may be characterized by its distribution of pore sizes. Each pore size present will contribute to the total adsorption isotherm in proportion to the fraction of the total area or pore volume of the sample that it represents. Mathematically, this relation is expressed by,

$$X(P) = \int x(P,H)f(H)dH \qquad\qquad (3.24)$$

where

$X(P)$ =   the experimental quantity adsorbed at pressure P,

$x(P,H)$ =   the quantity adsorbed per unit area at the same pressure, P, in a pore of size H, and

$f(H)$ =   the total area of pores of size H in the sample.

The integration is over all pore sizes in the sample. The function x(P,H) is called the *kernel function* and describes the model isotherms that have been evaluated numerically using density functional theory. The function f(H) describes how pore area is distributed by size in the sample and is easily converted to a pore volume distribution by size. Because there are no analytic equations for any of these functions, the problem must be solved in a discrete form; the integral equation becomes a summation:

$$X(P) = \sum x(P,H_i)f(H_i) \qquad\qquad (3.25)$$

Given a set of model isotherms, x(P,H), and an

experimental isotherm, X(P), the DFT software determines the set of positive values f(H) that most nearly, in a least-squares sense, solve the equation shown above. DFT also allows a selectable regularization constraint to be applied to avoid *over-fitting* in the case of noisy data. This process is referred to as *smoothing* in the DFT program.

3.3   APPARENT DENSITY

The apparent density of carbon is the mass in grams of 1 cm^3 of uniformly packed carbon in air. It is a measure of the physical quantity of carbon necessary to accomplish certain tasks. The apparent density is measured according to the ASTM method number D2854.

3.4   CHEMICAL BREAKTHROUGH ANALYSIS

The chemical breakthrough analysis was done on a test bench as illustrated Figure 3.6. A total flowrate of 30 $\ell.min^{-1}$ was used with a temperature of 20 ^{0}C and relative humidity of 70 %. The temperature was controlled by controlling the laboratory conditions and the humidity was generated by controlled air flow through a water bubbler.

The determination of the adsorption rate constants and capacities with the Wheeler equation requires a variation in the carbon mass in order to plot three points on the graph. The carbon mass was varied by means of varying the number of filters tested. The carbon was packed in filter cartridges (Figure 3.7) for application in the industry. The same packing was used and the carbon mass was accurately controlled as 45 g per filter cartridge. A special holder was manufactured in order to evaluate three filters in series and to monitor the breakthrough sequentially through one, two and three filters.
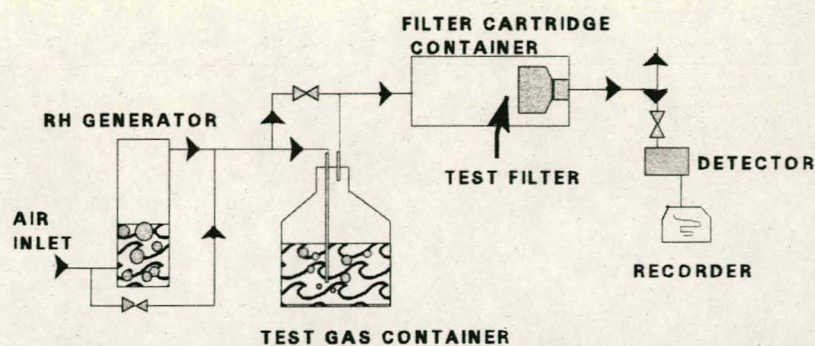
Figure 3.6 The filter test bench built for the evaluations
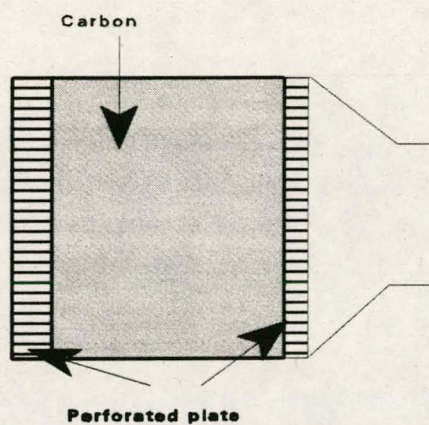
Figure 3.7   Filter cartridge used for the experiments

The detection is done by means of a flame ionisation detector (FID). The detector was installed in a gas chromatograph. The gas chromatograph conditions used are listed in Table 3.4.

Table 3.4: Gas chromatograph conditions

Detector temperature	250 °C
Oven temperature	100 °C
Hydrogen flow rate	50 ml.min^{-1}
Airflow rate	250 ml.min^{-1}
Carrier gas (test gas)	300 ml.min^{-1}

The 30 ml.min^{-1} was drawn from the outlet gas by means of a vacuum pump. The flow was set and controlled with a needle valve.

3.4.1 MATERIALS

Activated carbon

The coconut shell activated carbon was acquired from Haycarb in Sri Lanka and the coal-based carbon from CALGON in Belgium. The particle-size distribution used was 12 x 30 USS. The grades were HTO and BPL respectively and the carbon was impregnated with copper and chromium.

Chemicals

Carbon tetrachloride and Hydrogen cyanide were both AR grade. The addition of the test gas was done by two methods.

3.4.2 CCl$_4$ ADDITION

The addition of the CCl$_4$ was done by using a DOSIMAT dispenser. The liquid was disposed at a constant rate of 0,188 ml.min^{-1} and 0,094 ml.min^{-1}. This corresponded to an addition of 10 mg.l^{-1} and 5 mg.l^{-1} respectively. The calculation for the addition rate was as follows:

Density of CCl_4 =   1,5881

Flowrate   =   30 $l.min^{-1}$

Calculated addition   =   10 and 5 $mg.l^{-1}$

Dosage rate X Density / Flowrate = Addition

By utilising this method an accurate challenge concentration can be maintained.

3.4.3 HCN ADDITION

The addition of the hydrogen cyanide (HCN) as a gas was a problem. The reason being difficulty of control of addition as the pressure changed. As the boiling point of HCN is 22 ^{0} C and the experimental temperature was 20 ^{0}C it was possible to use the HCN in liquid form. The HCN was synthesized and collected in a vapour generator. The HCN temperature was maintained at 20 ^{0}C. The main flow rate was split and a flow of 3 $ml.min^{-1}$ was bubbled through the HCN as illustrated in Figure 3.6. The addition was controlled and the amount of HCN used determined by weighing the HCN before and after the test. The weighing was done on a four-decimal balance.

CHAPTER IV

RESULTS AND DISCUSSION

4.1 PHYSICAL CHARACTERISTICS

4.1.1 SPECIFIC SURFACE AREA

The BET (Brunauer-Emmett-Teller) adsorption method [49] is now universally accepted [10] as a standard procedure for the characterization of a variety of adsorbents. It is also recommended by IUPAC [9]. The surface area of the carbon in this study was determined with N_2 at 77K. The samples were conditioned overnight at 210°C. Outgassing was performed by heating the sample to volatilize and desorb any foreign material that may have contaminated its surface and pore space. The results obtained are listed in Table 4.1 and illustrated in Figure 4.1 and the isotherms are illustrated in Figure 4.2 and Figure 4.3.

TABLE 4.1 Active surface of unimpregnated, impregnated (Cu/Cr/Ag) and impregnated carbon exposed to HCN

SAMPLE	BET SURFACE AREA $m^2.g^{-1}$	
	COAL	COCONUT
Unimpregnated carbon	1243	1 450
Impregnated carbon	730	950
Exposed Impregnated carbon	623	811

Note: These are averages of two analyses per sample, and two samples of each were analysed. Where the standard deviation exceeded 2σ, a third analysis was done.
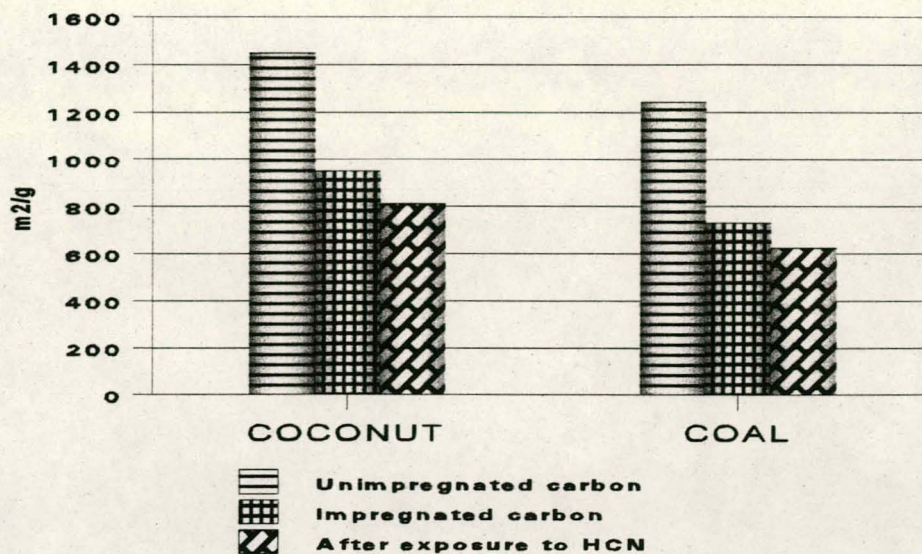
Figure 4.1. The active surface as function of the impregnation and HCN exposure
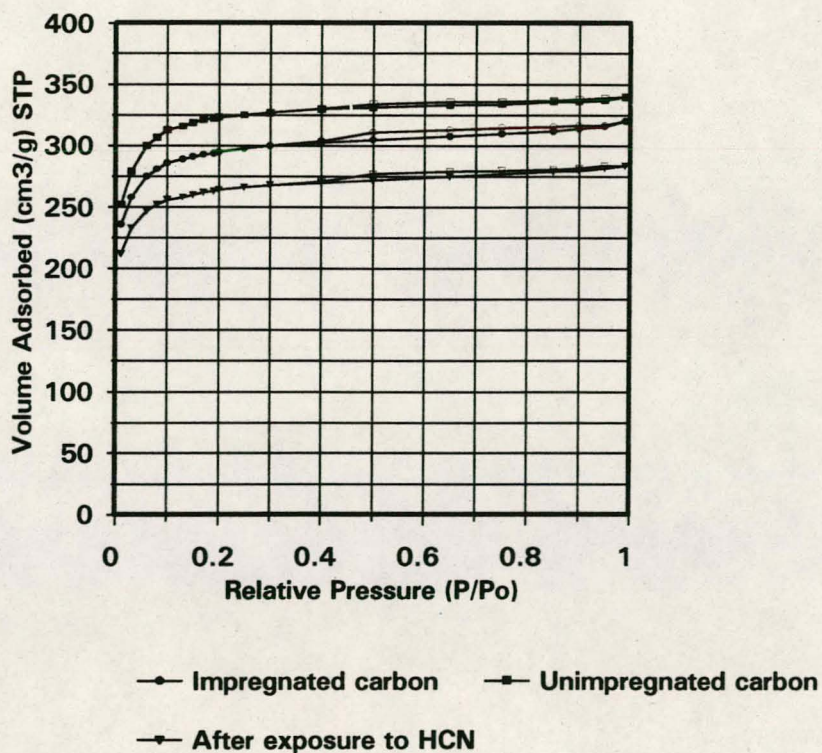
Figure 4.2 The adsorption/desorption isotherms of the unimpregnated and impregnated coconut shell carbon and the impregnated carbon after exposure to HCN.

Figure 4.3 — legend:
- Unimpregnated carbon
- Impregnated carbon
- After exposure to HCN
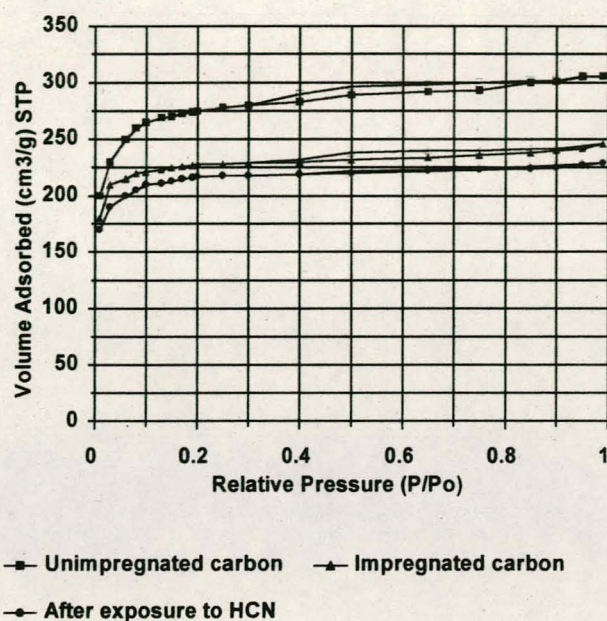
Figure 4.3 **The adsorption/desorption isotherms of the unimpregnated and impregnated coal carbon and the impregnated carbon after exposure to HCN.**

The adsorption isotherms of both the coconut shell and coal-based carbons had typical Type I profiles. This was typical of microporous adsorbents. The coal-based carbon isotherms showed a slight increase in the central portions of the isotherms and which was indicative of the presence of some mesopores. The uptake did not increase continuously as with Type II isotherms, but came to a limiting value in a plateau. This limit was reached because the pores was so narrow that they could not accommodate more than a single layer on their walls; the plateau thus corresponded to the completion of the monolayer. Very small hysteresis values were measured. Micropore filling was significant at relative low partial pressures, typically < 0,1 P/P° The adsorption process was basically complete at 0,5 P/P°. The very steep region at low P/P° was due to the filling of very narrow pores and the limiting uptake depended on the accessible micropore volume [50]. The reduction in the available

pores was clear from the adsorption isotherms. The typical Type I isotherms were maintained due to the microporous structure but the pore volume decreased because of the shifts from the unimpregnated to the impregnated after exposure to the HCN.

The results show two important factors, namely, the reduction of approximately 35% (coconut shell carbon) and 42% (coal-based carbon) in the active surface area after the metal catalysts were impregnated on the carbon. The reason for this was the partial blocking of the pores by the impregnants.   This effect can be illustrated as follows;

CARBON GRANULES

Impregnants

Unimpregnated Carbon   Impregnated Carbon
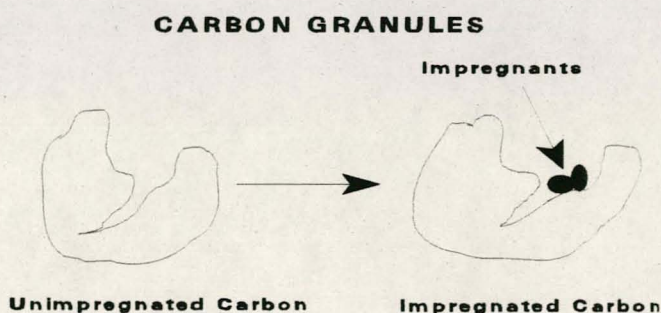
Figure 4.4   Illustration of partial blocking of the pores after impregnation

The further 14% (coconut carbon) and 15% (coal-based carbon) reductions, respectively, in the surface area after exposure to HCN were the direct result of the filtration reaction, since the HCN reacted with the Cu/Cr complex deposited on the carbon. The decrease was also reflected in the adsorption isotherms as illustrated in Figure 4.2 and Figure 4.3. The accessibility of the micropores was directly affected by both the impregnants and the reaction products. This had a direct influence on the filtration capacity of the impregnated carbon used in respirator filters. The effect of this is discussed in paragraph 4.2. The results showed that the reduction in the active surface as

function of impregnation and exposure to HCN was not a function of the carbon.

4.1.2 PORE-VOLUME DISTRIBUTION

The increasing use of activated carbons has increased interest in that region of the pore-size spectrum near a few molecular diameters. Most commonly, routine methods employ the data of nitrogen adsorption taken at 77 K and use the Kelvin equation to correlate pore size to the pressure at which condensation in the pore takes place, together with a relation to correct for the thickness of the adsorbed layer at the point of condensation. The method of *Barrett, Joyner* and *Halenda* [51] is typical, and the thickness curves of *de Boer, Halsey* or *Harkins* and *Jura* are frequently employed [52].

While the Kelvin equation may be regarded as exact in the large-pore area, its accuracy decreases as the pore dimensions become less than a large multiple of molecular size.

The determination of pore size distributions in the micropore region (defined as 2 mm and below) enjoys less consensus. Methods based on potential theory of the Dubinin School [53], t or alpha plots [54] or the MP method [55] are in wide use. More recently, *Horvath* and *Kawazoe* [56] published a quasi-thermodynamic method akin to the Kelvin equation in that is describes a step-function mapping of equilibrium relative pressure for pore-filling to micropore size modelled as width of slit-like pores. This theory has since been extended to include cylindrical pores by *Saito* and *Foley* [57]. While these authors understandably praise the "Kelvin-like simplicity" of the method, it seems that the reality of adsorption in micropores may be somewhat more complex.

During the past decade great advances have been made in the understanding of the structure and thermodynamics of

inhomogeneous systems of simple molecules, including surface tension and density profile of the free liquid-vapour interface. This has led to investigations of the behaviour of fluids at free solid surfaces [58] and fluids confined by parallel or cylindrical walls [59]. Density functional theory has been especially useful in these investigations, together with computer simulations which can serve as a definitive reference [60].

In 1989, *Seaton, Walton* and *Quirke* [61] published the first description of a method by which model isotherms calculated from density functional theory were used to determine a pore-size distribution from experimental isotherms. A slit geometry was assumed. It was further assumed that the size distribution could be described by a bimodal lognormal distribution function.

Olivier and *Conklin* [62] recalculated the model isotherms of Seaton et al using similar assumptions, and showed that it was feasible to extract the pore-size distribution from experimental data by a deconvolution technique without the restriction of assuming a functional form for the distribution. The methods are thus applicable to the entire range of pore sizes accessible by the adsorptive molecule, and they approach the Kelvin result at the large-size limit.

A comparative study was done by Russel and LeVan [63] of different pore-size distribution measurement methods, that is, the M.P. method, theory of volume-filling of micropore (TVFM) method, the Horvath and Kawazoe method, the Seaton, Walton and Quirke method and the utilization of the water desorption isotherm. It was concluded that the Seaton, Walton and Quirke method "offers the greatest flexibility and scope for refinements". They also stated that each model embodies a degree of uncertainty, and that it is difficult to discern which is the most accurate.

It was therefore decided to use the DFT method for the determination

of the pore size distributions. The distributions were determined for the unimpregnated carbon, the impregnated carbon and the distribution after exposure to HCN. The three distributions are illustrated in Figure 4.5 and Figure 4.6. The results are listed in Table 4.2 and illustrated in Figure 4.7.
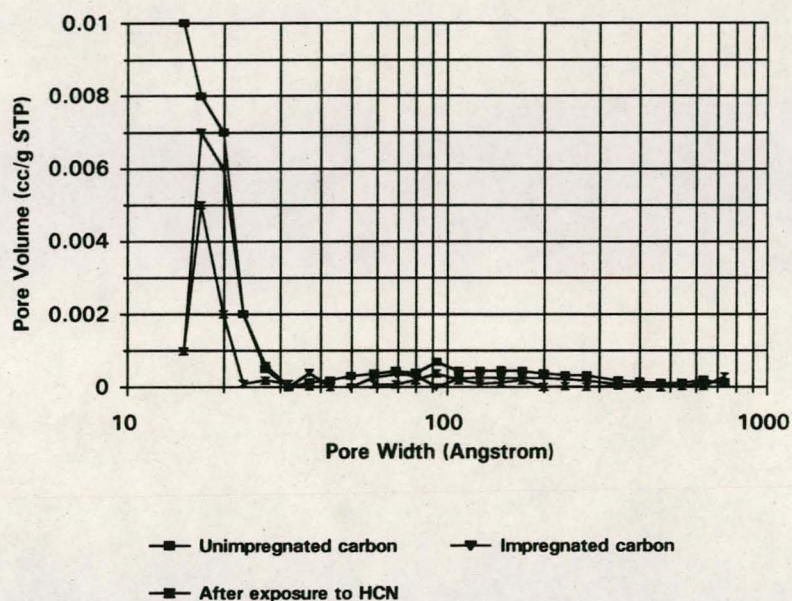
Figure 4.5 **Pore-size distribution of the coconut-based unimpregnated and impregnated carbon and the impregnated carbon after exposure to HCN as determined using the DFT method.**
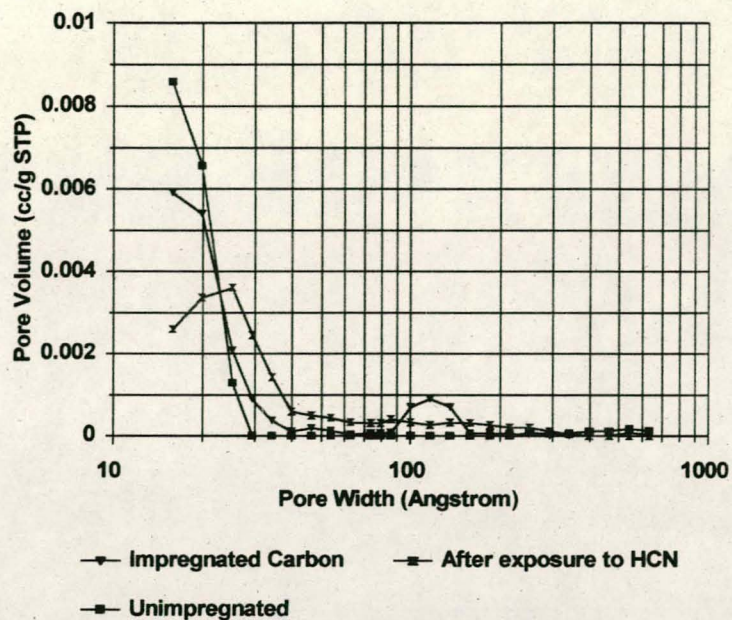
Figure 4.6   Pore-size distribution of the coal-based unimpregnated and impregnated carbon and the impregnated carbon after exposure to HCN as determined using the DFT method.

TABLE 4.2.   The micropore and mesopore volumes as determined with the DFT-method.

SAMPLE	PORE VOLUME DISTRIBUTION (ml.g^{-1})			
	MICROPORE		MESOPORE	
	COCONUT	COAL	COCONUT	COAL
Unimpregnated	0,65	0,59	0,19	0,27
Impregnated	0,58	0,52	0,09	0,19
After exposure to HCN	0,36	0,36	0,07	0,08
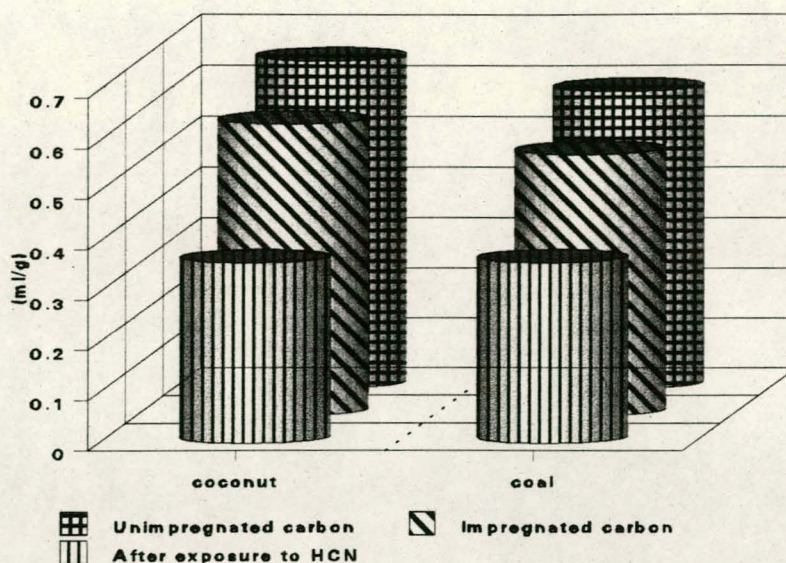
Figure 4.7   The micropore volumes as function of impregnation and exposure to HCN, respectively

The reduction in the available pores is clear from the adsorption isotherms. The typical Type I isotherms are maintained due to the microporous structure but the reduction in the pore volume caused for the shifts from the unimpregnated to the impregnated, to the impregnated, after exposure to the HCN.

The reduction in the micropore volume of the coconut based carbon was 11% and 12% for the coal-based carbon with the addition of the impregnants. The micropore volume of the coconut-shell carbon was reduced further by 37,9% and the coal-based carbon micropore volume was reduced by 30,8% after exposure to HCN. This aspect has not been reported previously in the literature and it was never regarded as a problem. The reduction in micropore volume was a two-fold effect. First, the micropore volume was reduced by the addition of the impregnants. It was therefore a masking effect by the impregnants which were deposited in the micropores and macropores. Little has been reported regarding this effect of adsorbate capacities on carbons containing various amounts of impregnants [64, 65].

The second reduction was due to the reaction products formed when

the HCN reacted with the impregnants. These reaction products can be summarized as follows:

HCN in the presence of Cu^{2+} tends to be oxidised preferentially to cyanogen, (CN_2) , in a heterogeneous reaction [66] analogous to the well-documented oxidation of cyanide ion in aqueous solution;

$$Cu^{2+} + 2\,CN^- \rightarrow CuCN + \tfrac{1}{2}(CN)_2$$
$$(CN)_2 + 2H_2O \xrightarrow{Cr\ 6+} H_2N-\underset{\substack{\parallel \\ O}}{C}-\underset{\substack{\parallel \\ O}}{C}-NH_2$$

oxamide
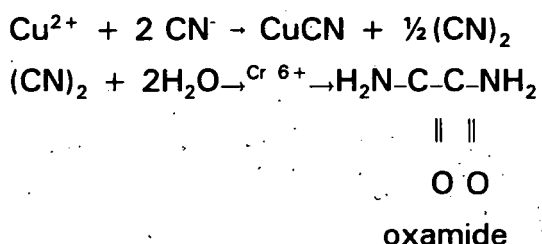
A detailed description of the reaction of HCN with a copper-impregnated and chromium-impregnated carbon was given by *Alves* and *Clark* [67].

The second reduction in the micropore volume after exposure to HCN was therefore a direct result of the deposition of the oxamide. The oxamide partially blocked the micropores. This aspect has never been mentioned in the literature, and is discussed further in paragraph 4.2. The reduction was not affected by the use of different base carbons. It was thought that the larger mesopore volume of the coal-based carbon would result in a smaller reduction in the pore volume, but this dit not happen. It is also clear from Figure 4.6 that the mesopore volume was drastically reduced after impregnation and exposure to HCN. This was an indication that the impregnant was adsorbed in the mesopores.

4.2   CHEMICAL PROTECTION

4.2.1 CCl$_4$ PROTECTION

The protection times (the time at which the exit concentration is equal to 10% of the challenge concentration) as function of relative humidity, carbon base material, challenge concentration and carbon weight for 1,2 and 3 filter cartridges are listed in Table 4.3 and illustrated in Figure 4.8 and Figure 4.9.

TABLE 4.3. Protection time against CCl$_4$ as function of carbon weight carbon base material, challenge concentration and relative humidity

CARBON WEIGHT (g)	PROTECTION TIME (min)			
	CONCENTRATION 10 mg.l^{-1}			CONCENTRATION 5 mg.l^{-1}
	0% RH		70% RH	0% RH
	COAL	COCONUT	COCONUT	COCONUT
45	82	97	75	197
90	172	197	172	413
135	275	290	253	623
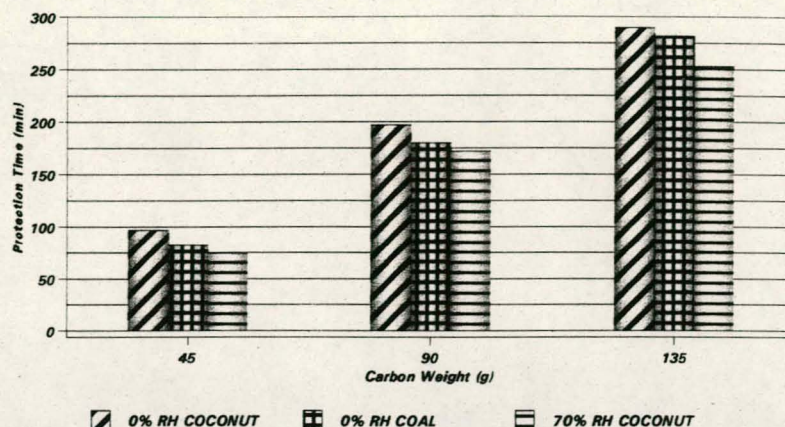
Figure 4.8. **Protection against CCl$_4$ as function of carbon weight, base material and %RH**

Consider the Wheeler equation (paragraph 2.5) applied in the following format, namely;

$$t_b = \frac{W_e}{C_o Q}\left[W - \frac{\rho_B Q}{k_v}\,\ln\left(\frac{C_o}{C_x}\right)\right] \qquad (2.28)$$

where Q is the flow rate (cm^3.min^{-1}), t_b the protection time (min), C$_x$ the exit concentration (g.cm^{-3}), C$_0$ the inlet concentration (g.cm^{-3}), ρ_B the bulk density of the packed bed (g.cm^{-3}), k$_v$ the first-order adsorption rate constant (min^{-1}), W the carbon weight (g) and W$_e$ the kinetic saturation capacity (g.g$_c^{-1}$).
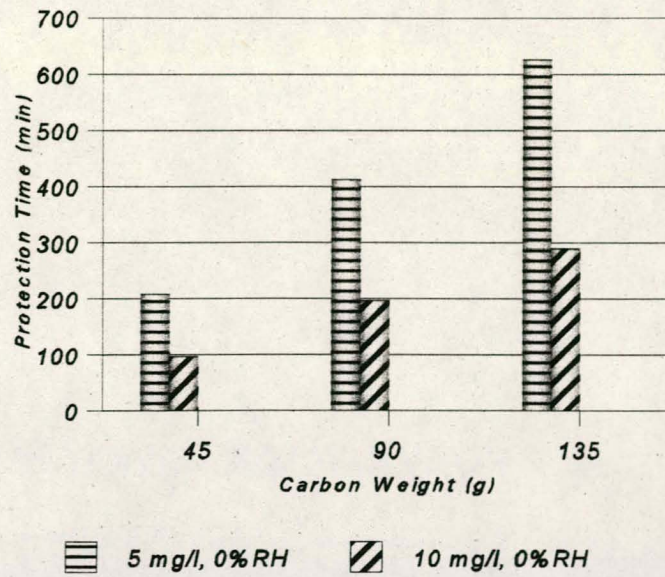
Figure 4.9 **Protection of the coconut base carbon against CCl$_4$ as function of challenge concentration**

The experimental values of the protection time ,t_b , as a function of the carbon-bed weight, W, were subjected to linear regression analysis in the form of y = a + bx. The results of these analysis are shown in Table 4, Table 5 and illustrated in Figure 4.9 and Figure 4.10.

A simple transformation of equation (2.28) can be shown as

$$t_b = \frac{W_e \rho_B}{C_o k_v} \ln\left(\frac{C_o}{C_x}\right) + \frac{W_e W}{C_o Q} \tag{4.2}$$

from which similarity considerations lead to the identities

$$a = \frac{W_e \rho_B}{C_o k_v} \ln\left(\frac{C_o}{C_x}\right) \tag{4.3}$$

$$b = \frac{W_e}{C_o Q} \qquad\qquad (4.4)$$

for the regression graph. The kinetic adsorption capacity W_e was calculated from the slope of the experimentally determined straight-line equation, and insertion into equation (4.4) of the values for the inlet concentration C_0 and the flow rate Q. The pseudo-first-order adsorption rate constant k was calculated from the y-intercept of the regression equation, and insertion into equation (4.3), of the bulk density of the packed bed ρ_B, the inlet to exit concentration ratio C_0/C_x, the value for C_0, and the determined value of W_e. By setting $t_b = o$ in the regression equations of Table 4.4, and solving for W, it was possible to obtain the value of W_c, the critical weight of the carbon bed, since by definition

$$W \cong W_c \qquad\qquad (4.5)$$

when $t_b = 0$ and the inlet concentration is instantaneously reduced to the exit concentration by the carbon bed. The value for W_c was calculated from the following equation ($t_b = 0$ in equation (4.2)):

$$W_c = \frac{\rho_\beta Q}{k_v} \ln\left(\frac{C_o}{C_x}\right) \qquad\qquad (4.6)$$

or the value was taken from the graph by measuring the x-axis intercept. The values of W_c, W_e and k_v in units of min^{-1} are shown in Table 4.5.

TABLE 4.4. Regression equation for the CCl$_4$ protection time

CHALLENGE CONCENTRATION	RH(%)	REGRESSION EQUATION	COEFF OF CORRELATION
10 mg.l^{-1}	0 (COCONUT)	$t(min) = -7,67 + 2,2W$	0,9995
	0 (COAL)	$t(min) = -18 + 2,22W$	0,9998
	70 (COCONUT)	$t(min) = -11,33 + 1,98W$	0,9973
5 mg.l^{-1}	0 (COCONUT)	$t(min) = -15 + 4,73W$	0,9995

TABLE 4.5. Adsorption variables for CCl$_4$ derived from the regression equations

	UNIT	Challenge concentration 10 mg/l						Challenge concentration 10 mg/l	
		0%RH (COAL)		0%RH (COCONUT)		70%RH (COCONUT)		0%RH (COCONUT)	
		CALC	EXP	CALC	EXP	CALC	EXP	CALC	EXP
Adsorption capacity (W$_e$)	g.g^{-1}	0,665	0,591	0,660	0,649	0,594	0,545	0,709	0,675
Critical bed weight (W$_c$)	g	8,0		3,5		5,7		3.2	
Adsorption rate constant (k$_v$)	min^{-1}	9528		22191		13520		24411	
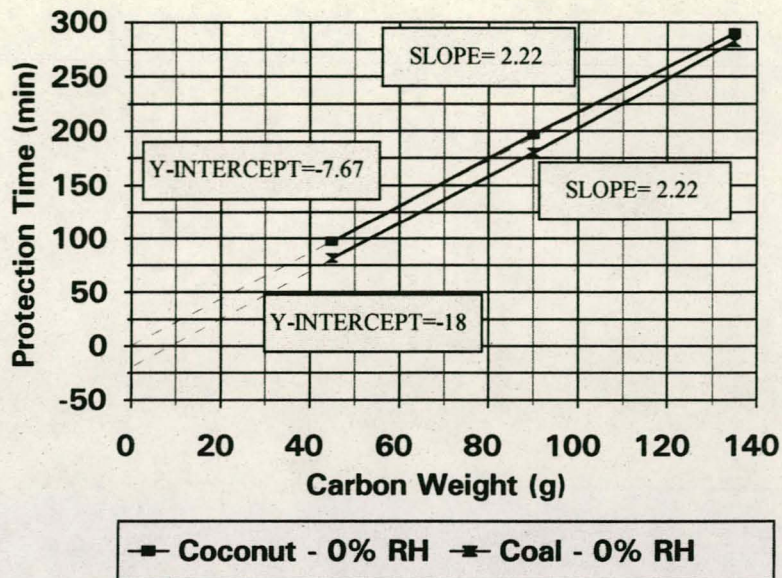
Figure 4.9 The regression analysis of the CCl_4 protection as function of carbon weight and the relative humidity
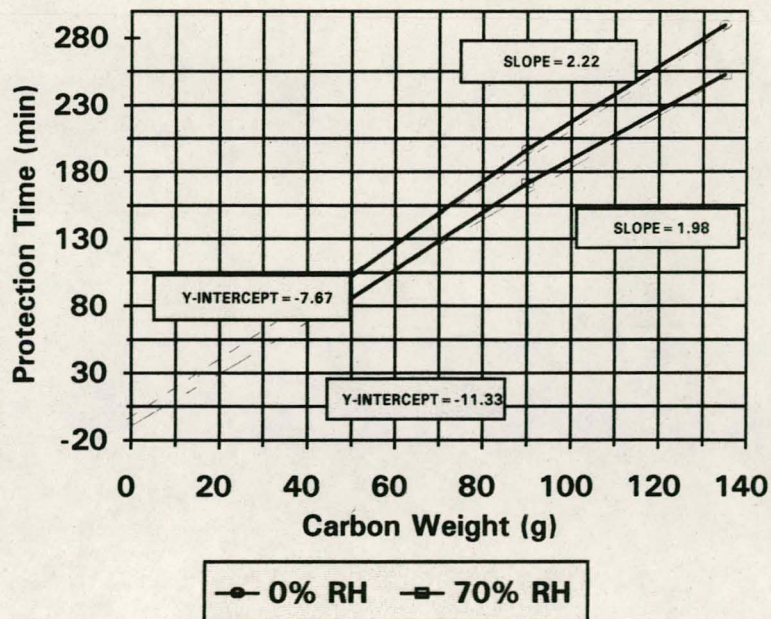
Figure 4.10 The regression analysis of the CCl_4 protection as function of carbon weight and carbon type

Since *Levenspiel* [72] has shown that passage of vapour through a bed of packed granules can be approximated by plug flow, the CCl_4 vapour mixture had a mean residence time of 0,16 s for one filter cartridge, 0,32 s for two filter cartridges and 0,48 s for three filter cartridges in the bed. During the duration of the test, the adsorption-rate constant for 0% RH for coconut-based carbon was 22191 min^{-1} and for 70% RH 13520 min^{-1} (Table 4.5). In accordance with the concept of a first-order reaction it was perceived that a limit of 22191 and 13520 volumes of gas-air mixtures (containing1 x 10^{-3} g CCl_4 .cm^{-3}) for 0% RH and 70% RH respectively, could be reacted with or adsorbed by the carbon per minute. Therefore, the CCl_4 in each volume of CCl_4 -air mixture was adsorbed by the carbon in 0,0027 s and 0,0044 s respectively. Even under these extreme conditions the time of adsorption occurred in only 1,7% (one filter cartridge; 0% RH), 0,6% (three filter cartridges, 0% RH), 2,8% (one filter cartridge, 70% RH) and 0,9% of the residence time in the carbon bed. It was therefore assumed that the capacity values were optimal for the conditions used.

The CCl_4 adsorption mechanism and the thermodynamic aspects can be defined as follows: If it is assumed that the adsorption mechanism can be represented by the process

$$V + S \underset{K_2}{\overset{K_1}{\rightleftharpoons}} V.S \tag{4.7}$$

then the rate of the process is given by the following equation [68]:

$$-d(V)/dt = k_1(V)(S) - k_2(V.S) \tag{4.8}$$

where $(V)(S)$ and $(V.S)$ represent the concentration of adsorbable vapour and the unoccupied sites, respectively. The concentration is the number of molecules and sites per unit volume of bulk carbon. Since the number of active sites is large compared with that of the incoming vapour molecules, that is, $(S) >> (V)$, the rate equation

can be written as

$$-d(V)/dt = k_1'(V) - k_2(V.S) \tag{4.9}$$

since (V) becomes the limiting step.   Material balance shows that

$$(V_0-V) = (V.S) \tag{4.10}$$

and equation (4.9) becomes

$$-d(V)/dt = (k_1' + k_2)(V) - k_2(V_0) \tag{4.11}$$

If k_2 is markedly less than k_1', then pseudo-first-order kinetics would appear, a fact which was experimentally established.

The carbon granule was viewed as being surrounded by a volume of space within which there was a specific concentration of gas, starting with the inlet concentration C_0 at $t_b = 0$. As adsorption of the gas in this surrounding volume proceeded with time, the number of gas molecules per unit volume capable of being adsorbed decreased. The rate of this decrease was the rate of gas adsorption and its concentration dependence determined the order.

If CCl_4 molecules were to be placed on a surface as close as possible to one another, and assuming a cross-sectional area of $36,7 \times 10^{-16}$ cm^2 per molecule and no interactions, there would be $2,7 \times 10^{14}$ molecules per cm^2 . On the assumption that one gas molecule is adsorbed onto one active site, there would then be a maximum of $2,7 \times 10^{14}$ active sites per cm^2 . *Hayward* and *Trapnell* [69] state that there are an average of 10^{15} active sites per cm^2 on a clear metal

surface. Since the activated carbon had an internal pore area of 950 m^2/g there would be a maximum of 2,57 x 10^{21} active sites per gram of carbon. Assuming that all the sites were available for CCl_4 adsorption, it would be possible for 2,57 x 10^{21} CCl_4 molecules to be adsorbed per gram of carbon.

The mean inlet concentration in this experiment of 10^{-3} g CCl_4.cm^{-3} air at 25°C was equivalent to 3,96 x 10^{16} CCl_4 molecules.cm^{-3} of air.

Since the airflow rate was 30 000 cm^3.m^{-1}, the addition of the CCl_4 amounts to 1,188 x 10^{21} molecules.m^{-1}. This was 53,5% of the calculated available active sites of 2,57 x 10^{21}. The theoretical capacity for the 0% RH with the coconut based-carbon was 0,660 g.g^{-1} carbon, which amounts to 2,61 x 10^{21} CCl_4 molecules.g^{-1} carbon, and the experimental capacity was 0,630 g.g^{-1} carbon, which amounts to 2,49 x 10^{21} CCl_4 molecules.g^{-1} carbon. This corresponds well with the calculated value of possible CCl_4 adsorption. The theoretical capacity at 70% RH was 0,594 g.g^{-1} carbon which amounted to 2,16 x 10^{21} CCl_4 molecules.g^{-1} carbon. This amounts to 16% less adsorption than the calculated value of 2,57 x 10^{21} CCl_4 molecules.g^{-1} carbon. These results were in line with what *Wood* [70] reported on his studies. He calculated the number of pores per gram of carbon with CCl_4 to be 3,7 x 10^{21} for dry conditions and the average number of pores per gram of carbon 2,6 x 10^{21}. The reduction with humidity in the number of molecules per gram carbon is a direct effect of occupation of the adsorption sites by water molecules. This is illustrated in Figure 4.11.
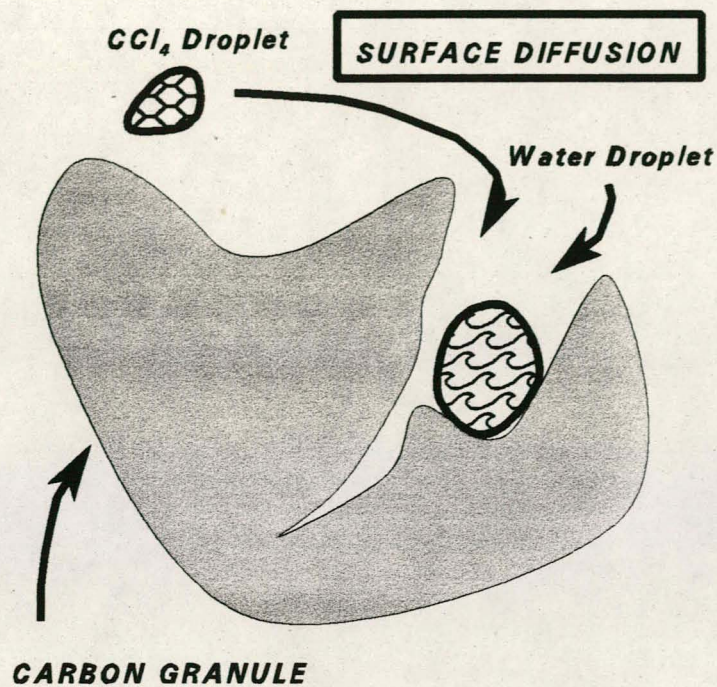
Figure 4.11 **An illustration of the occupation of active sites by water molecules**

However, the water can be displaced by the CCl_4. This phenomenon was reported by *Hall et al* [71] who investigated the filtration of trichloronitromethane as function of humidity, as illustrated as in Figure 4.12.
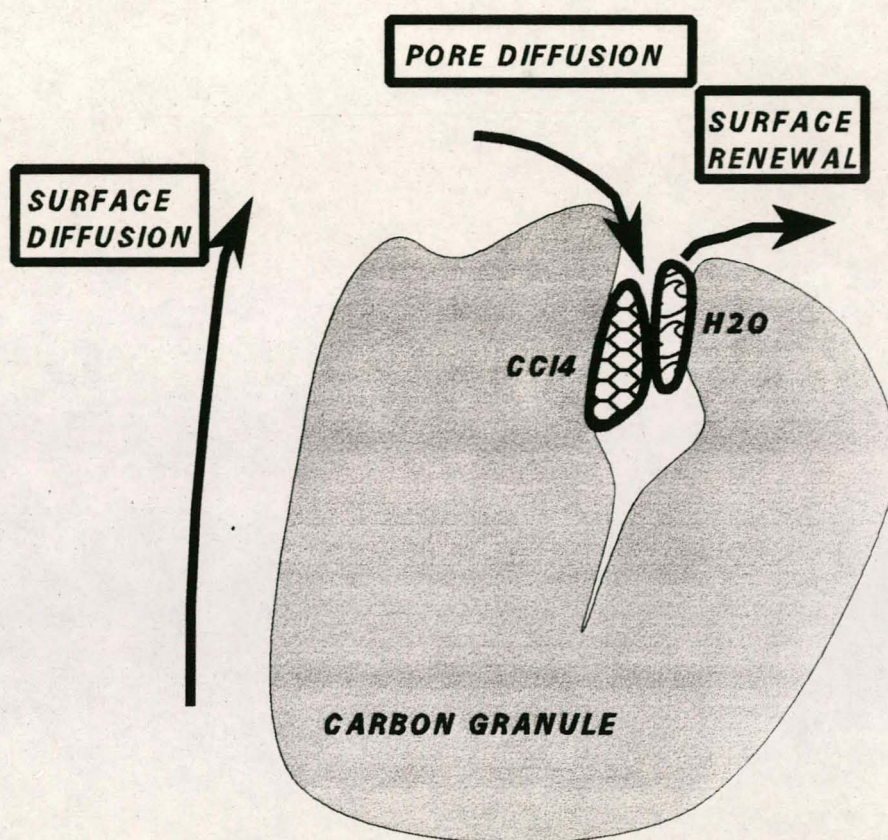
Figure 4.12 An illustration of the displacement of water from the surface

The CCl_4 is not affected by the impregnants, so that pure adsorption is represented by these characteristics. This was confirmed by results reported by *Ackley* [73]. The different processes during the physical adsorption of CCl_4 can then be illustrated as in Figure 4.13.
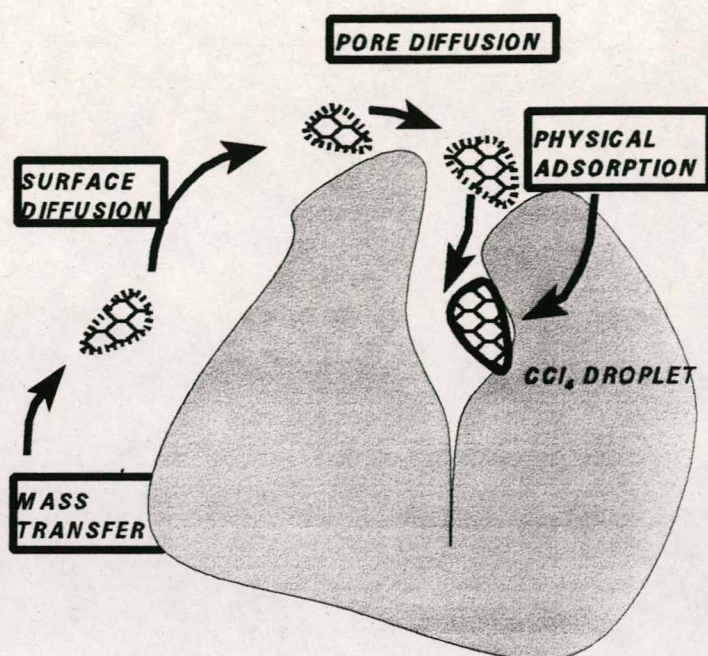
Figure 4.13 An illustration of the different processes during physical adsorption

4.2.2 AGAINST HCN PROTECTION

The protection time against HCN was evaluated for only the coconut-based carbons since the chemisorption of HCN is a function only of the impregnants. The protection times as functions of one, two and three filter cartridges are listed in Table 4.6 and illustrated in Figure 4.14.

TABLE 4.6. Protection time against HCN as function of carbon weight and relative humidity

RESIDENCE TIME	CARBON WEIGHT	PROTECTION TIME (min)	
(sec)	(g)	0% RH	70% RH
0,16	45	15	13
0,32	90	48	50
0,48	135	98	102
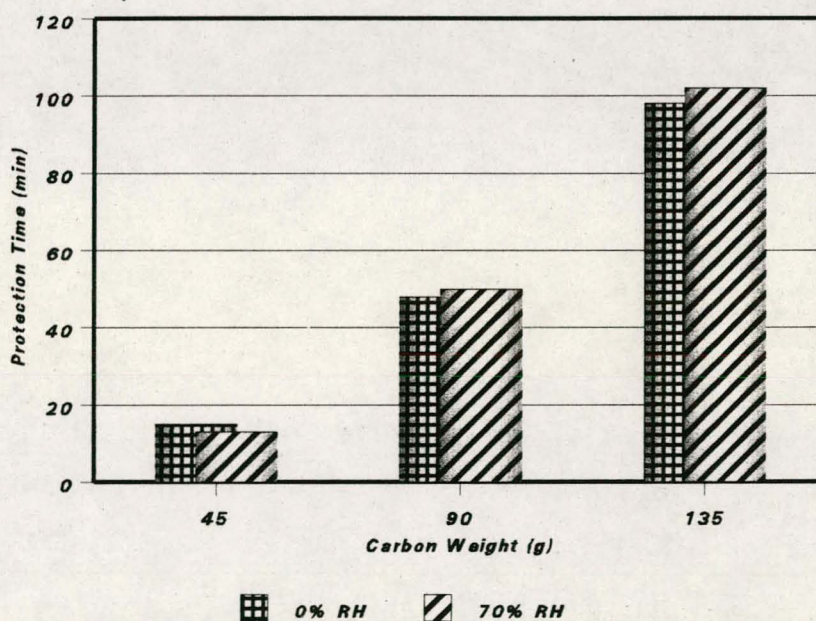
Figure 4.14 Protection against CCl_4 as function of carbon weight and % RH.

The filtration of HCN is entirely dependent on the impregnants (Cu^{2+} and Cr^{6+}) since HCN was filtered only by chemisorption. The filtration reactions are listed in paragraph 4.1.2

If plug flow is assumed for the movement of gas through the carbon bed, the mean residence time τ in the bed can be shown as

$$T = \frac{L}{V_l} = \frac{V}{Q} = \frac{W}{\rho_B \, Q} \qquad (4.12)$$

where L =   bed depth (cm)

             V_l =   superficial linear velocity (cm.min^{-1})

             V =   volume of the bed (cm^3)

             ρ_B =   bulk density of the carbon bed (g.cm^{-3})

             Q =   volumetric flow (cm^3.min^{-1}).

Substitution into the Wheeler equation, eq.(4.1), gives t_b as a function of T:

$$t_b = \frac{W_e \, \rho_B}{Q} \left[T - \frac{1}{k_v} \ln \left(\frac{C_o}{C_x} \right) \right] \qquad (4.13)$$

In heterogeneous catalysis (chemisorption), in contrast with heterogenous adsorption, the attenuation of C_0 to C_x can be independent of time, and therefore the kinetics of this process were studied under steady-state conditions. Under these conditions, the first-order equation relating the concentration attenuation is

$$\frac{C_x}{C_o} = \exp k_c T \qquad (4.14)$$

where k_c is the first-order catalytic rate constant (min^{-1}).

If, in the kinetics of gas adsorption, a finite concentration left the bed immediately and if the concentration remained relatively steady and independent of time, equation (4.1) could be applied to these conditions by setting $t_b = 0$.

Then it can be shown for the non-trivial case that

$$\ln\left(\frac{C_x}{C_o}\right) = -\frac{k_v W}{\rho_\beta Q}$$

(4.15)

and from equation (4.12) that

$$\frac{C_x}{C_o} = \exp k_v \tau$$

(4.16)

Equation (4.14) and (4.16) are thus equivalent in form, with the rate constant k_v denoting adsorption and k_c denoting chemisorption. The essential difference between adsorption and chemisorption is that in adsorption, the concentration attenuation is dependent on both residence time τ and test time t_b, whereas in chemisorption it is dependent only on τ.

If t_b vs τ is plotted the equation predicts a straight line with the slope and y-intercept as follows:

$$a = \frac{W_e \rho_B}{C_o k_v} \ln\left(\frac{C_o}{C_x}\right)$$

(4.17)

$$b = \frac{W_e \, \rho_B}{C_o} \qquad\qquad (4.18)$$

The results from the linear regression analysis for the results obtained in this study are summarized in Table 4.7 and Table 4.8 and illustrated in Figure 4.15 for bed-weight variances and in Figure 4.16 for residence-time variances.

TABLE 4.7. Regression equations for the HCN protection time

RH(%)	REGRESSION EQUATION	COEFF OF CORRELATION
0	t(min) = -29,33 + 259,38W	0,9862
70	t(min) = -34 + 278,13W	0,9906

TABLE 4.8. Modified Wheeler equation values for HCN calculated by the weight-variation approache and residence time variation.

		0% RH		70%RH	
		BED WEIGHT	RESIDENCE TIME	BED WEIGHT	RESIDENCE E TIME
PARAMETERS	UNIT	CALC	CALC	CALC	CALC
Adsorption capacity (W_e)	$g.g^{-1}$	0,055	0,056	0,059	0,059
Critical bed weight (W_c)	g	30	N/A	34	N/A
Adsorption rate constant (k_v)	min^{-1}	2420	2461	2238	2238

119
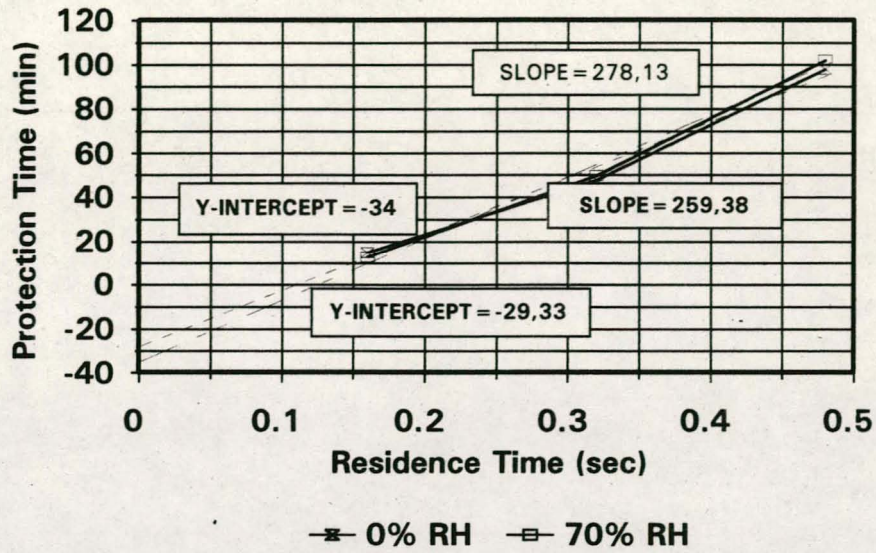
Figure 4.15 The regression analysis of the HCN protection as function of carbon weight and the relative humidity
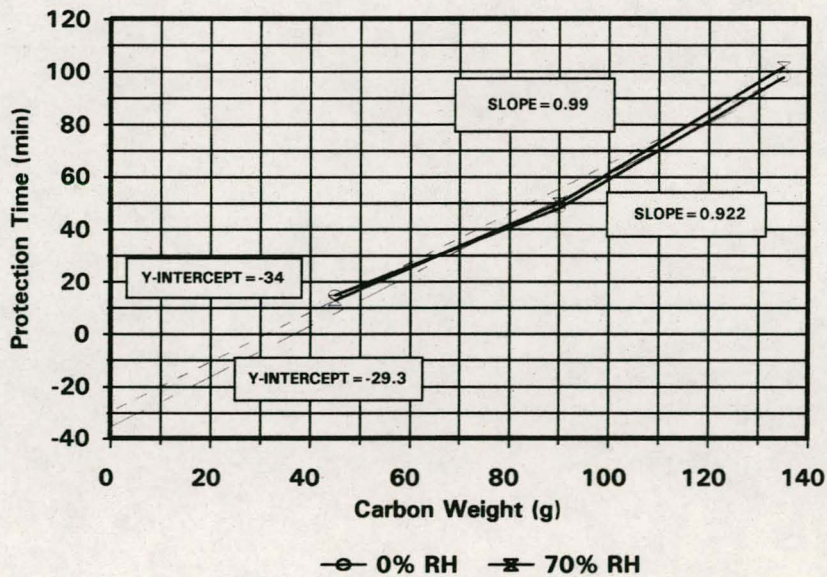
Figure 4.16 The regression analysis of the HCN protection as function of residence time and the relative humidity

The major reaction between HCN and Cu/Cr impregnated carbon was suggested by *Zabor* [74]to be;

$$4HCN + 2CuO \rightarrow 2CuCN + 2H_2O + C_2N_2$$
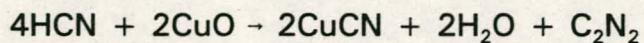
The stoichiometric ratio between HCN and Cu is therefore 2:1. The carbon used contained 0,0005823 moles of Cu per gram of carbon. The capacity absorbed is equivalent to 0,0011857 moles of HCN per gram of carbon, giving an approximate ratio of HCN to Cu of 2:1. This is an indication that all of the impregnants were accessible to the HCN molecules that entered the carbon bed. This is illustrated in Figure 4.17.
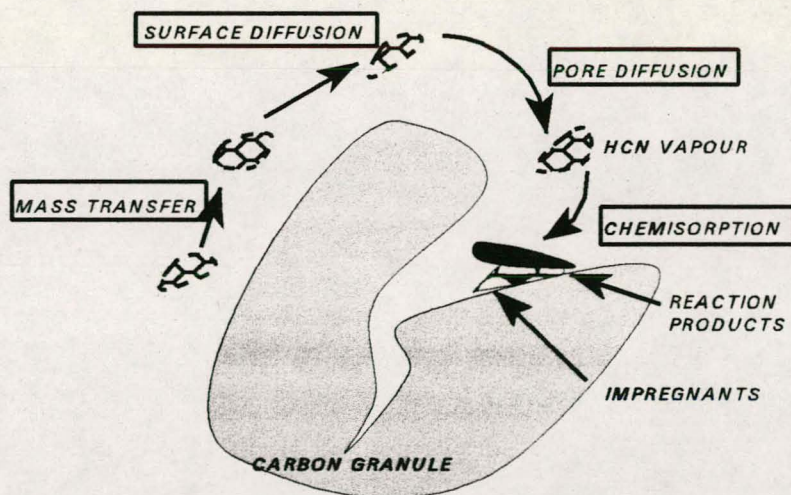
Figure 4.17 An illustration of the process of chemisorption

4.2.3 PROTECTION AGAINST HCN AND CCl$_4$ SIMULTANEOUSLY

The protection times obtained against the exposure of CCl$_4$ and HCN simultaneously with one, two and three filter cartridges are listed in Table 4.9 and illustrated in Figure 4.18.

TABLE 4.9. **Protection time against HCN and CCl$_4$ as function of carbon weight, relative humidity and simultaneous exposure to CCl$_4$ and HCN**

CARBON WEIGHT (g)	COCONUT			
	CCl$_4$		HCN	
	0% RH	70% RH	0% RH	70% RH
45	71	59	10	12
90	148	132	46	56
135	220	187	90	92
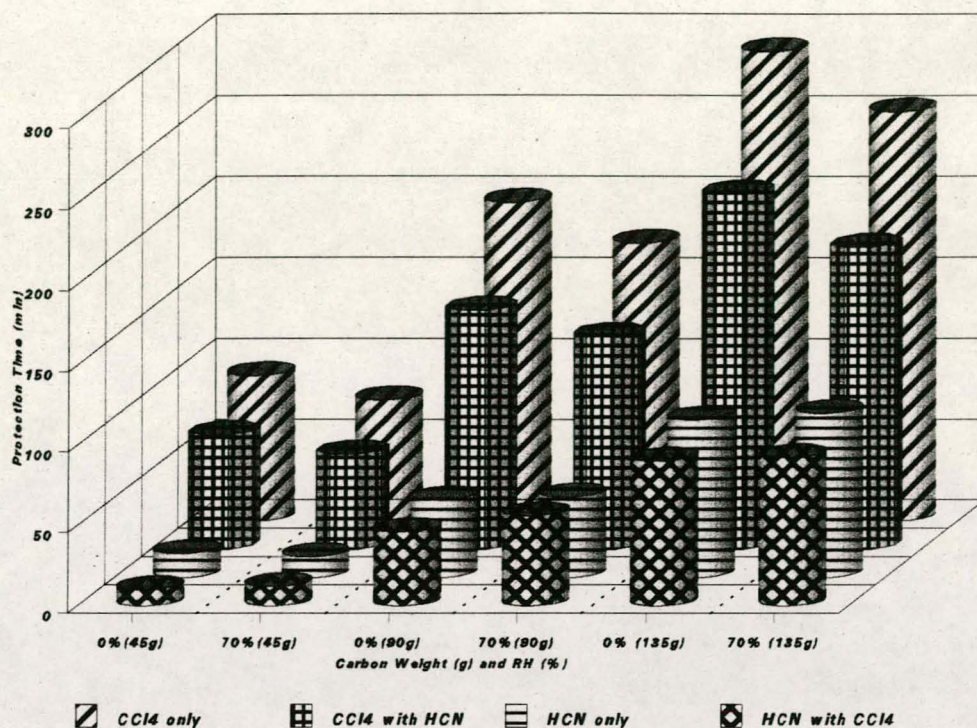
Figure 4.18   The protection time against CCl_4 and HCN as a function of carbon weight, %RH and simultaneous exposure to HCN and CCl_4

The filtration of HCN is not a function of the active surface area but is a function of impregnation. The efficiency of filtration is therefore dependent on the residence time (τ) and to less extent dependent on the porosity. The porosity determines the efficiency of impregnation. As illustrated in paragraph 4.1.1, the deposition of the impregnants in the pore structure reduces the active surface area. The important difference between the simultaneous exposure and the individual exposure is the reduction in the capacity of the carbon for CCl_4. The reduction was, on average, 25%, which had a significant effect on the protection time as illustrated in Fig 4.18. Possible reaction steps can be illustrated as shown in Figure 4.19.
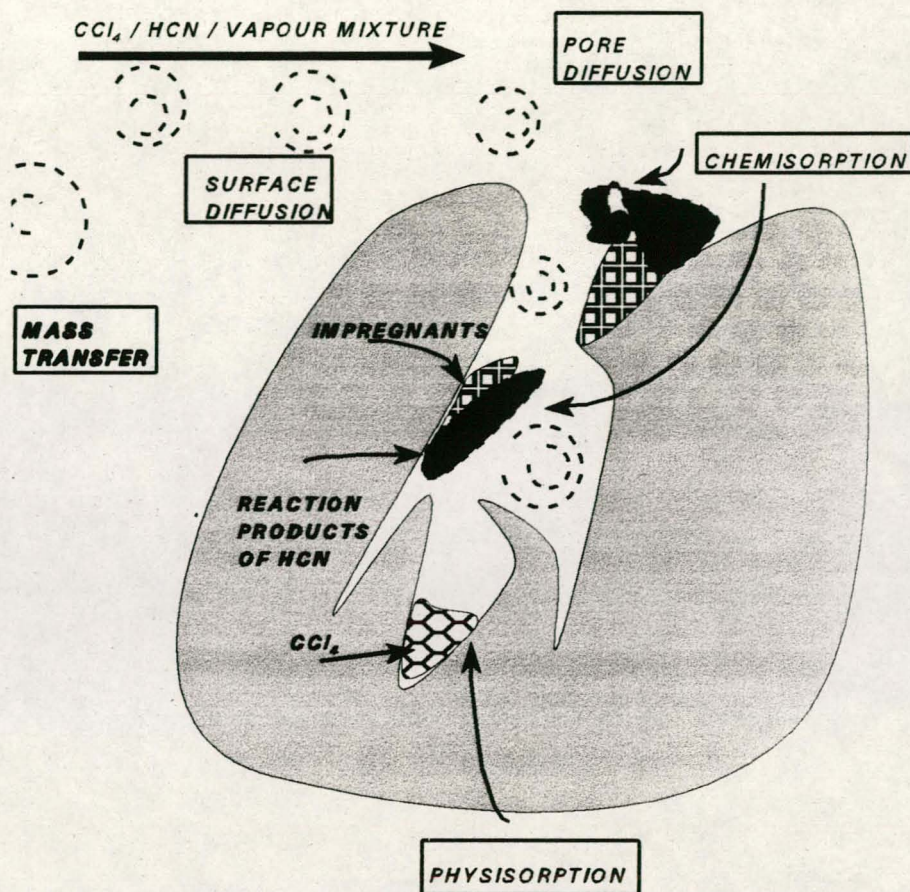
Figure 4.19   **An illustration of possible reaction steps during simultaneous exposures to HCN and CCl$_4$**

Both mechanisms of physisorption and chemisorption take place simultaneously until the reaction products start to block the pore openings. The CCl$_4$ vapour must penetrate the pore in order that capillary condensation will take place in the micropores. The availability of micropores is evident from the pore distribution analysis discussed in section 4.1.2. The effect of the reaction products on the availability of micropores was investigated by determining the nitrogen adsorption isotherm and the determination of the BET active surface. These results were discussed in section 4.2.1. The isotherms

were shown in Figure 4.2. The reduction of the active surface area from 950 m².g⁻¹ to 811 m².g⁻¹ corresponds to a reduction of 15 %. The masking effect of the reaction products had a direct influence on the availability of active sites for physisorption.
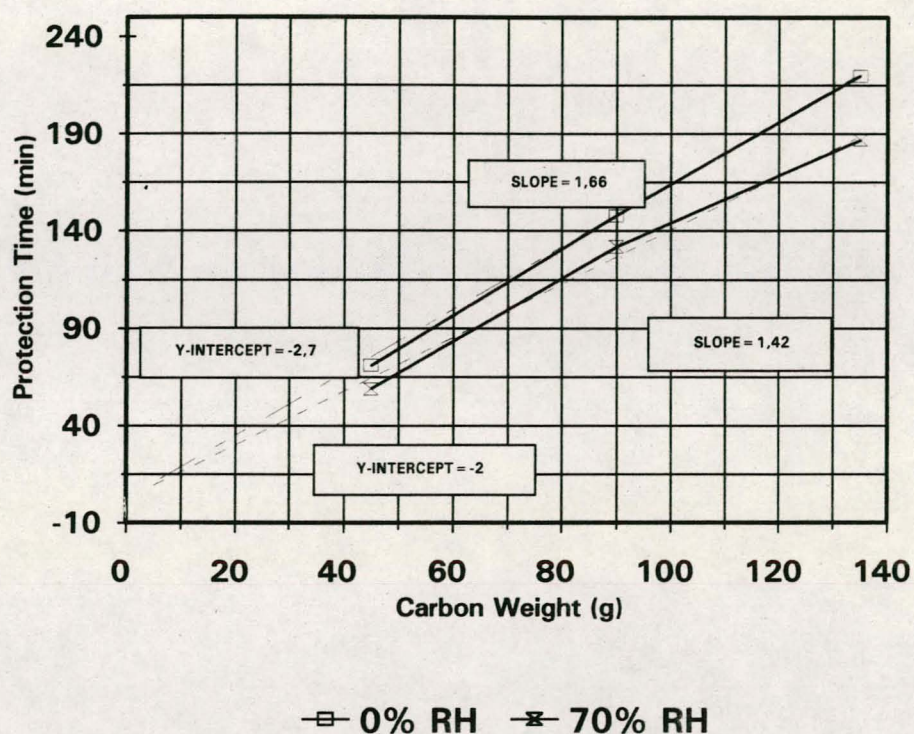
Figure 4.20   **The linear regression for CCl₄ as a function of the simultaneous exposure with HCN and relative humidity.**

The protection time afforded by the carbon against HCN did not change appreciably during the simultaneous exposure with CCl₄, as shown in Figure 4.18. The chemisorption of the HCN was therefore not affected by the CCl₄. The drastic reduction in the CCl₄ protection time with the simultaneous exposure to HCN was also reflected in the

adsorption rate constant. The linear regression graph is shown in Figure 4.20 and the adsorption capacities for CCl_4 as functions of the simultaneous exposure is listed in Table 4.10.

TABLE 4.10.The adsorption capacity and critical bed weights for CCl_4

PARAMETERS	UNIT	CCl_4		CCl_4 with HCN	
		0%	70%	0%	70%
Adsorption capacity (W_e)	$g.g^{-1}$	0,660	0,594	0,496	0,426
Critical bed weight (W_c)	g	3,5	5,7	5	8

In order to verify the importance of individual variables a sensitivity analysis was performed. This was done to determine whether the reduction in protection time as a function of simultaneous exposure to an organic and an inorganic substance was more significant than the other factors relating to the protection time of a gas mask filter, that is, relative humidity, base carbon, carbon weight and challenge concentration. The protection time obtained for the values specified by the SABS 1455 Specification were used as reference. The percentage variation per variable is shown in Table 4.11 and illustrated in Figure 4.21.

TABLE 4.11 Variation in CCl$_4$ protection time as a function of the different variables

VARIABLE	PROTECTION TIME (min)	CAPACITY (g.g^{-1})	VARIANCE (%)
Coconut, 90g, 10 mg.l^{-1}, 0%RH	197	0,657	0
Coconut, **135g**, 10 mg.l^{-1}, 0%RH	275	0,611	-7
Coconut, 90g, **5 mg.l^{-1}**, 0%RH	413	0,688	+4,7
Coconut, 90g, 10 mg.l^{-1}, **70%RH**	172	0,573	-12,8
Coal, 90g, 10 mg.l^{-1}, 0%RH	172	0,473	-12,8
Coconut, 90g, mg.l^{-1}, **simultaneous with HCN**	148	0,493	-25
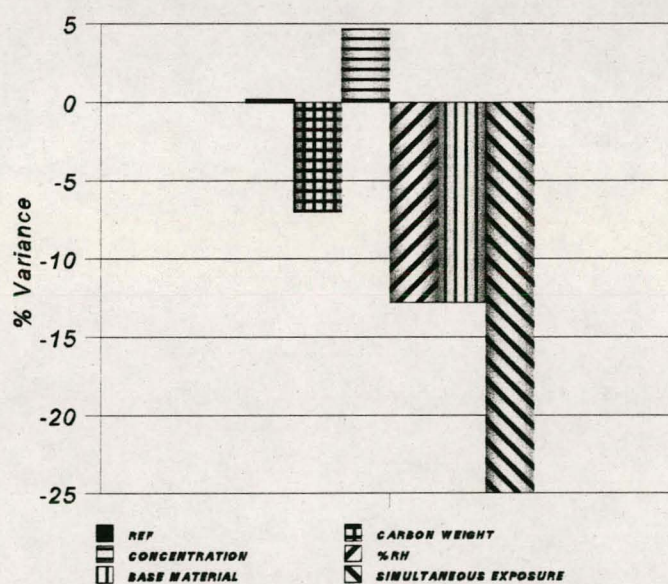
Figure 4.21   The percentage variance as functions of the variables tested

This phenomenon of a reduction in adsorption capacity when the filter is exposed to binary contaminants where the one contaminant relies on the impregnants is unique, and has never been reported

previous. The implications for this are great since all gas-mask filters are qualified against one test gas only when approvals are issued. The concept of exposure against a mixture of organic solvents and test vapours is reported in the literature. [75-79]. It is not a problem when binary vapours are adsorbed only by physical adsorption, because the capacity of the carbon bed is qualified for approvals. The capacity per vapour is affected in such instance, but the capacity of the filter is not affected.

Binary exposure, in which the one challenge vapour relies on the impregnation, becomes a problem since respiratory filters are currently marketed and approved internationally [79] in the following categories:

Type A	-	ORGANIC VAPOURS
Type B	-	INORGANIC VAPOURS
Type E	-	SULPHUR DIOXIDE AND OTHER ACID GASSES
Type K	-	AMMONIA

Type A operates only by physical adsorption and is therefore dependent on the active surface and porosity of the carbon. No impregnation is required. Types B, E and K all operate only by chemisorption.

Each Type is qualified against single test gases but other ranges of filters are marketed worldwide, namely

Type ABEK

Type ABE

Type BE

In these instances users of these filters will have problems, especially when the user is exposed to two vapours, one of which is dependent on physical adsorption, porosity and surface area, and one which is dependent on impregnation. The filters are still only qualified against single test-gas exposures and are approved accordingly. This aspect is of concern since a simultaneous exposure to a chemisorption-dependent vapour and a physisorption-dependent vapour could cause the filter not to have the required approval capacity because of the reductions observed in this study. A wearer could find himself in a situation in which protection is inadequate because of binary exposure.

CHAPTER V

CONCLUSION

5.0 CONCLUSION

The results of this study have shown that the application of gas-mask filters in an environment containing mixtures of gas contaminants could be detrimental to the health of the wearer especially when highly volatile organic vapours are present. The reason, as shown in this study, is the reduction in capacity for organic compounds, which relies on the physical adsorption process and which is due to the occupation of pore space by the reaction products of the chemisorption process. It was necessary to investigate the phenomenon as this aspect has never been encountered or reported on before. The implication is significant since legislation now protects the worker and furthermore the employer is now responsible for the health of the individual; but the employer can supply "approved" filters from a manufacturer without conforming to the legislation. The obvious question is the relevance of this study in all instances. In other words will this be the case with all combination filters? The answer is yes if the worker is exposed to both organic and inorganic substances (which are dependent on the impregnants). This study highlights the important reasons for this and can be summarized as follow

a)   Impregnated carbons, irrespective of their origin (e.g. coal, coconut, peat, etc) are susceptible to partial pore-blocking due to formation of reaction products in the pores. This was illustrated and proved by the studies of different carbons in terms of the change in pore-volume distribution and the reduction in surface area after exposure of the carbon to HCN.

b)   The consistency in the results with regard to the chemisorption in a single or a binary exposure is a further indication that the reduction

in capacity for organic substances is a consequence of inhibition of physical adsorption.   Steric effects in terms of pore diffusion and to a lesser extent intra-granular diffusion are the main reasons for the reduction in protection time.

c)   The adsorption rate constant and the carbon-bed capacity, in terms of the Wheeler equation, was used to determine theoretically and experimentally the influence of exposure to filters of binary mixtures on the capacity of the filter. It was bound that the adsorption rate constant could change only if there was a change in the physical characteristics of the carbon, for example, surface area, pore volume and density of the carbon.   It could also change if the thermodynamic environment changed, for example, exothermic or endothermic reaction with large temperature swings or large pressure changes, or lastly, if there was a change in challenge concentration and airflow rate. In order to quantify the extent of the problem and to imitate practical usage conditions, the following aspects were kept constant, e.g. challenge concentration, constant experimental temperature and pressure and constant airflow rate.   The only contributing aspects to the phenomenon of a reduction in capacity and adsorption rate constant was the change in physical characteristics.

REFERENCES

1.   J.W. Hassler: "Activated Carbon", pp. 2-237. Chemical Publishing Co., New York, (1963).

2.   S.M. Levine and M. Schneider: Am Ind. Hyg Ass. J.43, 423-426, (1982).

3.   C.L. Mantell: "Adsorption", 2-161, McGraw-Hill Book Co., New York, (1951).

4.   M. Smisek and S. Cerny: "Active Carbon Manufacture Properties and Applications", 2-197. Elsevier Publishing Co., Amsterdam, (1970).

5.   Calgon Corporation, "Basic Concepts of Adsorption on Activated Carbon", Pittsburg, Pennsylvania.

6.   M. James Montgomery Consulting Engineers: "Water Treatment Principles and Design", 174-197, John Wiley and Sons, New York. (1985).

7.   S. Brunauer: "The Adsorption of Gases and Vapours", Volume 1. Physical Adsorption, 3-187. Princeton University Press, Princeton, New Jersey. (1943).

8.   S. Brunauer, L.S. Deming, W.S. Deming and E. Teller: J. Amer. Chem. Soc. 62, 1723, (1940).

9.   K.S.W. Sing, D.H. Everett, R.A.W. Haul, L. Moscou, R.A. Pierotti, J. Rouquerol and T. Siemieniewska: Pure and Applied Chem., 57 (4), 603 (1985).

10. S.J. Gregg and K.S.W. Sing: "Adsorption, Surface Area and Porosity", Academic Press, London, (1967).

11. A. Bailey, D.A. Cadenhead, D.H. Davies, D.H. Everett and J.A. Miles: Trans. Faraday Soc., 67, 231, (1971).

12. F.M. Barrer and J.S.S. Reay: "Proc. Second Int. Cong. Surface Activity, II" 79, Butterworths, London, (1957).

13. A.R. Miller: "The Adsorption of Gases on Solids" 20-61. Cambridge University Press., Cambridge, England, (1949).

14. M.M. Dubinin: "Progress in Surface and Membrane Science", V 9, 1-70, Academic Press, New York, (1975).

15. De Boer, J.H.: "The Dynamic Character of Adsorption", Oxford, Clarendon Press, (1953).

16. Zsigmondy, R.Z.: Anorg. Chem., 71, 356 (1911).

17. Langmuir, I.: J. Am. Chem. Soc., 38 : 2221 (1916); 40 : 1361 (1918).

18. Hutchins, R.A.: "New Method Simplifies Design of Activated Carbon Systems". Chem. Eng. 133, (1973).

19. Brunauer, S., Deming, L.S., Deming, W.E. and Teller, E.J.: J. Am. Chem. Soc. 62, 1723 (1940)

20. Polanyi, M.: Verhandl. Deut. Physik. Ges. 18 : 55 (1916).

21. Dubinin, M.M.: "Porous Structure and Adsorption Properties of Active Carbons, Chemistry and Physics of Carbon", Ed., P.L. Walker, Jr. 2, 55. (1966).

22. Kadlec, O. and Dubinin, M.M.: J. Coloid. Interfaced Sci. <u>31</u>, 479 (1969).

23. Reucroft, P.J., Simpson, W.H. and Jonas, L.A.: J. Phys. Chem. <u>75</u>, 3526 (1971).

24. Handbook of Chemistry and Physics, 66th Ed. CRC Press, Inc. Boca. Raton, FL (1985 - 1986).

25. Dubinin, M.M. and Radushkevich, L.V.: Zhur, Fiz. khim. <u>23</u>, 469, (1949).

26. Dubinin, M.M. and Astakhov, V.A.: Adv. Chem. Ser. 102, 69 (1971).

27. Dubinin, M.M. and Stoeckli, H.F.: J. Colloid Interface. Sci., <u>75</u>, 34 (1980).

28. Jaroniec, M. and Madey, R.: Carbon, <u>25</u>, 579, (1987).

29. Rozwdowski, M. and Wojsz, R.: Carbon, <u>22</u>, 363, (1984).

30. Dubinin, M.M.: Carbon, <u>23</u>, 373, (1985).

31. Bering, B.P., Dubinin M.M. and Serpinsky, V.U.: J. Colloid Interfaced Sci, <u>27</u>, 378, (1966).

32. Wheeler, A. and Robell, A.: J. Catalysis <u>13</u>, 229 (1969).

33. Jonas, L.A. and Rehrmann, J.A.: Carbon, <u>10</u>, 657 (1972).

34.	Jonas, L.A. and Rehrmann, J.A.: Carbon, <u>12</u>, 95 (1974).

35.	Emmett, P.H.: Catalysis, Vol. II, 150, Reinhold Publishing Co., New York, (1955).

36.	Rehrmann, J.A. and Jonas, L.A.: Carbon, <u>16,</u> p.47 (1978).

37.	Jonas, L.A., Tewari, Y.B. and Sansone, E.B.: Carbon, <u>17,</u> 345, (1979).

38.	Grubner, O. and Underhill, D.W.: Separation Science, <u>5</u>, 555, (1970).

39.	Atkins, P.W.: "Physical Chemistry", Oxford Univ Press, 837, (1978).

40.	Knudsen, J.G. and Katz, D.L.: "Fluid Dynamics and Heat Transfer", 18 McGraw-Hill, New York, (1958).

41.	Wheeler, A: "Progress Report", Army Contract DA 18-035-AMC-279 (a), 22, (1966).

42.	Gilliland, E.R., Baddour, R.F., Perkinson, G.F. and Sladek, K.J.: Ind. Eng. Chem. Fund. <u>13</u>, 95 (1974).

43.	Sladek, K.J., Gilliland, E.R. and Baddour, R.F.: Ind. Eng. Chem. Fund. <u>13</u>, 100 (1974).

44.	Satterfield, C.N.: "Mass Transfer in Heterogeneous Catalysis", MIT Press, Cambridge, (1970).

45.	Kennard, E.H.: "Kinetic Theory of Gases", McGraw-Hill, New York, 302, (1938).

46. Wheeler, A.: Catalysis, Vol. II, 127, Reinhold, New York, (1955).

47. Wheeler, A.: "6th Bimonthly Progress Report" (Edited by Makowski J.), Army Contract DA 18-035-AMC-279(A), 85, Sept. (1965).

48. Carbon Adsorption Handbook, ed. by Cheremisinoff, P.N. and Ellerbusch, F., 334, (1980).

49. S. Brunauer, P.H. Emmett and E. Teller., J. Amer. Chem. Soc. 60,,306, (1938).

50. K.S.W. Sing: Colloids and Surfaces, 38,113, (1989).

51. E.P. Barrett, L.G. Joyner and P.H. Halenda, J. Am. Chem. Soc. 73, 373, (1951).

52. J.H. de Boer, B.G. Linsen and Th. J. Onsinga, J. Catalysis, 4, 643, (1965).

53. M.M. Dubinin and L.V. Radushkevich, Doklady Akad. Nauk. S.S. S.R., 55, 327, (1947).

54. B.C. Lippens and J.H. de Boer, J. Catalysis, 4, 319, (1965).

55. S. Brunauer, R. SL. Mikhail and E.E. Bodor, J Colloid Interface Sci 24, 451, (1967).

56. G. Horvath and K. Kawazoe, J. Chen. Eng. Japan, 16, 470, (1983).

57. A. Saito and H.C. Foley, AIChE, Journal, 37, 429, (1991).

58.   D.E. Sullivan and M.M. Telo da Gama, In Fluid Interfacial Phenomena, C.A. Croxton, ed, Wiley, New York, (1987).

59.   R. Evans and P. Tarazona, Phys. Rev. Letters, 53, 557, (1984).

60.   J.P.R.B. Walton and N. Quirke, Chem. Phys. Letters, 129, 382, (1986).

61.   N.A. Seaton, J.P.R.B. Walton and H. Quirke, Carbon 27, 853, (1989)

62.   J.P. Olivier and W.B. Conklin, presented at 7th Int. Conf. On Surf. And Coll. Sci., Compiegne, France, (1991).

63.   B.P. Russell and M.D. LeVan, Carbon 32, (5), 846, (1994)

64.   P.J. Reucroft and Chion, C.T., Carbon 15, 285, (1977).

65.   J. Kloubek.: "Investigation of Impregnant Deposition in Activated carbon", Carbon 19, 303, (1981).

66.   T.H. Williams, Thesis, Bath University, (1975).

67.   B.R.Alves and A.J. Clark, Carbon 24, 287, (1986).

68.   L.A. Jonas and W.J. Svirbely, J. of Catalysis, 24, 446, (1972).

69.   D.O. Hayward and B.M.W. Trapnell, Chemisorption, Butterworths, London, 18, (1964).

70.   G.O. Wood, Am. Ind. Hyg. Assooc. J., 48 (8), 703, (1987).

71. C.R. Hall, R.J. Holmes and I.W. Lawston, Adsorption Science and Technology, <u>8</u>, 69, (1981).

72. D. Levenspiel, Chemical Reaction Engineering, Wiley, New York, 465, (1962).

73. M.W. Ackley, Am. Ind. Hyg. Ass. J. <u>46</u> (11), 679, (1985).

74. G.W. Zabor, UNMARY Tech. Report of Div. D. NORL, Chap. 7, (1946).

75. N. Vahdat., P.M. Swearengen and J.S. Johnson, Am. Ind Hyd. Assoc. J. <u>55</u> (910), 909, (1994).

76. J. Hemeth, S. Baticz, M. Peter-Horanyi, Gy. Szukaand. P. Regenyi, Hungarian Journal of Industrial Chemistry, <u>14</u>, 411, (1986).

77. P.M. Swearengen and S.C. Weaver, Report UCRL - 93430 - Pt. 1, 1, (1985).

78. B. Buuczek, A. Swiatkowski and J.Goworek, Carbon <u>33</u>, 129, (1995).

79. European Standard, prEN 141, (1988).

80. West, R.E. "Effect of Porous Structure on Carbon Activation"., EPA Report EP 1.16: 17020 DDC (1971).

81. De Boer, J.H. "The Structure and Properties of Porous Materials", D.H. Everett and S. Stone, Eds. London: Butterworths, 68, (1958).

82. Lowell, S.J. Anal. Chem., <u>45</u>, 1576, (1973).

139

83.   Lippens, B.C., Jinsen, B.G. and de Boer, J.H., J. Catalysis, 3, 32, (1964).

84.   De Boer, J.H., Linsen, B.G. and Osind, T.J., J. Catalysis, 4, 643, (1965).

85.   Cranston, R.W. and Inkley, F.A., Adv. Catalysis, 9, 143, (1957).

86.   Halsey, G.D., J. Chem. Phys., 16, 931, (1948).

CONFIDENTIAL

The Processes and Factors Controlling Air Filtration by Impregnated, Activated Carbon and its Application in Environmental Pollution

CA BARNARDT

VOLUME B

1.0 SUMMARY

This section summarises the results of a study of single-metal and combination-solution impregnation processes as means for producing carbons giving increased protection against toxic agents. Processes were developed for the impregnation of carbon with cupric oxide, chromium trioxide, silver nitrate, molybdenum oxide and vanadium pentoxide.

Spectrographic analysis of impregnated samples of carbon showed that impregnants were present on these carbons in the expected concentration ranges. BET surface-area analysis proved that material deposited by impregnation caused less loss of surface area than expected. Pore-size distribution calculations revealed that impregnation processes deposited material in the carbon macropores.

Impregnation was used to add to the carbon a material which it does not contain normally and which promoted the adsorption of specific toxic agents. The impregnation technique, the equilibrium time and the drying procedure are discussed. The equilibrium time was short (5-10 min) and was only the time needed to completely saturate the carbon with the impregnation solution. Drying was done in three stages. Three combinations of impregnants were used, namely, Cu/Cr/Ag, Cu/Mo/Ag and Cu/V/Ag. These impregnations were all successful.

Test procedures were developed to test the various impregnated carbons against agents such as HCN, CNCl and chloropicrin. The chloropicrin protection time was good but showed a decrease with increased impregnation due to reduction of surface area. Protection against HCN was significant only for the Cu, Cu/V, Cu/Cr/Ag, Cu/Mo/Ag, Cu/V/Ag

impregnated carbons, and the single Ag, Cr and Mo carbons could not remove HCN.

The Cu/Mo/Ag impregnated carbons exhibited the best protection time of 125 min for CNCl.

Evaluations were made of the impregnated carbons against mixtures of agents, agents plus solvents and agents plus impurities. Mixtures adversely affected protection times by blocking pores. Impurities did not have a significant influence on protection times. The reasons were similar to those for mixtures of agents. The protection time of chloropicrin decreased drastically during the simultaneous exposure to HCN and CNCl. This was attributed to partial masking of the micropores by the reaction products formed when the HCN and CNCl react with the impregnants.

The impregnated carbons were also compared with two available international impregnated carbons, namely Calgon BPL and PICA NBC carbon. The comparisons were done on the basis of the impregnation, surface area, pore volumes and the protection time against HCN and chloropicrin. Comparison of the protection times showed that the capacity for HCN of the local Cu/Cr/Ag impregnated carbon was similar to that for the Calgon and PICA carbons, and that the chloropicrin capacities were higher for the local Cu/Cr/Ag impregnated carbon.

2.0 OPSOMMING

Hierdie afdeling dien as opsomming van die totstandkoming van 'n program van impregneringsprosesse met oplossings om koolstowwe te vervaardig wat langer beskerming teen toksiese agense bied. Impregneringsprosesse van koolstof met koperoksied, chroomtrioksied, silwernitraat, molibdeenoksied en vanadium pentoksied is ontwikkel.

Spektrografiese analises van geïmpregneerde monsters het aangetoon dat impregnante in die koolstof in die verwagte konsentrasies teenwoordig is. BET oppervlak studies het bewys dat minder aktiewe oppervlak as gevolg van die impregnering beset is, as wat verwag is. Porieverspreidingstudies het getoon dat impregneringsprosesse materiaal in die makroporië neerlaat.

Impregnering word gebruik om 'n materiaal tot die koolstof toe te voeg wat nie op die koolstof gewees het nie en wat spesifieke agens adsorpsie bevorder. Die impregnerings tegniek, die ekwilibriumtyd en die drogingsprosedure is bespreek. Die ekwilibriumtyd is kort (5-10 minute) en is slegs die tyd nodig om die koolstof met die impregnerings oplossing te versadig. Droging is in drie fases gedoen. Drie kombinasie impregnerings is gedoen naamlik, Cu/Cr/Ag, Cu/Mo/Ag en Cu/V/Ag. Hierdie impregnerings was almal suksesvol.

Toetsprosedures is ontwikkel om die verskillende geïmpregneerde koolstowwe teen agense soos HCN, chloorpikrien en CNCl te evalueer. Die beskerming teen chloorpikrien was goed, maar het 'n afname getoon met 'n toename in impregnering as gevolg van 'n afname in aktiewe oppervlakte. Beskerming teen HCN was slegs insiggewend vir Cu, Cu/V, Cu/Cr/Ag, Cu/Mo/Ag, Cu/V/Ag geïmpregneerde koolstof terwyl enkel Ag, Cr en Mo

geen beskerming teen HCN gebied het nie.

Die Cu/Mo/Ag geïmpregneerde koolstof het die beste beskerming teen CNCl gelewer, naamlik 125 minute.

Hierdie bylae bespreek verder die evaluasie van die geïmpregneerde koolstowwe teen agensmengsels, agense plus oplosmiddels en agense plus onsuiwerhede. Mengsels affekteer leeftye nadeling deur porieë te blokkeer. Onsuiwerhede het nie 'n beduidende invloed op die leeftye nie. Die redes is soortgelyk aan die vir mengsels van agense. Die beskermingstyd teen chloorpikrien het drasties afgeneem tydens die gelyktydige blootstelling met HCN en CNCl. Dit is toegeskryf aan die gedeeltelike afskerming van die mikroporiëe as gevolg van die reaksieprodukte wat vorm as HCN en CNCl met die impregnante reageer.

Die geïmpregneerde koolstowwe is ook met die internasionale koolstowwe, naamlik Calgon BPL en PICA KBC, vergelyk. Die vergelykings is ten opsigte van impregnering, aktiewe oppervlakte, porievolumes en die beskerming teen HCN, chloorpikrien en CNCl gedoen. Die beskermingstye met die plaaslik geïmpregneerde koolstof was soortgelyk aan die wat met Calgon en PICA behaal is terwyl die beskermingstyd vir chloorpikrien met die plaaslik geïmpregneerde Cu/Cr/Ag koolstof groter was.

CONTENTS

CONFIDENTIAL

3.0 LIST OF ABBREVIATIONS

CNCl	-	Cyanogen chloride
CCl_3NO_2	-	Chloropicrin
HCN	-	Hydrogen cyanide
Cu	-	Copper
Cr	-	Chromium
Ag	-	Silver
Mo	-	Molybdenum
V	-	Vanadium
$mg.l^{-1}$	-	milligram per litre
$cm.g^{-1}$	-	cubic centimeter per gram
$g.l^{-1}$	-	gram per liter
$ml.l^{-1}$	-	milliliter per liter
$g.ml^{-1}$	-	gram per milliliter

4.0 INTRODUCTION

There is a continuing need for improving activated carbons capacity to remove toxic gases from the air. Since this capacity is due primarily to adsorption on the carbon surface, the amount of toxic material removed from the air is determined by the amount of surface area of the carbon and the affinity of the carbon for the particular toxic agent. Furthermore, the agent is not chemically altered by the carbon, and desorption results in recontamination of the air by the toxic compound.

The extentby which adsorption capacity can be measured by enlarging surface area through greater activation has practical limits. Therefore, further increases in capacity must come from methods which increase carbon's affinity for the particular agent. One such method consists of impregnating an active carbon with a metal or metal salt capable of reacting with the particular toxic agent. Ideally, the impregnant should catalytically decompose or alter the toxic species to form a non-toxic compound. Then, provided that the catalyst impregnant is not poisoned, the impregnated carbon would offer protection indefinitely. Protection can be increased greatly by impregnations of the carbon with compounds which chemically react to decompose or combine with toxic species.

Generally, the impregnation of active carbons is achieved by a solution process in which a suitable carbon is soaked in a solvent, usually water, containing the impregnant. Subsequent drying of the carbon then results in precipitation of the impregnant on the carbon surface.

This section covers the impregnation of batches for evaluation, physical characterisation of the carbons, and subsequent evaluation of the treated carbon against various aggressors.

With many of the carbon filters it was not only the gas agents that influenced protection times. Other factors such as impurities present in the agents, solvents and mixtures of agents will also influence protection time. Impurities in some agents have not been properly refined. Solvents could be used when agent gases were too volatile to be persistent for example, HCN and CNCl. Mixtures were used to cause more rapid breakthrough for example, chloropicrin and HCN.

6.0 RESULTS AND DISCUSSION

6.1 IMPREGNATION RESULTS

Table 1 lists the results of the metal analysis on the impregnated carbons.(NH_4^+ given as NH_3 and $CO_3^=$ as CO_2)

TABLE 1 - METAL ANALYSIS OF IMPREGNATED CARBONS

SAMPLE I.D.	METAL ANALYSIS(%)						
Cu	9.0						
Cr	1,9						
Ag	0,13						
Mo	3,6						
Cu-V	8,0 Cu; 2,7 V						
	Cu	Cr	Ag	Mo	V	CO_2	NH_3
Cu/Cr/Ag	7,9	2,3	0,17	-	-	9,0	10,0
Cu/Mo/Ag	7.2	-	0,12	3,7	-	9,2	10,3
Cu/V/Ag	7,5	-	0,15	-	2,38	8,9	9,8
Calgon	6,9	1,9	0,1	-	-	-	-
PICA	5,8	2,1	0,1	-	-	-	-

These results show that the batch impregnations were successful and that the calculated concentrations were achieved with the impregnation.

6.2 PHYSICAL CHARACTERISTICS OF IMPREGNATED CARBON

6.2.1 SURFACE AREA

The surface areas of the impregnated carbons are illustrated in Figure 2. The results are listed in Table 2.

TABLE 2 : SURFACE AREAS OF IMPREGNATED CARBON

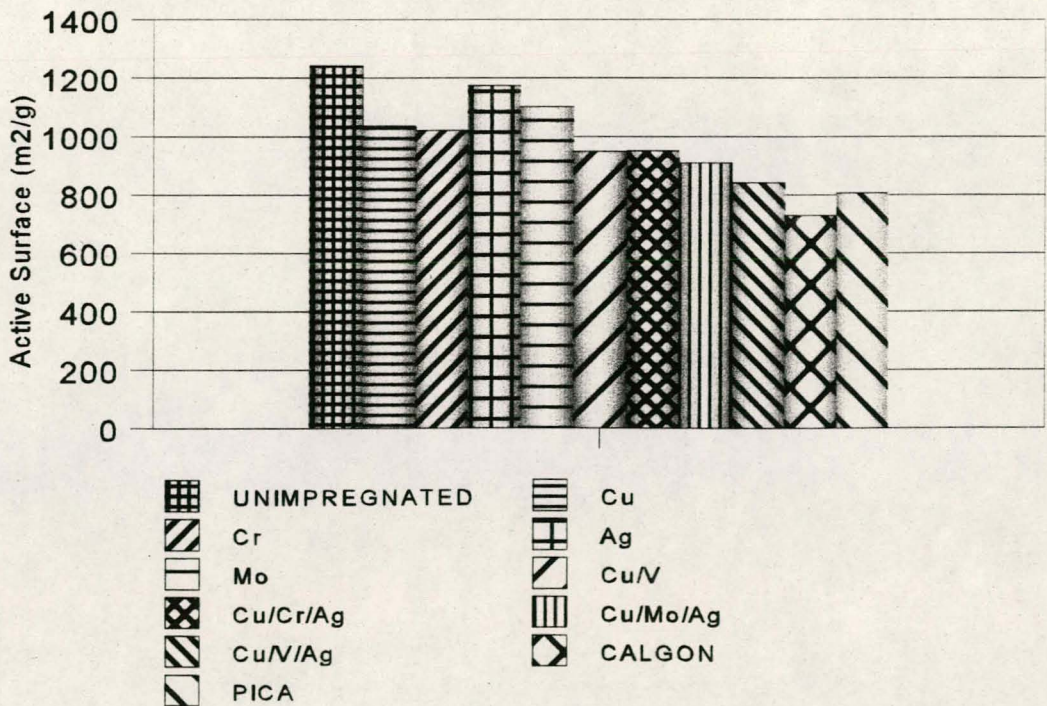| SAMPLE I.D.	ACTIVE SURFACE (m^2/g)
UNIMPREGNATED	1243
Cu	1037
Cr	1020
Ag	1175
Mo	1103
Cu-V	949
Cu/Cr/Ag	950
Cu/Mo/Ag	910
Cu/V/Ag	842
Calgon	730
PICA	805

Figure 2   The comparative active surface areas as functions of the impregnation and supplier.

It can be seen that impregnation had an effect on the surface area, although, in some cases, this has been small. Silver impregnation had the least effect on surface area and this was not unusual as there was only 0,1% silver on the carbons and very little surface area would have been occupied. Molybdenum impregnation, which was 3,6%, showed a markedly lower effect on surface area than chromium did. The surface area, however, was consistent with the higher total pore and micropore volumes measured. High surface area is usually coupled to high micropore volumes. A possible explanation for the high surface area for molybdenum-impregnated carbon is that a batch of the base material may have had a higher surface area than the batches used for the other impregnations.

The copper-vanadium-silver impregnated carbon had the highest content of impregnants, containing 8% copper and 2,9% vanadium, 0,1% silver and the surface area of 842 $m^2.g^{-1}$ was not unexpected. In general, impregnation was successful with regard to surface area as there had been no drastic drop with any of the impregnated carbons. The low surface area for the Calgon carbon was expected since it is a coal-based carbon which normally has a smaller micropore volume.

6.2.2 PORE VOLUME DISTRIBUTION

The pore volumes for the impregnated carbons are illustrated in Fig 3. The results are listed in Table 3.

TABLE 3 :   PORE-VOLUME DISTRIBUTION OF IMPREGNATED CARBON

SAMPLE I.D.	MESOPORE VOLUME $(ml.g^{-1})$	MICROPORE VOLUME $(ml.g^{-1})$
Unimpregnated	0,19	0,65
Cu	0,10	0,55
Cr	0,19	0,59
Ag	0,16	0,53
Mo	0,13	0,58
Cu-V	0,11	0,55
Cu/Cr/Ag	0,09	0,58
Cu/Mo/Ag	0.10	0,52
Cu/V/Ag	0.09	0,52
Calgon	0,19	0,52
PICA	0,07	0,48
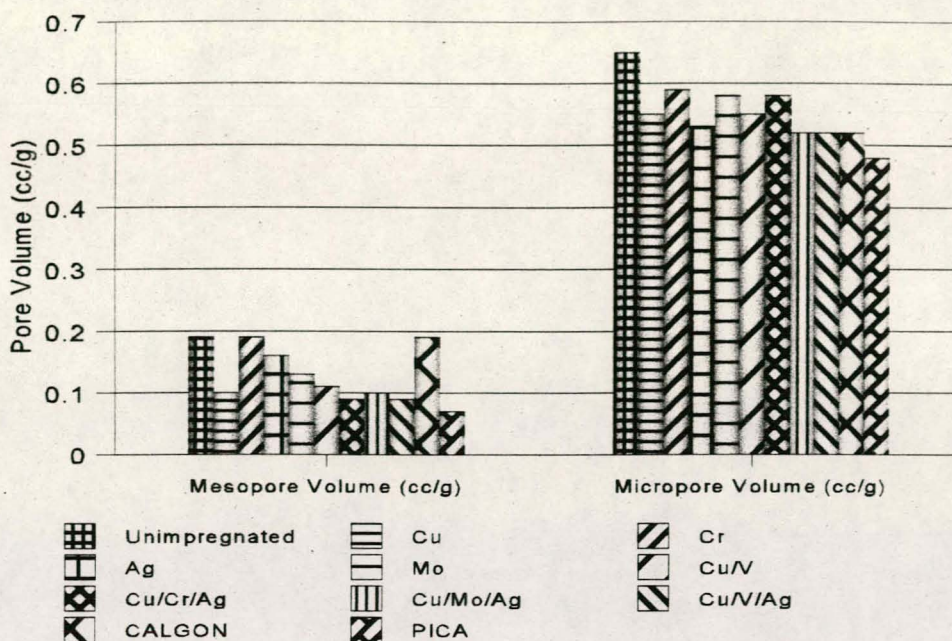
Figure 3   The mesopore and micropore volumes as functions of impregnation and the comparison with international carbons.

It is clear from the results that impregnation influenced the pore sizes and that the micropore volumes were lower. It appears, therefore, that impregnation partially blocked the micropore region of the carbon. However the impact of this partial blocking was negligible and in fact, unavoidable, because of the deposition of the impregnants in the mesopore and macropore regions.

6.2.3 SKELETAL DENSITY

The skeletal densities of the impregnated carbons are illustrated in Fig 4. The results are listed in Table 4.

TABLE 4 : SKELETAL DENSITY OF IMPREGNATED CARBON

SAMPLE I.D.	SKELETAL DENSITY (g.ml^{-1})
Unimpregnated	2,09
Cu	2,20
Cr	2,14
Ag	2,09
Mo	2,14
Cu-V	2,20
Cu/Cr/Ag	2,40
Cu/Mo/Ag	2,38
Cu/V/Ag	2,43
Calgon	2,13
PICA	2.21

Unimpregnated	Cu	Cr	Ag
Mo	Cu/V	Cu/Cr/Ag	Cu/Mo/Ag
Cu/V/Ag	Calgon	PICA	
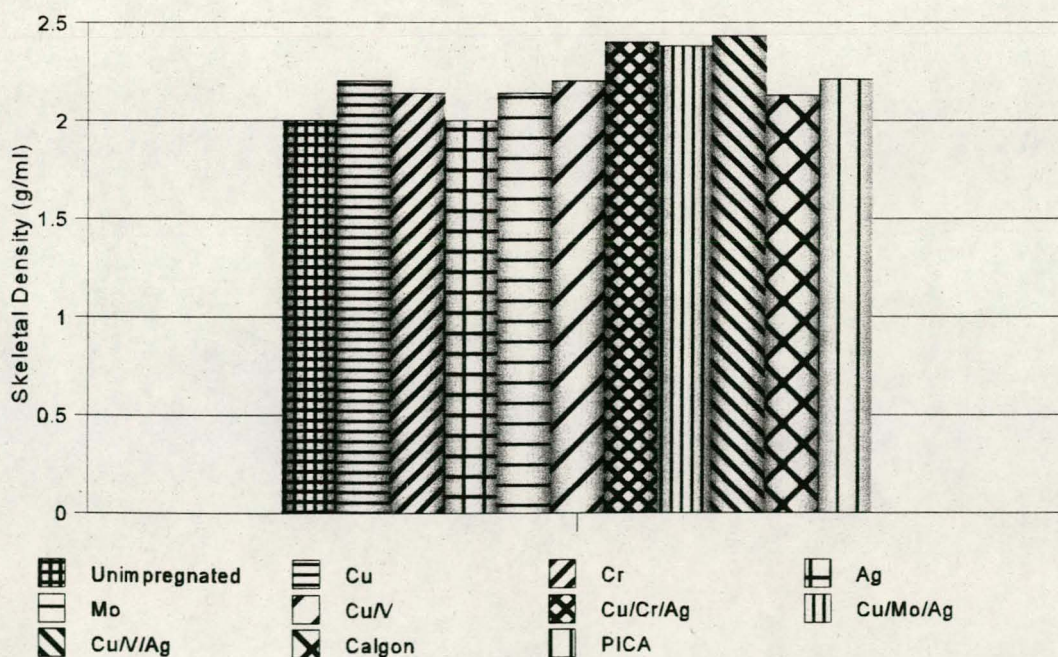
Figure 4   The skeletal densities as functions of the impregnation and comparison with international carbons.

Skeletal densities were slightly affected by impregnation. The combination impregnations resulted in the highest skeletal densities and were consistent with the higher degree of impregnation of these carbons. Cr and Mo carbons were impregnated to a lesser degree and subsequently had lower skeletal densities. Ag carbon had very low impregnation and was the same as unimpregnated carbons.

Skeletal densities, therefore, correlated with the level of impregnation and were observed to increase slightly with increasing degree of impregnation.

6.2.4 APPARENT DENSITY

The apparent densities of impregnated carbons are illustrated in Fig 5. The results are listed in Table 5.

5.0 IMPREGNATION PROCEDURES

5.1 IMPREGNATION OF THE ACTIVATED CARBON WITH SINGLE IMPREGNANTS

5.1.1 COPPER IMPREGNATION

For the evaluation against the aggressors approximately 2 kg of impregnated carbon was necessary for each of the tests. An impregnating solution, containing 8% copper, 9% carbonate and 10% aqueous ammonia, mixed in equal volumes with activated carbon, produced a carbon containing approximately 8% copper.

Four litres of an aqueous impregnating solution were made up to contain

(1)	$CuCO_3.Cu(OH)_2$	-	167,0 g.l^{-1}
(2)	$(NH_4)_2 CO_3.H_2O$	-	194,0 g.l^{-1}
(3)	NH_4OH (25%)	-	567,0 ml.l^{-1}

Specific gravity of the solution was 1,2 g.ml^{-1}.

This was then mixed with 4 l (about 2 kg) of activated carbon for 10 min. It was shown in the single-impregnation study that impregnation was complete after 5 min of mixing.

The batch was shaken for a further 30 min as to ensure complete impregnation.

After impregnation the carbon was drained of excess solution and placed on a sieve in an oven at 90 °C for 60 min, at 150 °C for 180 min and then at 170 °C for 180 min to ensure complete drying. A sample was taken from the batch for analysis to determine the concentration of copper on the carbon.

5.1.2 CHROMIUM IMPREGNATION

An impregnating solution, containing 2,5% chromium oxide, 9% carbonate and 10% aqueous ammonia, mixed in equal volumes with activated carbon, produced a carbon containing approximately 1,7% chromium.

Four litres of an aqueous impregnating solution were made up to contain

(1) CrO_3 - 60,0 g.l^{-1}
(2) $(NH_4)_2 CO_3.H_2O$ - 280,0 g.l^{-1}
(3) NH_4OH (25%) - 350,0 ml.l^{-1}

Specific gravity of the solution was 1,2 g.ml^{-1}.

The impregnation procedure outlined in section 5.1.1 was then followed.

5.1.3 SILVER IMPREGNATION

An impregnating solution, containing 0,05% silver ions, 9%

carbonate, and 10% aqueous ammonia, mixed in equal volumes with activated carbon, produced a carbon with approximately 0,1% silver on it.

Four litres of an aqueous impregnating solution were made up to contain

(1)	$AgNO_3$	-	1,0 g.l^{-1}
(2)	$(NH_4)_2 CO_3.H_2O$	-	280,0 g.l^{-1}
(3)	NH_4OH (25%)	-	350,0 ml.l^{-1}

Specific gravity of the solution was 1,2 g.ml^{-1}.

The impregnation procedure outlined in section 5.1.1 was then followed.

5.1.4 MOLYBDENUM IMPREGNATION

An impregnating solution, containing 3,5% molybdenum oxide, 9% carbonate and 10% aqueous ammonia, mixed in equal volumes, with activated carbon, produced a carbon with approximately 3,9% molybdenum in it.

Four litres of an aqueous impregnating solution was made up to contain

(1)	$(NH_4)_6 Mo_7.O_{24}.4H_2O$	-	73,0 g.l^{-1}
(2)	$(NH_4)_2 CO_3.H_2O$	-	280,0 g.l^{-1}
(3)	NH_4OH (25%)	-	279,0 ml.l^{-1}

Specific gravity of the solution was 1,2 g.ml^{-1}.

The impregnation procedure as outlined in Section 5.1.1 was then followed.

5.1.5 VANADIUM IMPREGNATION

An impregnating solution, containing 8% copper combined carbonate, hydroxide, 2,9% vanadium oxide, 9% carbonate and 10% aqueous ammonia, mixed in equal volumes with activated carbon, produced a carbon with approximately 8% copper, 2,7% vanadium on it. Copper was necessary as the NH_4VO_3 was not readily soluble in water and the copper aided the rapid dissolution of NH_4VO_3.

Four litres of an aqueous impregnating solution was made up to containing

(1)	$CuCO_3.Cu(OH)_2$	-	167,0 g.l^{-1}
(2)	$NH_4 VO_3$	-	80,0 g.l^{-1}
(3)	$(NH_4)_2 CO_3 H_2O)$	-	194,0 g.l^{-1}
(4)	NH_4OH	-	462,0 ml.l^{-1}

Specific gravity of the solution was 1,2 g.ml^{-1}.

The impregnation procedure outlined in section 5.1.1 was then followed.

5.2 IMPREGNATION OF THE ACTIVATED CARBON WITH COMBINATION IMPREGNANTS

5.2.1 COPPER/CHROMIUM/SILVER

For the evaluation against the aggressors approximately 6 kg of impregnated carbon was necessary for all the tests. An impregnating solution, containing 8% Cu, 1,7% Cr, 0,1% Ag salts, 13% carbonate and 10% aqueous ammonia, mixed in equal volumes with activated carbon, produced a carbon with approximately 9% Cu, 1,8% Cr, 0,2% Ag on it.

Twelve litres of an aqueous impregnating solution was, therefore, made up to contain

a.	$CuCO_3.Cu(OH)_2$	-	167,0 $g.l^{-1}$
b.	CrO_3	-	39,2 $g.l^{-1}$
c.	$AgNO_3$	-	1,9 $g.l^{-1}$
d.	$NH_4HCO_3.NH_2.NH_4COO$	-	219,1 $g.l^{-1}$
e.	NH_4OH (25%)	-	450 $ml.l^{-1}$

Specific gravity of the solution was approximately 1,2 $g.ml^{-1}$.

This was then mixed with 12 litres (about 6 kg) of activated carbon for 10 min. It was shown in the single impregnation study that impregnation was complete after 5 min of mixing. The batch was shaken for a further 30 min to ensure complete impregnation.

After impregnation the carbon was drained of excess solution

and placed on a sieve in an oven at 90 °C for 60 min, at 150 °C for 180 min and then at 170 °C for 180 min to ensure complete drying. A sample was taken from the batch to determine the copper, chromium and silver concentrations on the carbon.

5.2.2 COPPER/MOLYBDENUM/SILVER IMPREGNATION

An impregnating solution, containing 9% copper carbonate combined, hydroxide, 5% molybdenum, 0,1% silver salts, 13% carbonates and 10% aqueous ammonia, mixed in equal volumes with activated carbon, produced a carbon with approximately 7% Cu, 4% Mo, 0,15% Ag on it.

An aqueous impregnating solution was, therefore, made up into 12 litres containing

a.	$CuCO_3.Cu(OH)_2$	-	167,0 g.l^{-1}
b.	$(NH_4)_6 Mo_7O_{24} 4H_2O$	-	86,1 g.l^{-1}
c.	$AgNO_3$	-	1,9 g.l^{-1}
d.	$NH_4HCO_3.NH_2.NH_4COO$	-	219,1 g.l^{-1}
e.	NH_4OH (25%)	-	280 ml.l^{-1}

Specific gravity of the solution was approximately 1,2 g.ml^{-1}

The impregnation procedure outlined in Section 5.2.1 was then followed.

5.2.3 COPPER/VANADIUM/SILVER IMPREGNATION

An impregnating solution, containing 8% copper carbonate combined, hydroxide, 2,9% vanadium oxide, 0,1% silver salts, 13% carbonates and 10% aqueous ammonia, mixed in equal volumes with activated carbon, produced a carbon with approximately 9% Cu, 2,5% V and 0,1% Ag on it.

Twelve litres of an aqueous impregnating solution was made up to contain

a.	$CuCO_3.Cu(OH)_2$	-	167,0 g.l^{-1}
b.	NH_4VO_3	-	79,9 g.l^{-1}
c.	$AgNO_3$	-	19 g.l^{-1}
d.	$NH_4HCO_3.NH_2NH_4COO$	-	219,1 g.l^{-1}
e.	NH_4OH (25%)	-	340 ml.l^{-1}

The impregnation procedure outlined in section 5.2.1 was then followed.

5.3   IMPREGNATION PROCESS

The critical aspect of the impregnation process was the sequence of chemical addition and   monitoring of the temperature. Both endothermic and exothermic reactions occurred during preparation of the solution. The sequence of chemical addition for the Cu/Cr/Ag impregnation was:

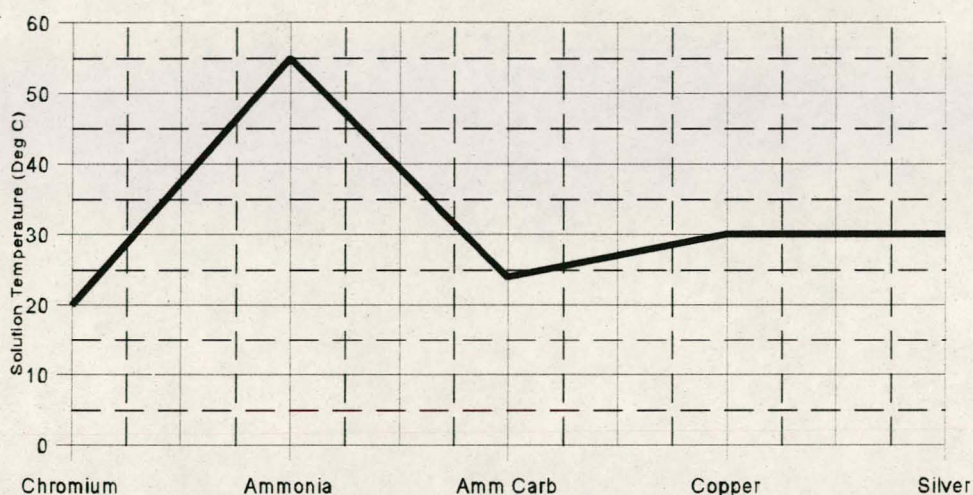| 1	Water + Chromium	Wait until fully dissolved
2	Add NH_4OH	Monitor temperature
3	Add NH_4 carbonate	Add heat to dissolve
4	Add copper carbonate	Wait to dissolve
5	Add silver nitrate	Stir for 30 minutes

The variation in the solution temperature is illustrated in figure 1.

Figure 1   An illustration of the endothermic and exothermic reactions during the preparation of the impregnation solution.

It is clear from the graph that heat was required as soon as the ammonium carbonate is added. This was necessary in order to effectively dissolve the ammonium carbonate.

5.4 MEASUREMENT OF PHYSICAL CHARACTERISTICS AND DETERMINATION OF PROTECTION TIMES

These measurement methods, theories and apparatus are discussed in the first section of the thesis.

TABLE 5 : APPARENT DENSITY OF IMPREGNATED CARBON

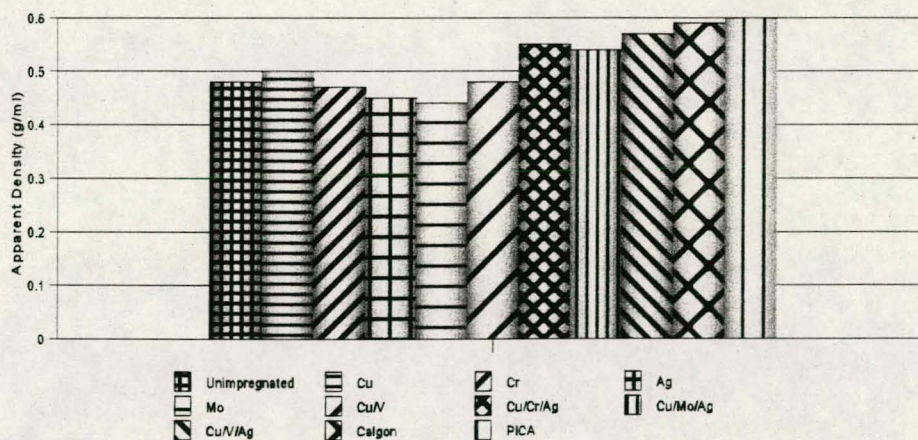| SAMPLE I.D.	APPARENT DENSITY (g.ml^{-1})
Unimpregnated	0,48
Cu	0,50
Cr	0,47
Ag	0,45
Mo	0,44
Cu-V	0,48
Cu/Cr/Ag	0,55
Cu/Mo/Ag	0,54
Cu/V/Ag	0,57
CALGON	0,59
PICA	0,60

Figure 5   The apparent densities as functions of the impregnation and comparison with international carbons

Apparent densities show that the impregnation contributed to the apparent or packing density. This had an effect on the filter mass;   the higher the impregnation loading the higher the apparent density was.

6.2.5 HARDNESS

The hardness of the impregnated carbons is illustrated in Fig 6. The results are listed in Table 6.

TABLE 6 : HARDNESS OF THE IMPREGNATED CARBONS

SAMPLE I.D.	HARDNESS (%)
Unimpregnated	94
Cu	95
Cr	97
Ag	94
Mo	95
Cu-V	94
Cu/Cr/Ag	93
Cu/Mo/Ag	94
Cu/V/Ag	95
Calgon	89
PICA	90

The hardness remained very much unaltered by impregnation, and the carbon thus appeared to retain its abrasive resistance despite

impregnation. The Calgon carbon was less hard due to the coal-base raw material which initially had a lower hardness.
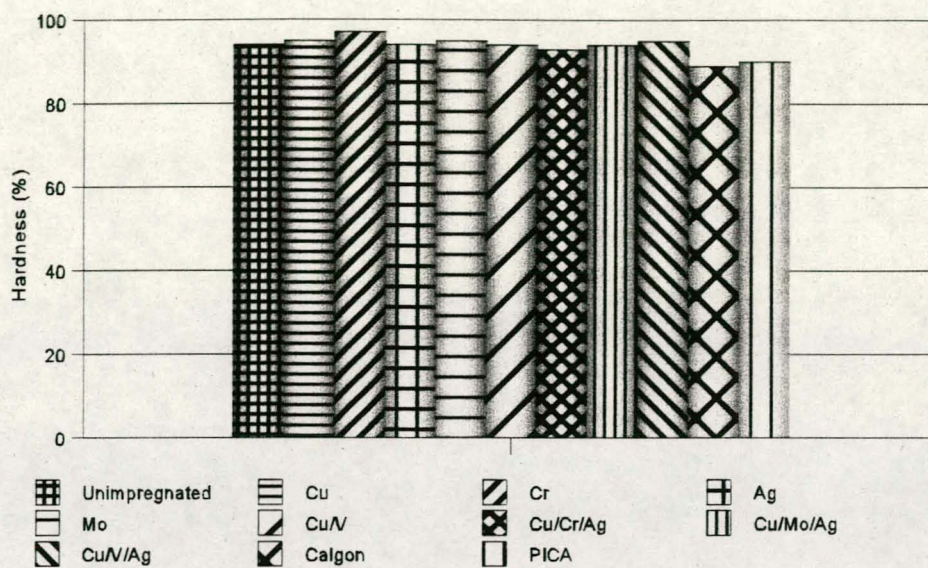

Figure 6   The hardness as functions of the impregnation

6.2.6 ASH CONTENT

The ash content of the impregnated carbons is illustrated in Fig 7. The results are listed in Table 8.

TABLE 8 : ASH CONTENT OF IMPREGNATED CARBON

SAMPLE I.D.	ASH CONTENT (%)
Unimpregnated	2,1
Cu	10,6
Cr	6,0
Ag	1,7
Mo	6,3
Cu-V	14,6
Cu/Cr/Ag	16.3
Cu/Mo/Ag	15
Cu/V/Ag	17
Calgon	15
PICA	17
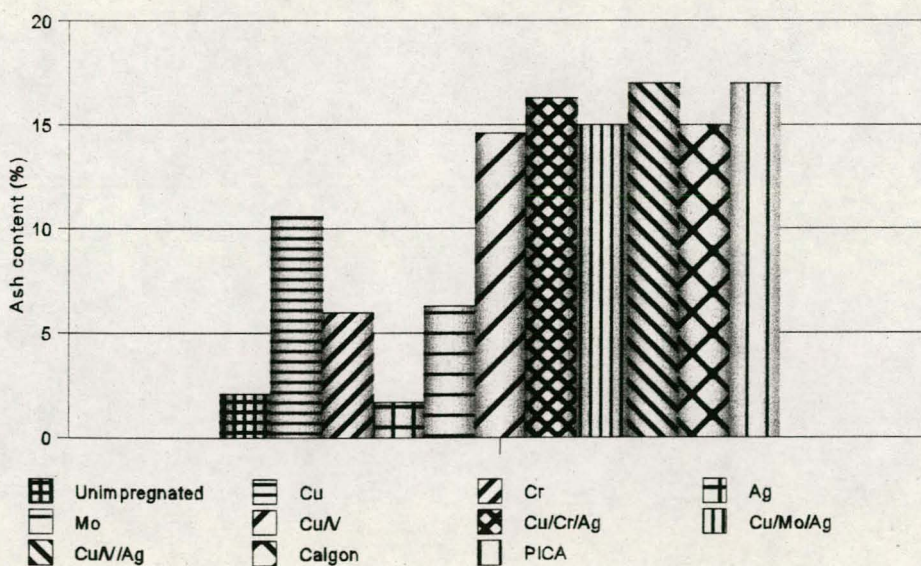
Figure 7   The ash content as functions of the impregnation

Ash contents of the carbons gave a good idea of the degree of impregnation by each of the impregnants. Copper-vanadium-silver impregnation yielded 17% ash which was consistent with the impregnation with 9% copper and 3,5% vanadium and 0,1% silver. Copper, chromium and molybdenum also yielded ash contents that were consistent with their levels of impregnation. Silver-carbon had an ash content of 1,7% which was similar to the values for unimpregnated ash. As only 0,1% silver was impregnated and on the base carbon's ash content ranged from 1 to 3%, it was impossible to see whether the carbon had been impregnated.

6.2.7 MOISTURE CONTENT

The moisture contents of the impregnated carbons are illustrated in Fig 8. The results are listed in Table 9.

TABLE 9 : MOISTURE CONTENT OF IMPREGNATED CARBONS

SAMPLE I.D.	MOISTURE CONTENT (%)
Unimpregnated	3,8
Cu	1,6
Cr	5,1
Ag	3,8
Mo	0,9
Cu-V	4.1
Cu/Cr/Ag	2
Cu/Mo/Ag	1.5
Cu/V/Ag	3
Calgon	5
PICA	4

The moisture contents of the carbons were very good and an indication that the drying procedure was efficient in drying the carbon to acceptable moisture levels. A high moisture content could have altered the oxidation state of the impregnants and therefore affected the protection time.
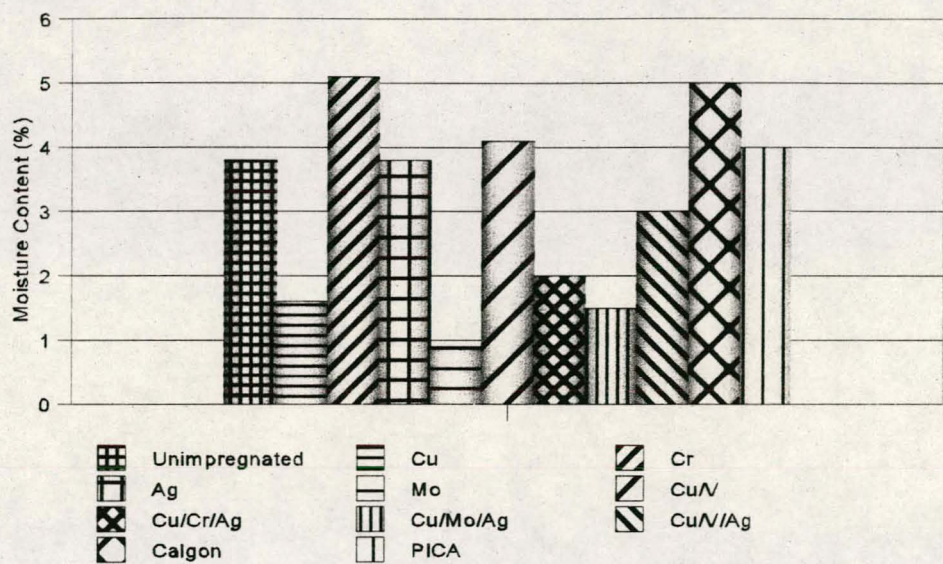

Unimpregnated	Cu	Cr	
Ag	Mo	Cu/V	
Cu/Cr/Ag	Cu/Mo/Ag	Cu/V/Ag	
Calgon	PICA		

Figure 8   The moisture contents as functions of the impregnation

6.3   EVALUATION OF IMPREGNATED CARBONS

6.3.1 CHLOROPICRIN EVALUATION

Figure 9 compares the carbon protection times for the single impregnated carbons.   Table 10 gives the results of the evaluation.

TABLE 10 :   PROTECTION TIME OF IMPREGNATED CARBONS AGAINST CHLOROPICRIN

SAMPLE I.D.	Protection time (min)
Unimpregnated	225
Cu	180
Cr	160
Ag	200
Mo	180
Cu-V	150
Cu/Cr/Ag	121
Cu/Mo/Ag	119
Cu/V/Ag	124
CALGON	103
PICA	105
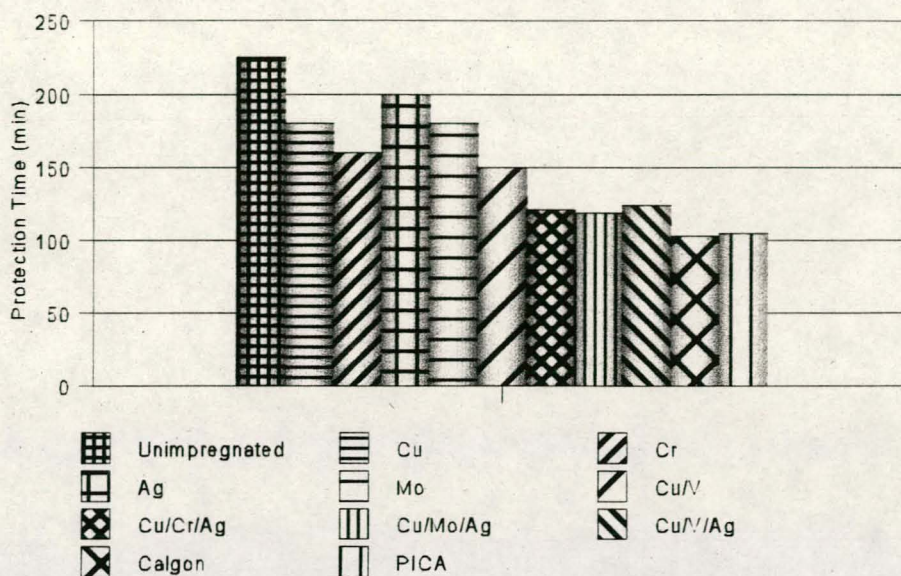
Figure 9　　The chloropicrin protection times as functions of impregnation

It can be seen that unimpregnated carbon gave the longest protection time against chloropicrin.　The least effective in the removal of chloropicrin was the Calgon impregnated carbon. Chloropicrin did not adsorb chemically, but physically onto the surface of the carbon, so that the surface area was the factor that determined the adsorption of chloropicrin.

The unimpregnated carbon and the silver-impregnated carbon had the greatest surface areas and also the longest protection times against chloropicrin, as was expected.　Calgon carbon had the lowest surface area and showed the shortest protection time against chloropicrin, decreasing by 54% as compared with unimpregnated carbon. The reason for this was the smaller micropore volume of the coal-based carbons.

6.3.2 HCN EVALUATION

Figure 10 compares the carbon protection times for the impregnated carbons.   Table 11 lists the results of the evaluation.

TABLE 11 :   PROTECTION TIME OF IMPREGNATED CARBONS AGAINST HCN

SAMPLE I.D.	Protection time (min)
Unimpregnated	0
Cu	35
Cr	7
Ag	0
Mo	5
Cu-V	37
Cu/Cr/Ag	50
Cu/Mo/Ag	48
Cu/V/Ag	43
Calgon	57
PICA	49

The Cu, Cu/V, Cu/Cr/Ag, Cu/Mo/Ag, Cu/V/Ag, Calgon and PICA were the only carbons able to remove HCN. The reason for this was the reaction of the Cu with HCN, so that chemisorption appears to be the means by which HCN was removed from the gas stream. The basic reaction was
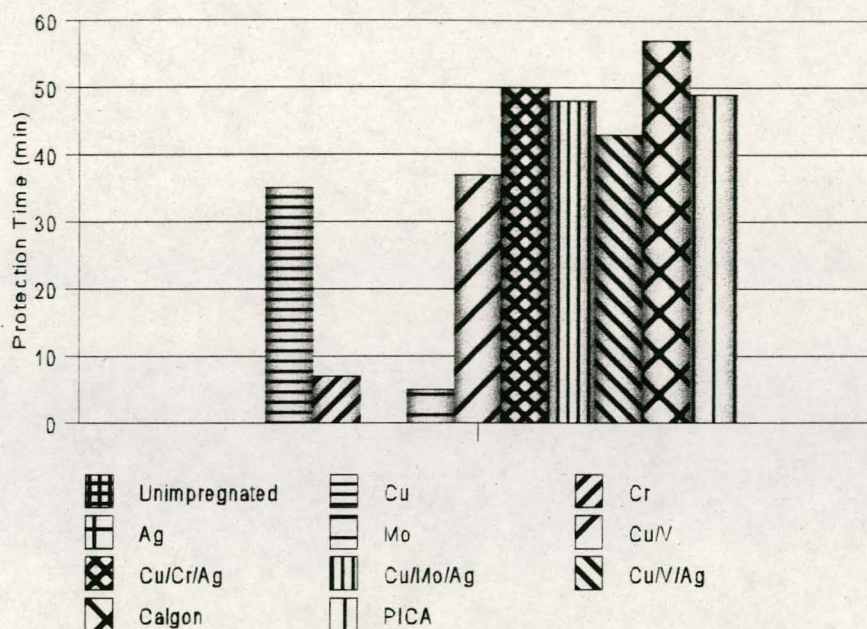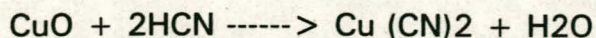
CuO + 2HCN ------> Cu (CN)2 + H2O

Figure 10   Protection against HCN as functions of the impregnation.

The influence of vanadium (as V_2O_5) with the copper seemed to increase the removal of HCN as the carbon protection time increased.   The silver-impregnated carbon protection time was expected to be similar to that of the unimpregnated carbon, as the HCN would adsorb only chemically onto the surface, and only was 0,1% Ag-impregnated. Although Ag can react with cyanides, 0,1% it was insufficient to increase the carbon protection time. The protection times with the combinations were very good. The higher protection time of the Calgon carbon was a direct consequence of the more open structure of the coal-based carbon in which the impregnants were more

CONFIDENTIAL

accessible for filtration.

7.0 EVALUATION OF IMPREGNATED CARBONS AGAINST MIXTURES, IMPURITIES, SOLVENTS AND DIESEL FUEL

7.1 MIXTURE EVALUATION

7.1.1 CNCI AND CHLOROPICRIN

Only five impregnated carbons were used for the evaluation. There were Cu/Cr/Ag, Cu/Mo/Ag, Cu/V/Ag, Calgon and PICA.

The chloropicrin and the CNCl were added to the carbon simultaneously. The addition of the chloropicrin is discussed in Section A of the thesis. The CNCl was added directly from a gas cylinder, and the gas flow rate was controlled with a mass-flow controller.

Figure 11 compares the protection times and Table 12 give the results for the evaluations.

TABLE 12 : CARBON PROTECTION TIMES AGAINST CHLOROPICRIN AND CNCI

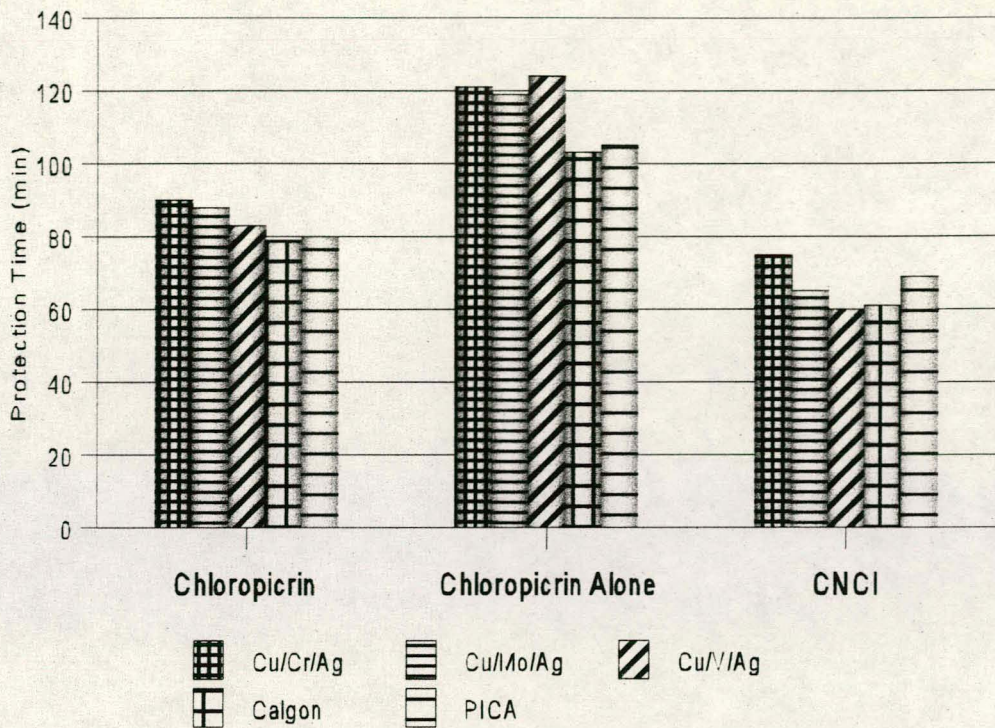| SAMPLE I.D.	Protection time (min)		
	CHLOROPICRIN alone	CHLOROPICRIN mixed	CNCI
Cu/Cr/Ag	121	90	75
Cu/Mo/Ag	119	88	65
Cu/V/Ag	124	83	60
Calgon	105	79	68
PICA	105	75	64

Figure 11   The protection times as functions of simultaneous exposure of the carbons to chloropicrin and CNCl

The protection times against chloropicrin in a mixture were considerably shorter than those against pure agents. This was not unexpected as the chloropicrin and CNCl were dosed together at the same concentrations (5,0 mg.l^{-1} and 2,0 mg.l^{-1} respectively) used in the pure agent evalutions. A flame ionization detector was used. The protection time against the CNCl did not alter with change from single to simultaneous exposure. The five impregnations gave very similar results with the CNCl, but the results with the chloropicrin showed a

reduction in protection of approximately 30%. The explanation given in Section A of the thesis applies also to the CNCl/chloropicrin, namely, the masking effect of the reaction products.

7.1.2 HCN AND CHLOROPICRIN

Figure 12 compares the protection times and Table 13 gives the results of the evaluations of simultaneous exposure of HCN and chloropicrin. The addition was done as discussed in Section A of the thesis. The concentration of the HCN was 2 mg.l^{-1}.

TABLE 13 : CARBON PROTECTION TIMES AGAINST HCN AND CHLOROPICRIN

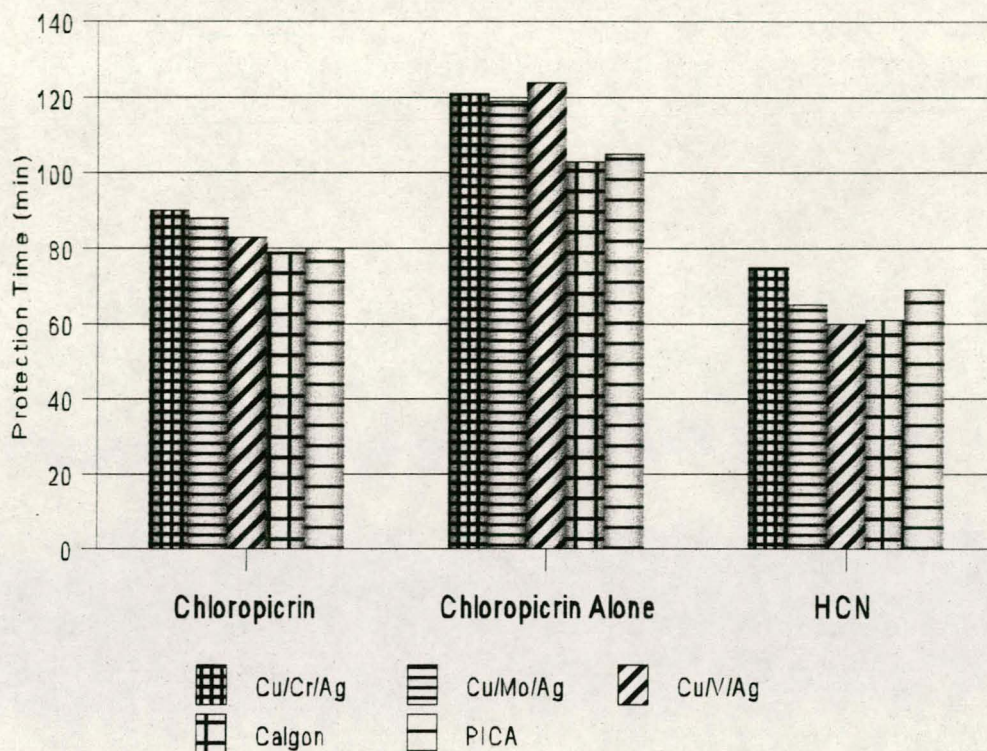| SAMPLE I.D.	Protection time (min)		
	CCl_3NO_2 Alone	CCl_3NO_2	HCN
Cu/Cr/Ag	121	92	50
Cu/Mo/Ag	119	85	50
Cu/V/Ag	124	81	43
Calgon	105	77	54
PICA	105	77	48

Figure 12   Carbon protection time against CCl_3NO_2 and HCN

As with the CNCl, the chloropicrin protection time was reduced by approximately 28% when exposed simultaneously by HCN. The problem of reaction products masking the micropores is a serious problem in multiple gas exposure.

7.2 IMPURITY EVALUATION

7.2.1 CHLOROPICRIN AND IMPURITY

Impurities such as nitromethane and sodium hypochlorite used in chloropicrin synthesis were added to pure chloropicrin in 5 vol. % quantities each to simulate impure chloropicrin.

Figure 13 compares their protection times and Table 14 gives the results of the evaluations.

TABLE 14 : CARBON   PROTECTION   TIMES   AGAINST CHLOROPICRIN AND IMPURITIES

SAMPLE I.D.	Protection time (min)	
	PURE	IMPURE
Cu/Cr/Ag	121	110
Cu/Mo/Ag	119	106
Cu/V/Ag	124	98
Calgon	105	89
PICA	105	93

The results appeared to show slightly shorter protection times than those for pure chloropicrin. This was unexpected as the chloropicrin concentration was only approximately 90% pure and a slightly longer protection time would have been expected. The shorter protection times may have been due to the presence of hypochlorite which contained chlorine. Chlorine is a highly volatile gas which is removed only by reduction. This was probably what was detected as having broken through the filter.
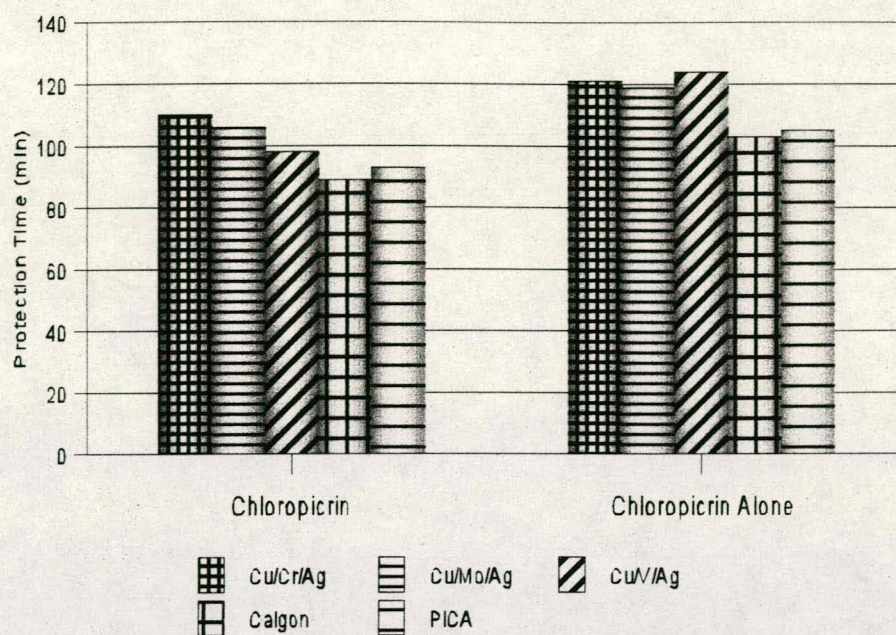
Figure 13   Carbon protection times against chloropicrin and impurities

7.2.2 HCN AND IMPURITIES

The only impurities present in HCN synthesis are water and possible traces of sulphuric acid. Water was included as a 10% impurity for evaluation purposes.

Figure 14 compares the protection times of the five carbons and Table 15 gives the results of the evaluations.

TABLE 15 : CARBON PROTECTION TIMES AGAINST HCN AND IMPURITIES

SAMPLE I.D.	PROTECTION TIME (min)	
	PURE	IMPURE
Cu/Cr/Ag	50	55
Cu/Mo/Ag	50	52
Cu/V/Ag	43	50
Calgon	54	58
PICA	48	53

As expected, protection times increased. Water not only reduced the volatility of the solution (water has a lower volatility than HCN) but provided a reaction medium which increased removal. Aqueous neutralisation of cyanide is far more rapid than gaseous reactions, and for this reason moisture present on activated carbon did not detrimental to HCN removal but in fact aided its removal.
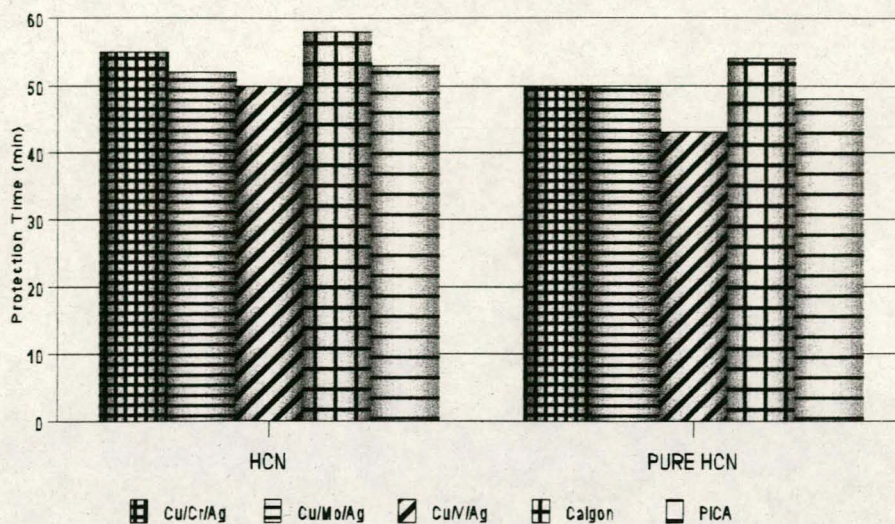
Figure 14   Carbon protection time against impure HCN

7.3 SOLVENT/AGENT EVALUATION

7.3.1 HCN AND SOLVENT

The most common solvent is ethanol and a 50/50 mixture was prepared. Figure 15 compares five carbon protection times and Table 16 gives the evaluation results.

TABLE 16   CARBON PROTECTION TIMES AGAINST HCN AND SOLVENT

SAMPLE I.D.	PROTECTION TIME (min)	
	PURE	WITH SOLVENT
Cu/Cr/Ag	50	56
Cu/Mo/Ag	50	58
Cu/v/Ag	43	48
Calgon	54	56
PICA	48	53

Longer protection times were expected as the volatility of ethanol is lower than that of HCN so that ethanol suppressed HCN vaporisation by lowering the solution volatility. The HCN concentration was therefore reduced.
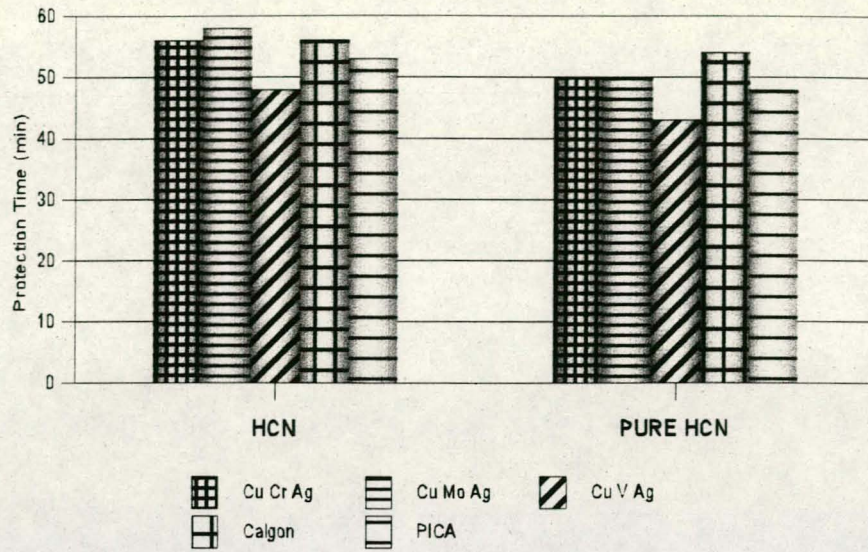
Figure 15   Carbon protection time against HCN and solvent

7.3.2 CNCl AND SOLVENT

The most common solvent is ethanol and a 50/50 mixture was used in the evaluation.

Figure 16 compares five carbon protection times and Table 17 gives the evaluation results.

TABLE 17 :   CARBON PROTECTION TIMES AGAINST CNCl
AND SOLVENT

SAMPLE I.D.	PROTECTION TIME (min)
Cu/Cr/Ag	79
Cu/Mo/Ag	69
Cu/v/Ag	65
Calgon	74
PICA	71

The increases in protection times were expected as ethanol suppressed the solution volatility which resulted in a lowering of CNCl vaporisation, that is, a lower CNCl concentration.
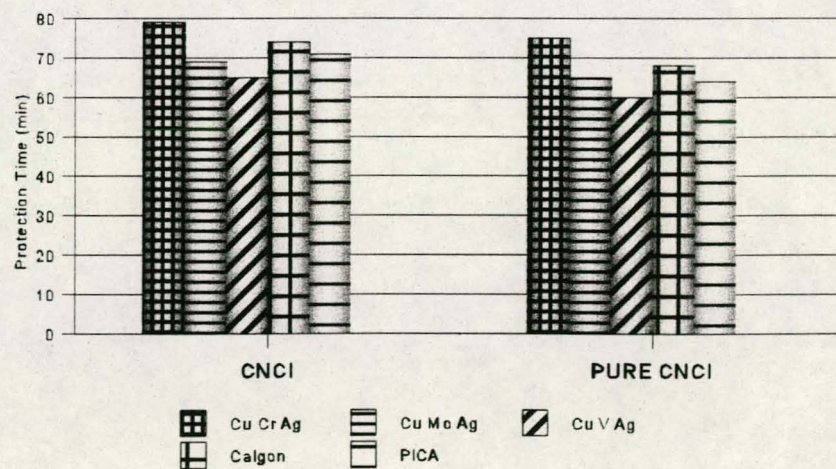

Figure 16   Carbon protection time against CNCl and solvent

7.0 CONCLUSIONS

a) Impregnation

i) The local carbons with Cu/Cr/Ag impregnations were comparable to the Calgon and PICA carbons as regards protection time and impregnation concentration.

ii) A combination impregnation was essential for the filtration of HCN and CNCl

iii) This study demonstrated the feasibility of impregnating carbons with catalysts by solution-deposition techniques. Tests performed on carbons, impregnated with Cu, Cr, Ag, Mo and V and combinations indicated that impregnation was effective. Surface-area measurements and pore-size distribution calculations showed that solution-deposition processes deposited material in the carbon mesopores and macropores. Surface areas of the carbon remained accessible even after impregnation.

With chloropicrin it was observed that surface area was important as physical absorption of this fairly large molecule is the means by which it is removed from air. It was found that the unimpregnated carbon was superior for removal of chloropicrin while impregnated carbons show a reduction in the protection time against chloropicrin.

Protection against HCN is dependent on the impregnation with Cu, and additional impregnants increase the protection time.

b)   Influence of mixtures

i)   Chloropicrin in combination with HCN and CNCl adversely affected the protection time of the chloropicrin because of masking effects of the reaction products.

c)   Influence of impurities

i)   Protection times of CNCl and HCN appeared to be slightly shorter, but the influence was not significant.

d)   Influence of solvents

i)   Solvents caused an increase in protection time, probably due to a lowering of solution volatility because the solvent (ethanol) was less volatile than the agents (HCN and CNCl). The concentration is therefore also lower.

The work emphasized the importance of recognising and understanding the capacities of the adsorbents in all their applications. Different levels of contamination and mixtures of contaminants may result in large reductions in protection times and the capacities of filters. The implication of this reduced performance is that many users of filters will be affected in many different applications. The knowledge of the extent of the contamination is a very important factor to be considered before the filters are used. Specifications are guidelines and as shown in this study they do not apply to all instances.